Sigmund Arntsønn Tronvoll

Doctoral thesis

Sigmund Arntsønn Tronvoll

On the applicability of fused deposition modeling for prototyping

Aspects of dimensional accuracy and structural integrity

NTNU
Norwegian University of
Science and Technology

NTNU
Norwegian University of
Science and Technology

NTNU

Sigmund Arntsønn Tronvoll

On the applicability of fused deposition modeling for prototyping

Aspects of dimensional accuracy
and structural integrity

Thesis for the Degree of Philosophiae Doctor

Trondheim, May 2019

Norwegian University of Science and Technology
Faculty of Engineering
Department of Mechanical and Industrial Engineering

◙ NTNU

Norwegian University of
Science and Technology

To Kjersti, my best friend and wife,
and Iver, my shortest buddy and dearest in life.

Preface

This thesis has been submitted to the Norwegian University of Science and Technology (NTNU) for the degree of Philosophiae Doctor (PhD). The work has been carried out at the Department of Mechanical and Industrial Engineering (MTP) at NTNU under the supervision of Professor Torgeir Welo and co-supervision of Professor Christer Westum Elverum. The project has been a part of the research project Systemflomvern 2020, which was funded by The Research Council of Norway and AquaFence AS.

Trondheim, February 2019

Acknowledgements

Abstract

During the last decade, *fused deposition modeling* (FDM) has managed to become the most used additive manufacturing technology for rapid prototyping. The surge in application of FDM is thought to be due to a severe price drop following the expiration of crucial patents in the decade mid-to-late 2000s. However, the process of compiling strings of molten material into three-dimensional objects has two major pain points; 1) poor dimensional accuracy; and 2) poor structural integrity. Hence, the FDM process is considered a sub-par choice for prototyping. To increase the prototyping applicability of FDM, this thesis aims to improve upon these two aspects. This, by generating knowledge for assessing and improving the part performance, while also generating design tools and knowledge to limit the impact of these major downsides. FDM is a very complex process, with many contextual factors that have implications for the performance of the end-result. The approaches utilized in this thesis are therefore directed towards trying to explore isolated effects and mechanisms, rather than assessing difficult-to-generalize overall performance parameters.

Dimensional accuracy is a well-established area of research, and drivers for defects and inaccuracies can be categorized into STL-conversion, printing fundament, positional accuracy, layer sampling and accuracy of material extrusion, where the contributions of this thesis are focused towards the two latter. The novelties presented here that target these, are; 1) an analysis of layer height and the sampling methods influence on the dimensional accuracy of threaded parts, through a novel method of digital image analysis; and 2) investigation of the performance of *pressure advance algorithms*, designed to improve the dimensional accuracy in regions of high acceleration/deacceleration of the printer. Findings suggests that both effects have significant influence on the dimensional accuracy of the FDM process.

Structural integrity of FDM is a less mature area of research, where the cause of the subpar performance compared to solid material is often debated. Most of the research within this domain tries to predict part performance based on input parameters, as with conventional material characterization research. This thesis explores an alternative approach, where the mechanical performance is estimated based on experimental investigation of the cellular structure. The novelties connected to this approach, presented in this thesis can be summarized as; 1) integration of statistical perspectives (weakest-link effect) in the assessment of FDM part strength; 2) assessment of through-thickness properties of the mesostructure of FDM, using a novel method for analysis of computed tomography data; and 3) structural analysis of FDM parts using a multiscale simulation approach, currently directed towards linear elastic behavior and strain energy density distribution. Findings suggests that previous work on the structural integrity of FDM parts is highly non-generalizable, due to a very complex mesostructure and strain energy density distribution.

The concepts presented in this thesis fills in some of the current gaps in the research literature on the performance of FDM parts, and provides models, frameworks and relations that can be utilized in further work.

X

Table of contents

Part 2: The appended papers

Part 1: Introductory overview

1. Introduction

"Prototyping is the shorthand of innovation"

- Tom Kelly, IDEO

1.1. Motivation and background

Being fluent in prototyping—the activity of building design proposals for the purpose of scrutiny—is a key asset for developing products that work as intended [1]. This is due to the limitation of the complexity of concepts that humans or computers can construct by deductive reasoning or prior empiric knowledge, without introducing design errors. The more novel the product, the more complex it becomes due to the lack of broken ground. This can be exemplified by Edison's lightbulb experiments, which took thousands of experiments before reaching a technically and commercially viable solution [2]. The lack of empirical knowledge at the start of a development process leads to what Ullman calls *"the design process paradox"* [3], which implies that the knowledge about the design problem, and hence the ability to design, increases throughout the development process, while the *design freedom* decreases due to the design choices taken. From a cost perspective view, this discrepancy persists. The cost to change a design or explore design alternatives, sometimes denoted cost of learning, is low in the beginning of a development project, when the knowledge of the design is low, and increases exponentially throughout the project [4].

The importance of the early-phase decisions on the final outcome is usually not reflected in the resources allocated. Prior literature explains that the majority of a product's life-cycle cost is locked-in through decisions made during the conceptualization and design phase of their projects, while these phases only attracts a small fraction of the life-cycle costs [5–7]. The sources to back up this inductive reasoning are scarce, and the disproportion would be dependent on e.g. product type, production volume and user characteristics, among others. However, a general overview given by Fabrycky and Blanchard [6] is provided in Figure 1-1. Thus, inexpensive tools and methods for allowing for rapid and thorough exploration are highly regarded in industry [8].
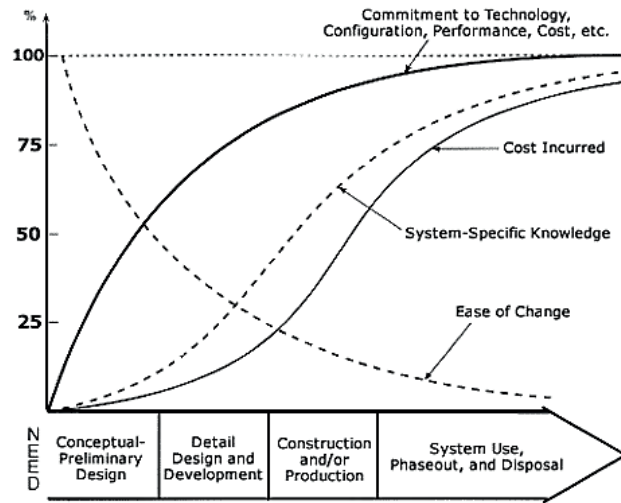
Figure 1-1 - Diagram of cumulative commitment vs. incurred cost for a general development program. Reproduced from Fabrycky and Blanchard [6].

This need for inexpensive tools for experimenting have contributed to the wide application of computer-aided methods. In this connection, computer-aided design (CAD) is the basis technology, allowing for detailed construction and dimensional analysis of an ideal geometry (e.g., as clearance/interference, weight, center of gravity). The extensions of CAD are targeting two different aspects: virtual experimentation and testing of mechanical aspects through computer-aided engineering (CAE); and aid for physical manufacturing and experimentation through computer-aided manufacturing (CAM). The combination of CAM and numerically controlled manufacturing methods has empowered companies and workers with manufacturing skills previously only held by highly experienced professionals, enabling creation of machine instructions to automatically manufacture designs that earlier had been found too complex to make. Some of these computer-controlled manufacturing methods that specifically targets design exploration due to their versatile manufacturing capability, go under the name *rapid prototyping* [9]. Although an agreed upon definition does not exist, rapid prototyping can be summed up as: *a relatively fast and automated method capable of making parts of a generic shape, with a very low level of user interaction.* This branch of tools, nowadays often associated with various *additive manufacturing* (AM) technologies, has surged in application throughout industry during the past decade, mainly due to improved affordability. After the low-end priced sub 5,000 USD additive manufacturing systems entered the market around 2007, the numbers of sold units have increased with a factor of 100, as seen in Figure 1-2, reported by Wohler et al. [10]. One single technology—*fused deposition modeling* (FDM)—is the main driver in this rise of rapid prototyping.
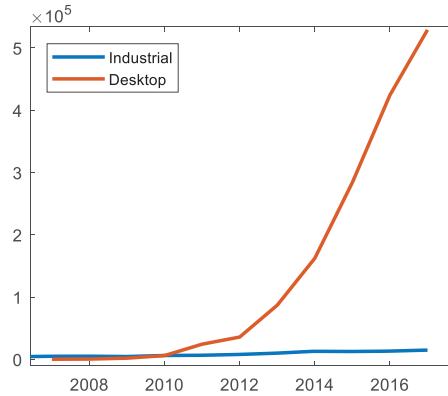
Figure 1-2: Comparison between estimated global sales of industrial (>5000 USD) vs desktop (<5000 USD, mainly FDM) AM systems, by number of sold units. Compiled from data given in Wohler et. al. [10].

While the term fused deposition modeling is trademarked by Stratasys Inc., it has become the *de-facto* standard for referring to processes where strings of extruded polymers, from a filament feedstock, are melted together and compiled into parts, layer-by-layer. The term for this type of manufacturing, according to ISO/ASTM52900:2015 would be *material extrusion additive manufacturing*. This term is however ambiguous, as the referred standard does not give any recommendations on how other material-extruding processes, using concrete, wax or non-polymeric biomaterial, should be named. FDM-like processes could be named *polymer filament-based material extrusion*, but no such convention currently exist. Some use the term *fused filament fabrication*, but this is not well adopted. This thesis will therefore use the term fused deposition modeling, but it must be mentioned that the research was not conducted using systems from Stratasys Inc.

Having a tool as FDM available gives the possibility of prototyping structures that were previously only achievable by a 5-axes CNC milling, available at a fraction of the cost. Other key characteristics are:

- high degree of integration with CAD;
- high degree of automation;
- low spatial requirements allowing it to be placed in close vicinity of the designer's workstations;
- high degree of open source design, software and firmware.

These aspects have made FDM the most commonly used rapid prototyping method throughout the industry. On the flip side, desktop FDM machines are also among some considered a sub-par additive manufacturing choice for prototyping, especially for *high-strength*, *high-consequence* or *fine-tolerance* applications. Some of the reasons for this are:

- poor build quality of machines [10,11], resulting in low reliability and repeatability;
- structural properties difficult to assess a priori [12], making use of CAE tools difficult (as *finite element analysis*);
- low dimensional accuracy [10,13–15], and commonly not possible to achieve the tolerance needed.

For applications demanding high accuracy and structural integrity, engineers therefore turn towards more high-end and hence high-cost methods, which would heighten the threshold for committing to build prototypes. Increasing the design space of FDM in terms of strength and accuracy or assessing what levels of strength and accuracy is possible, would therefore aid in lowering threshold for building prototypes. Followingly, with the aim to improve the applicability of FDM for cost efficient experimentation with physical prototypes, this thesis seeks to investigate key aspects connected to the structural integrity and dimensional accuracy provided by the method.

1.2. Research aim, questions and methods.

In an effort to increase product development performance through improved prototyping methods, the main objective of this thesis is as follows:

> **Objective:** *To improve the applicability of fused deposition modeling as a prototyping method by reducing the uncertainty in part performance, by building knowledge and establishing methods for assessing and improving their dimensional accuracy and structural integrity.*

During Chapter 2, this thesis will argue for why dimensional accuracy and structural integrity are key aspects in the context of prototyping in engineering design, through a compilation of conceptual studies and existing research. In this connection, this thesis will target the following research questions:

> **RQ1:** *What are the main drivers/factors influencing dimensional inaccuracy of FDM parts?*

> **RQ2:** *What are the main drivers/factors influencing structural integrity of FDM parts?*

These research questions are answered through exploring different concepts, using a combination of physical testing, non-destructive testing, numerical simulations and analytical work. This work has resulted in multiple novel methods for assessing dimensional accuracy and structural integrity. The results are provided in 4 scientific articles aiming to partially answer the research questions regarding dimensional accuracy and structural integrity of FDM parts. One additional article is appended which contributes to the connection between the manufacturing capabilities of FDM to the field of prototyping in specific.

1.3.   List of appended papers

The appended papers in this article collection-based PhD thesis relate to the overall objective as illustrated in Figure 1-1. Each paper has its own individual objectives, providing findings, methods and tools, contributing to the overall objective of this thesis as well as to the body of knowledge in general. As only three of the five papers are published, these will all be referred to as *appended Paper 1-4* and *Supporting paper*.
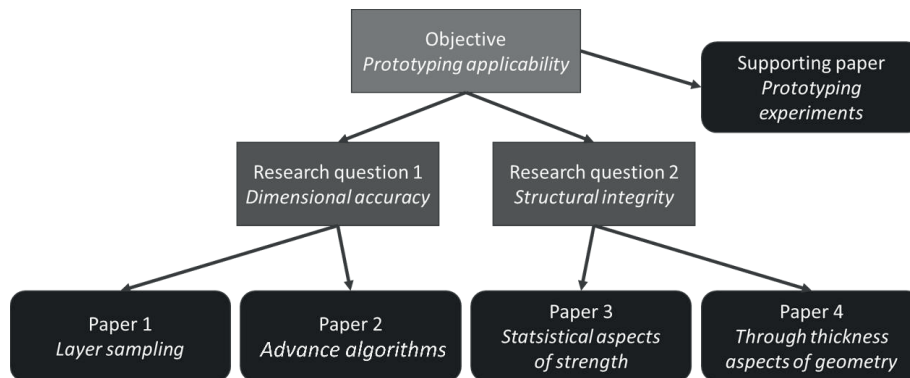
Figure 1-3: Relation between the of the papers' scope, the research questions and overall objective of this thesis.

These papers' contributions are further described in Chapter 6, while a brief description of their thematic is provided as follows:

Paper 1 – Dimensional accuracy of threads manufactured by fused deposition modeling. Tronvoll SA, Elverum CW, Welo T.

Status: Published in Procedia Manufacturing 2018;26:763–73.

Theme in-brief: This article explores the defects on FDM manufactured threads using a novel method of image analysis, and relates this to the geometric sampling used to generate the toolpaths.

Paper 2 – Investigating pressure advance algorithms for filament based material extrusion: Theory, practice and simulations. Tronvoll SA, Popp S, Elverum CW, Welo T.

Status: Manuscript approved to be published in Rapid Prototyping Journal.

Theme in-brief: This is the first-in-field article to describe and investigate the performance of (pressure) advance algorithms, whose scope is to minimize acceleration-related defects in FDM parts.

Paper 3 – The effects of voids on structural properties of fused deposition modelled parts: a probabilistic approach. Tronvoll SA, Welo T, Elverum CW.

<u>Status:</u> Published in International Journal of Advanced Manufacturing Technology 2018;97:3607–18.

<u>Theme in-brief:</u> This experimental study relates the strength of FDM parts to their mesostructure by using image analysis, and introduces the weakest link aspect into research on FDM.

Paper 4 – New method for assessing anisotropy in fused deposition modelling: Analysis of computed tomography data. Tronvoll SA, Vedvik NP, Elverum CW, Welo T.

<u>Status:</u> Manuscript submitted for publication in International Journal of Advanced Manufacturing Technology

<u>Theme in-brief:</u> This experimental study is the first-in-field to assess the 3D-internal structure of FDM parts, and to relate this to mechanical performance using a multiscale finite element-based approach.

Supporting paper – Prototype Experiments: Strategies and Trade-offs. **Tronvoll SA, Elverum CW, Welo T.**

<u>Status:</u> Published in Procedia CIRP 2017;60:554–9.

<u>Theme in-brief:</u> This conceptual study explores the trade-offs committed when designing prototype experiments and describes how this relates to their strategic design approach.

1.4. Limitations of the thesis

1.4.1. Approach to state-of-the-art

The recent price drop and subsequent sales surge for FDM systems are reflected in the numbers of papers on the subject. Using the keywords *fused deposition modeling, melt extrusion additive*, and *fused filament fabrication*, searching through title, abstract and keywords in the *Scopus* database reveals a leap in the numbers of scientific articles produced, around year 2010. It is now published at a rate of more than 866 articles per year (articles published in 2018, as reported January 7th, 2019), as seen in Figure 1-4. Even if the fundamental principles of fused deposition modeling have not altered much, the techniques, experimental results, and concepts are rapidly expanding. It is noteworthy that approximately 1/4 of the accumulated research on the topic is expected to be published within 2018 alone. For research trying to achieve a state-of-the-art overview of the field, therefore, might be outdated by the time of publication.
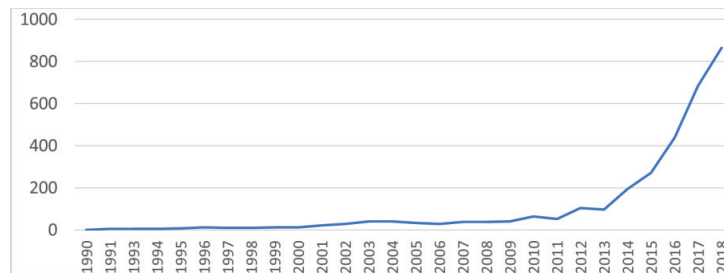
Figure 1-4: Research items published (excluding book chapters) on fused deposition modeling, melt extrusion additive*, or* fused filament fabrication *per year in Scopus database. Accessed January 7th, 2019. Other, more vague keywords, as* solid freeform fabrication *and* 3-D printing *are neglected.*

1.4.2. Engineering design, design and product development

This thesis will only assess prototyping of physical products as a part of the activities usually involved in product development. Although product development involves aspects as *business models, company/customer interaction, supply chains* and *marketing,* which can be investigated by prototyping, this work focuses on the construction and design of mechanical, dimensional and physical features of parts; that is, *engineering design.*

As this work is primary intended as a contribution to the engineering design community, its focus is directed towards technical and strategic aspects of using FDM in prototyping. This, rather than the *idioms* of the prototyping methods, as would possibly be the case if considering design as an art form.

1.4.3. Other methods of prototyping and additional processing

Combined with the geometric flexibility of the process, the low cost of FDM is a key argument for its attractiveness as a prototyping approach. Some companies do however have very large prototyping budgets, large workshops and trained personnel, and hence could utilize more expensive rapid prototyping methods or high-end manufacturing methods, e.g. 5 axes milling, and small series injection molding, without much lead time penalty. However, as shown by the surge in FDM-machine sales, for most practitioners, cost is an important issue. This thesis is; therefore, directed towards users and companies with relatively low prototyping budgets, mainly as in small-to-medium sized enterprises (SMEs).

There are many different needs for prototyping obviously not met by FDM, as e.g. fabric prototypes, high transparency prototypes, electronic prototypes. Hence, this thesis will be limited to prototyping of solid parts in the size range manufacturable by desktop FDM systems (normally in the range 100×100×100mm to 400×400×400mm). The focus has also been on printing with PLA, as this is the most dominant material in practitioner usage.

Furthermore, rapid prototyping by stereolithography (additive process abbreviated SLA, using UV light-reactive resin cured by a numerical controlled laser) is becoming increasingly popular due to recent reduction in cost. It is likely that this process will gradually take a larger share of the low-cost end of the rapid prototyping system market, as stereolithography is known for having better resolution and process control. As every method has its strengths and weaknesses, they could be considered complementary to each other. Therefore, exploring SLA and its applicability as a prototyping method, go beyond the scope of this thesis.

A large share of prior research goes into post-processing of FDM parts, for improved dimensional, functional or aesthetic properties. While this would include a large share of the conventional post-treatment methods of plastic parts, most of the FDM specific research deal with reducing the process' inherent surface roughness through sanding, filling or chemical smoothing, or for increasing part tolerance through e.g. post-machining. These are excellent contributions to FDM as a manufacturing method, and some of these techniques can be automated and included into FDM systems without inflicting with the method's ease of use. Most techniques do; however, complicate the process and hence moves the process further away from the rapid prototyping genre. To limit the scope, this thesis targets identifying and improving upon FDMs standalone performance, rather researching potential ways of handling its deficiencies through post processing.

1.4.4. Practitioner community activity

An important aspect of FDM is the size of the practitioner and developer community. As most software and printer firmware are open source, this allows for extensive experimentation for everyone having basic coding skills. This leads to several techniques and tools that are developed completely outside the academic sphere, leaving the academic community lagging in some areas.

1.5. Structure of thesis

The remainder of the introductory overview of is organized into six parts:

Chapter 2 displays the role of prototyping in engineering design, and what aspects of FDM are important in this context.

Chapter 3 offers a brief description of the FDM process.

Chapter 4 provides a synthesis of existing research explaining the various concepts and challenges associated with dimensional accuracy of FDM.

Chapter 5 provides a synthesis of existing research explaining the various concepts and challenges within the scope of structural integrity of FDM.

Chapter 6 lists the objectives and key contributions of the appended papers.

Chapter 7 provides summary and conclusions on the contribution of the thesis to the body of knowledge. Further work is also proposed.

2. Prototyping by fused deposition modeling – Contextual factors

2.1. The purpose of presenting prototyping theory in this thesis

The industrial application of fused deposition modeling is, with some exceptions, restricted to prototyping. To explain FDMs role in prototyping, and followingly why structural integrity and dimensional accuracy are important attributes in this context, the following aspects are covered:

- the role of prototyping in engineering design;
- the manufacturing need from physical prototyping.

This chapter will first go through the concept of prototyping in general, and then the role and approaches of physical prototyping will be discussed. These concepts, roles and approaches are then synthesized into a selection of manufacturing needs, which are elaborated on in the context of prototyping using FDM.

2.2. The concept of prototyping in engineering design

Product development is a set of sequential and iterative activities, which covers most of the work that is needed for bringing a product to market. The particular focus in this thesis is the development of *mechanical aspects* of the *product* and its *manufacturing process*. These aspects go by the definition of *engineering design* by Dixon and Duffey [16]. In a simplified way one could say that a general product development process consists of multiple phases, each with different main scopes, as described by Ulrich and Eppinger [17]:

Phase 0: Planning
Phase 1: Concept development
Phase 2: System level design
Phase 3: Detailed design
Phase 4: Testing and refinement
Phase 5: Production ramp-up

This could be a linear process, often referred to as a *waterfall model* [18], which is a description of Royce's proposal of how to manage software development projects [19], or *serial engineering* as named by Sobek, Ward and Liker [20]. However, many design decisions in a phase affects the requirements of the following phases, and a wider scope integrating the aspects from all phases is often beneficial for product development performance. This concept of integrating a more holistic viewpoint in all phases is named *concurrent engineering* by Sobek et. al. [20]. Iterations within each phase or between phases is also a common attribute of the development process, where one has to redo tasks based on new information, faulty initial design, or new design elements non-compliant

with previous elements [21]. In many cases, a real-world product development process will include elements from all these three characteristics.

It is acknowledged that design in general is a process which consists of different divergent and convergent activities, where one explores concepts (divergent) and thereby evaluates performance (convergent) related to different requirements, denoted the *generate-test cycle* by H.A. Simon [22]. If a concept is found insufficient, new concepts must be generated and subsequently tested. This includes activities throughout the whole development phase, although the relative changes between each cycle might be larger in the early phases, when the design space is more open. The dominantly divergent concept development phase, and later, more convergent activities is reflected in Ulrich and Eppinger's graphical description of the product development process as seen in Figure 2-1.

Phase 0:	Phase 1:	Phase 2:	Phase 3:	Phase 4:	Phase 5:
Planning	Concept development	System-level design	Detail design	Testing and refinement	Production ramp-up
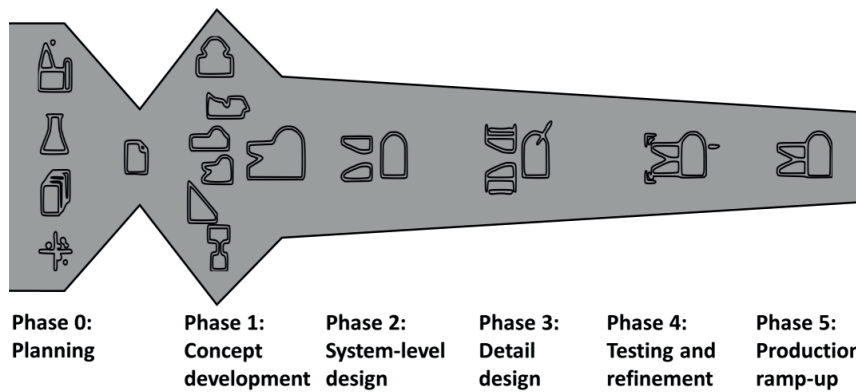
Figure 2-1: Illustration of a general product development process from Ulrich and Eppinger [17].

The generate-test cycles can either be of an accidental nature, needed to repair a design error, or they can be intentional and planned to solve a specific set of problems. Clark and Fujimoto call these *problem solving cycles* [23], and also state that these experiments can be found in form of e.g. thought experiments, physical tests, hand calculations and simulations. Kennedy, Kennedy and Sobek [1] argue that the generate-test cycles that should be avoided are those arising from errors on design elements that were expected to be final. Final elements are often used as input for many other design choices. These would have dependencies throughout the design, and redesign of such elements are therefore often costly. These unplanned cycles around expected-to-be-final parts of the design are often named rework [1,9]. Building on the concepts from Fabrycky and Blanchard [6], *rework risk* can be defined as the difference between the system-specific knowledge and the commitment, as seen in Figure 2-2. New tools and strategies therefore often target reducing this gap in the efforts to reduce rework. This is the key aspect of the generate-test cycles, as rather than only designing by *best guess* and/or *empirical knowledge,* the generate-test cycles seek to capture and test the product performance before the design of the end product is finished.
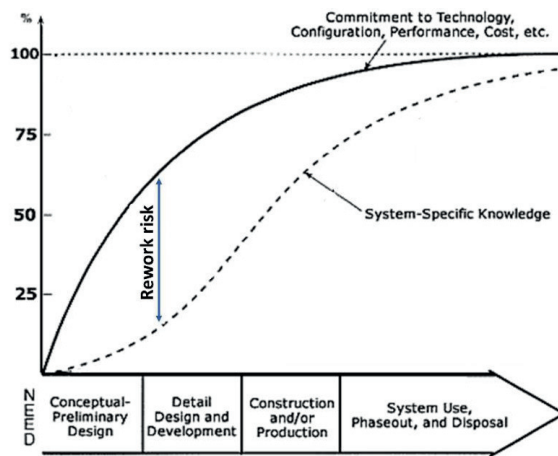
Figure 2-2: Rework risk as derived from knowledge and commitment. Modified illustration from Fabrycky and Blanchard [6].

Within the generate-test cycles, models of the design are evaluated against models of its environment, where both could be incomplete models, according to Thomke [24]. These models of the design in these cycles could go by the broad definition of a *prototype* as described by Ulrich and Eppinger [17]:

"(prototypes are…) an approximation of the product along one or more dimensions of interest"

This implies that prototypes could potentially obtain just a small selection of the product's functionality or components. It would be important to note that as one is evaluating the product against an environment, creating a test environment might be equally challenging as creating a prototype. Hence, making prototypes are parts of a larger context in form of creating prototype experiments. As shown by Tronvoll, Elverum and Welo [25] and in the appended Supporting paper, iterations could be around improving or changing the test environment, as well as the design itself. An important aspect affecting the choice of prototyping method is therefore assessing what variety of test environments the prototype should be compatible with.

For a binary experimental outcome, the correct interpretation of a prototype experiment could either be a subpar or adequate design, or that the experiment exhibits a type I or type II error, as illustrated in Table 2-1. As noted by Liker et al. [26], experimenting with prototypes made by rapid prototyping would often lead to Type I errors, as these are often underperforming compared to production-intent design.

Table 2-1: Interpretations of experiment outcomes.

Experiment failure	Experiment success
Subpar design	Adequate design
Underperforming prototype (Type I error)	Overperforming prototype (Type II error)
Too harsh environment (Type I error)	Too mild environment (Type II error)

The experiments in which the design is evaluated, are not necessarily controlled experiments, as performed in natural sciences. The appended Supporting paper elaborate on this topic by describing the experiment configuration as a trade-off between the following:

- *Iteration cost - What is the cost of the experiment?*
- *Iteration time - What is the time used on the experiment?*
- *Approximation level - How correct is the result?*
- *User level - How easy is it to use?*
- *Results presentation - How easy is it to draw conclusions from the data?*
- *Experiment flexibility - How easy is it to change conditions?*

Therefore, one might find prototypes as simple as a sketch for facilitating thought experiments, to multi-million *verification and validation* prototypes, with examples given in Figure 2-3. The test environment might also be everything from as simple as showing the design to a colleague or manager for facilitating though experiments, to a full real-life test, nearly identical to the intended use scenario.
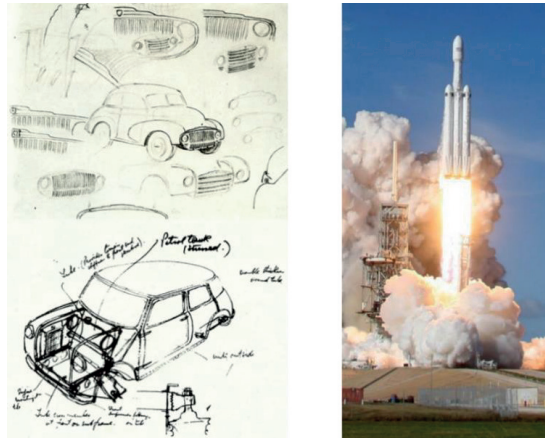
Figure 2-3: Two examples of prototypes: multiple early phase sketches for form-finding of the Morris Minor, and late-phase verification and validation prototype of the SpaceX - Falcon Heavy rocket. Image courtesy of Alec Issigonis and Reuters/Thom Baur, respectively.

Obviously, each prototype and environment should be tailored to its intended scope. Sometimes this could be as straightforward as a couple of hand calculations or static finite

element simulations. However, when one expects a more complicated part function as e.g.

- subject to multiple dependencies between components;
- multiple load cases difficult to analyze through CAE;
- subject to hard-to-model human interaction,

physical experimentation often has an edge compared to non-physical methods. As described by Ulrich and Eppinger [17]:

"… all of the laws of physics are operating when the [development] team experiments with physical prototypes."

Therefore, despite the rapidly expanding capabilities of CAE, the discipline of engineering design would still involve physical prototyping. One can also argue that technological advances within manufacturing, such as rapid prototyping techniques, will continue to improve and thereby improve the attractiveness physical prototyping

2.3. The types of physical prototyping and their manufacturing needs

Ulrich and Eppinger [17] classify prototypes along an *analytical* to *physical* axis, and Smith [9] classifies design approaches as either being *analyze first* or *make first*. Analyze first describes the approaches where the early phase prototyping is done using *analytical* methods, such as CAD and CAE, while *physical* methods might only be utilized for later stage verification and validation. Conversely, *make first* targets early and possibly extensive physical prototyping for learning about the design problem, which could then be used as input to analytical models for refinement. Elverum et al. [27] argues that the more novel the design problem is, the more favorable make-first approach becomes, due to less broken ground for which analytical tools are found accurate. For well-known design problems, analytical models usually have a validated domain of accuracy and analytical tools are often more refined in terms of user friendliness to improve speed of experimenting. Hence, physical prototypes play two different roles in these approaches, as tools for *risk-management* or as tools for *exploration* as defined by Schrage [28]. In a similar framework to the exploration/risk management classification proposed by Schrage, Smith [29] makes the same differentiation. He denotes the approaches *traditional* and *front-loaded prototyping*, building on the *front loading* conceptual framework from Thomke and Fujimoto [30] directed towards early exploration and learning through prototypes. Smith describes the different prototyping approaches as listed in Table 2-2. As the objectives of the prototypes are different, there is no immediate contradiction in utilizing both strategies in the same development project.

Table 2-2: Traditional vs. front-loaded prototyping. Reproduced from Smith [29].

Characteristic	Traditional prototyping	Front-loaded prototyping
Prototype cost	High	Low
Prototype build time	Slow	Quick
Numbers of prototypes	Few	Many
When used in development	Late	Throughout
Prototype's objective	Verify	Learn
Prototype's scope	Broad, vague	Specific, narrow
Prototype attractiveness	Refined	Perhaps crude
Department affiliation	Primarily engineering	Any

As an important note for build-first or front-loading methods, the constraints of the prototyping method could shape the design, rather than solely materializing a design idea. An example identified by Schrage, are the calculator product line from Hewlett-Packard, which drastically changed appearance after the designers changed from cardboard prototyping to foam shaping, resulting in a change from edgy plate-like designs to considerably more organic shapes [28]. For solely aesthetic features, this is not necessarily a problem, but for engineered features, the design should also be based on function, manufacturing capabilities and other constraining attributes.

Table 2-3 summarizes the different manufacturing needs of the two different prototyping approaches, by synthesizing the relevant parts of the trade-off dimensions from the Supporting paper and the prototype characteristics from Smith [29].

Table 2-3: Manufacturing needs from the two different prototyping approaches.

Traditional	Front loaded prototyping
Part performance should be accurate on a system level, and hence enable verifying the overall product performance	Part performance should be accurate in the scope investigated to generate rigorous knowledge
Preferably low cost	Low cost due to many cycles
Preferably short lead time	Low lead time due to short cycles
User involvement not essential	Low user involvement to enable experimenting without the need to involve 'expert users'.
Able to replicate as-built manufacturing methods	Flexible, to reduce chances for prototyping method derived design

Rapid prototyping methods, as FDM, are utilized for both traditional prototyping and front loading. However, front loading is where it has its main advantage, due to its key attributes of low cost, low lead time, low user involvement and high flexibility. As the lead time and prototyping budget is usually higher in traditional prototyping, FDM and rapid prototyping in general, is assumed to have less of an advantage. For traditional prototyping, the form freedom of FDM is its key aspect, enabling prototyping of parts difficult to achieve without high fixed-cost manufacturing methods, as injection molding and rotational molding.

What both traditional and front-loaded prototyping approaches require—an outcome FDM does not unreservedly guarantee—is accuracy. In this context, accuracy does not

implicate accurate according to specifications, intentions or drawings, but *form and function* compared with the to-be-manufactured design, to avoid a under or overperforming prototype. Traditional prototypes require accuracy on system level to rigorously be able to verify their overall performance. This would imply that some parts would need to be accurate across a whole specter of properties; e.g., *visual, physical, dimensional and mechanical*, as various tests might target all these aspects. Liker [26] disregards rapid prototyping as a viable method for anything that is novel or depending on aesthetics or structural integrity, and recommends traditional comprehensive prototypes for all those cases. This is based on findings from various industrial companies but does not mention to what extent these are preferences or practices. Front-loaded prototyping usually has a somewhat narrower scope; hence accuracy would not necessarily be needed across many different properties. In this connection, the choice of arms depends solely on what would be the easiest way to answer the questions at hand.

Within each scope of experimental testing, FDM would often have a design space where the performance is partially overlapping that of the intended manufacturing method, as illustrated in Figure 2-4. Liker argues that this is only existent within the scope of general form finding [26]. One could agree that the overlap is probably largest within that scope, but certainly there are overlaps within other scopes, as FDM prototypes are regularly being used both for structural and visual components. Within the overlapping region, the prototype performance and intended design could be taken as similar. However, if the optimal/intended design lies outside the viable design for FDM, the prototype would need to be redesigned for being manufacturable. It is therefore crucial that the results from any prototype experiment is analyzed to identify to which extent the performance is caused by the design itself, or the redesign for FDM. Whether the design is constructed with the final manufacturing method in mind, or whether this is disregarded, would alter the workflow differently, as displayed in Table 2-4 and Figure 2-4.

Table 2-4: Generate-test workflow through design for (final) manufacturing, and the altered workflow caused by primarily designing for FDM.

Design for final manufacturing method	Design for FDM
1. Generate a thought-to-be optimal design for the final manufacturing method	1. Generate design for FDM and print
2. Redesign for FDM and print	2. Test
3. Test	3. Calibrate results and redo cycle if subpar
4. Calibrate results and redo cycle if subpar	4. Redesign for final manufacturing method

As with the design in general, due to inaccuracies and knowledge gaps associated with the FDM process, the redesign and printing activities are often iterative. In contrast to making production-intent prototypes, where manufacturing issues directly translates to *design-for-manufacturing* aspects, the knowledge generated through iteratively trying to build FDM parts does not contribute to increased learning about the design. Iterations around the redesign for FDM should therefore be kept at a minimum to reduce wasteful activities.
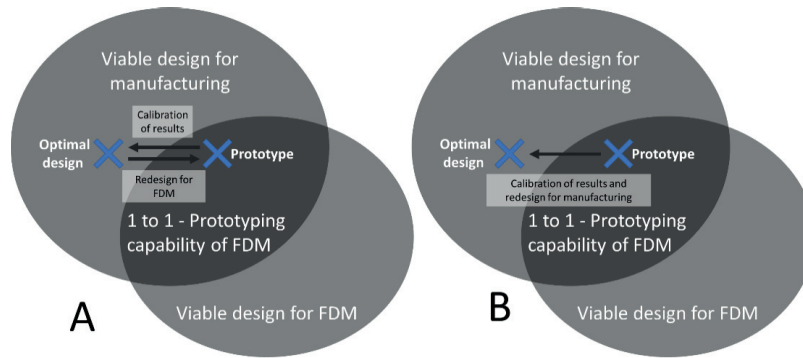
Figure 2-4: Design space of intended manufacturing method vs. design space for FDM. Way of redesign and calibration of results for A) design for final manufacturing *approaches, and B)* design for FDM *approaches.*

Referring to Figure 2-4, efforts to increase the prototyping applicability of FDM could target either of the following:

1. increase the overlap between design for various manufacturing methods and design for FDM (increase the capability of FDM);
2. generate knowledge about the performance of FDM parts for calibration of results;
3. generate tools and knowledge for design/redesign for FDM to decrease the performance gap or ease the transition to-and-from FDM prototypes (reduce waste).

These three aims are therefore the focus in this thesis, considering dimensional accuracy and structural integrity as key issues for using FDM as a prototype manufacturing method. The results in this thesis that targets these, aims as follows (with scope-number in parenthesis):

From Paper 1:
- knowledge about the dimensional accuracy of FDM threads (#2);
- tools for *design for FDM* to reduce the effects of dimensional deviations introduced during slicing (#3).

From Paper 2:
- knowledge on key relations between process parameters and extrusion accuracy for improved print quality (#1).

From Paper 3:
- knowledge about the mechanical performance of FDM parts, in terms of anisotropic behavior, for calibration of results (#2).

From Paper 4
- knowledge about the mechanical performance of FDM parts for calibration of results (#2);
- results can be used for design for FDM to decrease the performance gap (#3).

There are numerous cases where neither dimensional accuracy nor structural integrity are key performance parameters for prototyping. This could be for loosely specified tolerance parts, or where the strength and dimensional accuracy obviously meets the requirements or pose no risk if the prototype fails. It could also be prototypes for communication or geometric reasoning, as aid for mental processes. For many such applications, FDM is already a viable tool, and the challenge would rather be to integrate it into the development process, as this could require training, cultural change and process change according to Smith [9].

2.4. Motivational case from development project – Tightening knobs for flood barricades

In this prototyping case from late-stage development in the project *Systemflomvern-2020,* a prototype of a proposed door-opening flood barricade was to be made. A to-be-injection-molded knob for tightening the sides of the barricade to a wall was manufactured by FDM, where the conceptual layout can be seen in Figure 2-5, with detailed pictures of the parts in Figure 2-6. This was done as a part of a small series prototype deployment for user testing which involved 14 barricades, and hence 56 connections.
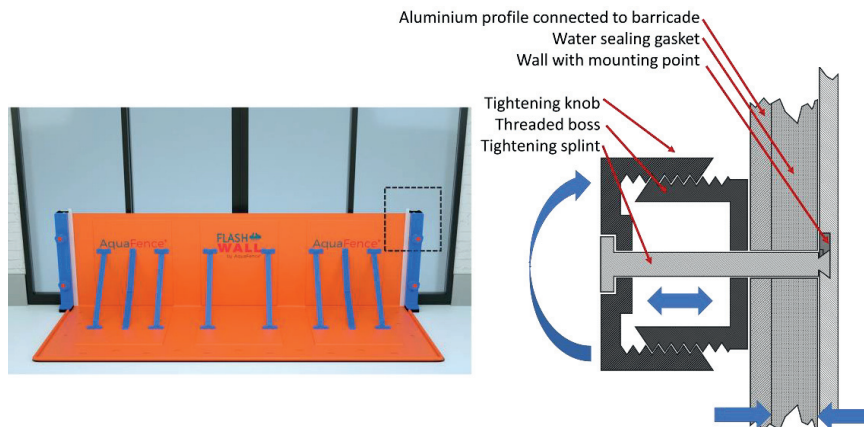
Figure 2-5: Flood barricade, and conceptual layout of wall connection assembly. Turning the knob makes the knob and boss extend while the gasket gets compressed to make a water tight seal.
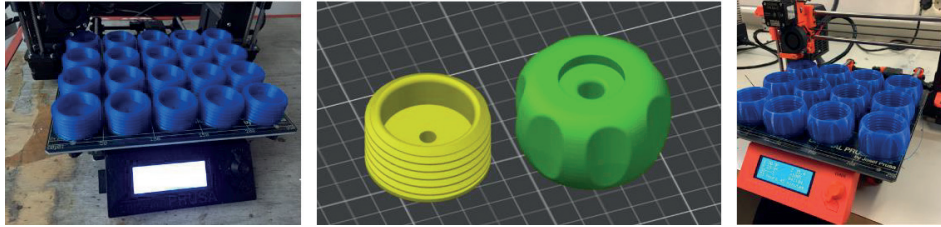
Figure 2-6: Threaded boss and tightening knob respectively.

The first prototype iteration revealed that, even though the inner diameter of the knob and outer diameter of the threaded hub indicated matching thread sections according to ISO-standard tables, they would not engage. This led to making a small set of knobs with altered thread profiles to find the optimal configuration, which took about a day of printing and testing. Thereafter, all prototypes were made and some deployed. This revealed a second flaw, as some knobs started breaking in the root of the countersink, as seen in Figure 2-7. The design was assumed to be strong enough for injection molding, and the failure was attributed to the relatively low structural integrity of FDM parts. It was, therefore, decided to provide spare parts until the injection molded parts could be manufactured. This compromised the development process due to the extra development time, production of various thread alternatives and production of spare parts, which can be considered waste in this context. However, the most problematic aspect was the following uncertainties that were pushed forward in the development process:

- Is the original thread profile from CAD incorrect, or is it the FDM process that is not capable to achieve the correct geometry?
- Would the injection molded part be strong enough? The knob design could easily have been redesigned to reduce the stress in the failed region by improving the design.

The injection molded knobs were luckily found to perform adequately, but the uncertainty did impose a risk to the development project. Therefore, having methods for assessing or minimizing the uncertainties would have helped to reduce the rework risk for this specific development project.
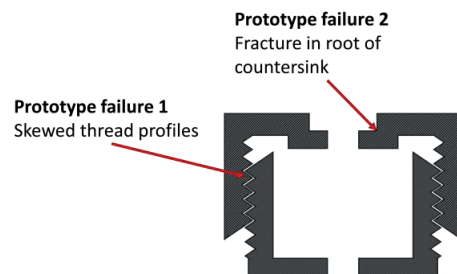
Figure 2-7: The different failed elements of the prototypes.

3. Description of the FDM process

Developed by Scott Crump, founder of Stratasys Inc. in the late 1980's, and patented in 1989 [31], fused deposition modeling is now the most used method of additive manufacturing in the world. After this patent expired, the market has become dominated by *open source* machine designs, or designs built on open source concepts. The development of these open source designs started in 2004 with the *RepRap Project* by Adrian Bowyer at University of Bath [32], with a goal to create a self-replicating machine. After their release of the *Darwin 1.0* design and *RepRap* machine firmware, many others have developed their own versions for both commercial or non-commercial purposes. As open source generally does not prohibit commercial application, open source designs are very common for commercially available printers.

FDM printers work by melting and depositing building material, most often supplied as thermoplastic filament, using a numerically controlled x-y-z coordinate system. This is done in a line-by-line and layer-by-layer fashion, so that what seemingly looks like a block of material consist of many individual strands of material compiled into a geometry. A conventional printer arrangement, can be seen in Figure 3-1, and an extruder arrangement (heating and feeding assembly) in Figure 3-2.
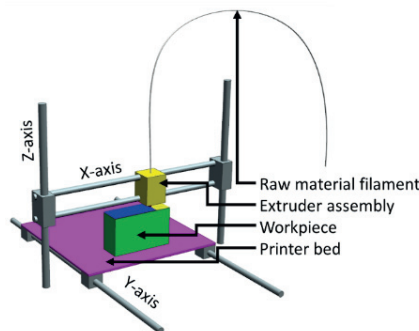
Figure 3-1: X-Y-Z configuration for a Prusa i3 setup, with a gantry controlling, x, y and z-movements, and bed travel controlling y-movement.

The lines of molten material deposited from the heating arrangement are squeezed down into the bed or workpiece, hence getting a compressed shape, as illustrated in Figure 3-3. As these lines are the elementary building blocks of FDM manufactured components, the height and width of their cross section are the major process parameters and will hereby be referred to as to as *layer height* and *line width*. Assuming that these strands of plastic have elliptic cross sections, or rectangular with perfectly circular rounded or parabolic ends, is convenient for analytical models of e.g. surface roughness [33,34]. While this assumption tends to be quite accurate for the exterior, most experimental results from the interior show an asymmetric cross section of the deposited lines [35], typically having a

21

planar bottom and top surface, and with smaller radius on the side facing upwards as illustrated in Figure 3-4.
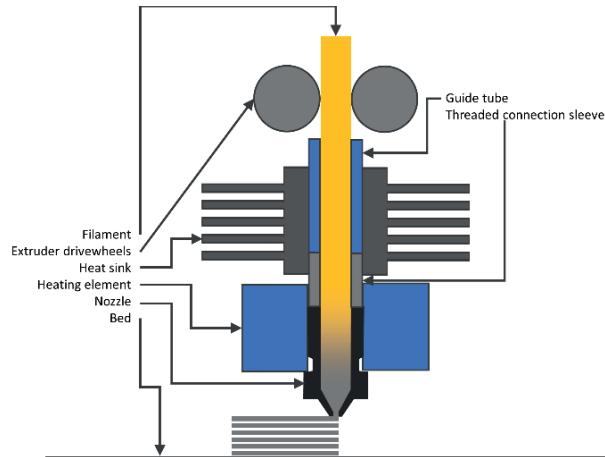
Figure 3-2: General overview of an extruder setup.
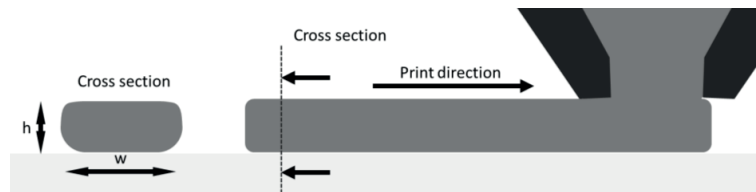
Figure 3-3: Cross section of extruded line of material, with line width, w, *and layer height,* h.
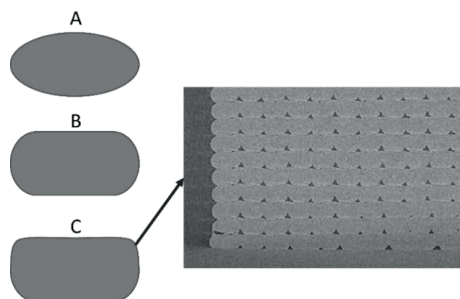
Figure 3-4: A) elliptical and B) rectangular cross sections used for analytical solutions, and C) shape generated by a Prusa i3 MK2.5 desktop printers, analyzed using CT scan.

Commercial desktop FDM printers generally parse machine G-code into mechanical movements, where the G-codes are dictated by a computer-aided manufacturing (CAM)

software. If tailored for FDM, the software is commonly known as a *slicer*. The common workflow for making FDM parts could be described as follows:

1. Design part in CAD;
2. Parse into a STL (stereolithography) file;
3. Convert the geometry into G-code toolpaths by a slicer;
4. Print the geometry using an FDM printer.

Figure 3-5: Images of the different results from each step in the path from design to physical part using FDM: 1) CAD model, 2) STL file visualization, 3) G-code toolpaths, 4) printed geometry. Image from appended Paper 1.

The STL-file is the conventional input to the slicer software and consists of a point cloud connected by planar facets. Any surface in the CAD model that is originally curved would, therefore, end up distorted, as illustrated in Figure 3-6, with a magnitude depending on the sampling resolution.
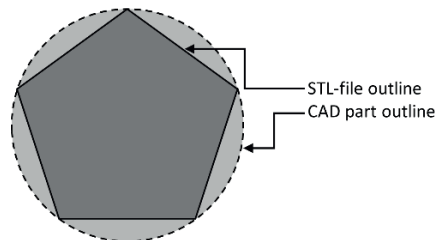
Figure 3-6: Illustration of how STL-file format distorts original geometry.

The slicer samples the STL geometry at different horizontal planes along the vertical axis, and generates toolpaths in the following order:

1. one or more perimeters of the geometry, creating a shell for non-horizontal surfaces;
2. dense horizontal bottom and top surfaces;
3. volumetric infill in the enclosed volume;
4. additional external structures for increased printability;
   - support structures for increasing printability of overhangs;

- brims for improved bed adhesion.

The infill is generally a repeating pattern of a cellular structure geometry as honeycomb, cubic structures or linear raster. Top and bottom surfaces, which usually are near-dense, are filled with linear raster patterns. Normal configurations for these domains are illustrated in Figure 3-7. Double supported overhangs, called bridges, is usually defined as an own domain. As these domains have different boundary conditions and purpose, they should be tuned accordingly, promoting either speed, strength, dimensional accuracy or printability.
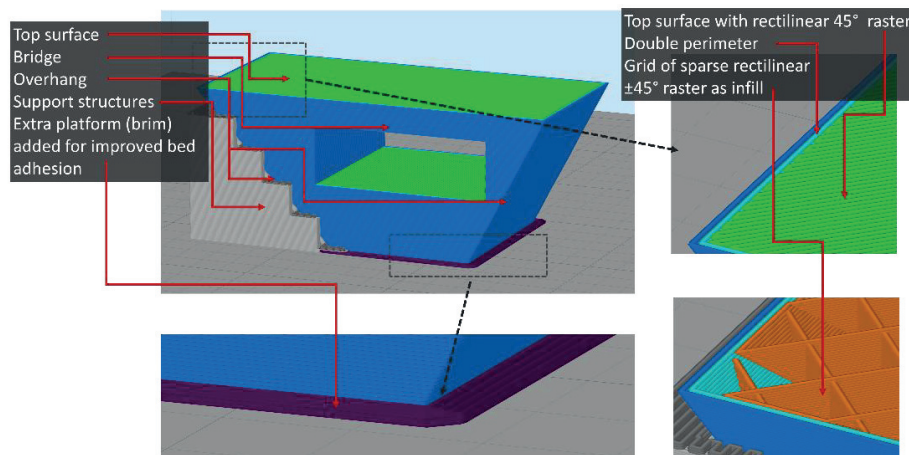
Figure 3-7: Toolpath visualization for part showing the different printing domains.

As shown in this chapter, the overall performance of the FDM process used as a prototyping method is not merely a result of the capability of the machine and material, but also affected by the STL file conversion, slicing procedure and the design of the part, as well as additional assisting structures. Changes done to either element can affect the performance of the other elements. This increasing uncertainty throughout the process from-CAD-to-part is in this thesis named *context dependency*, as illustrated in Figure 3-8. Low context-dependent improvement efforts have less previous elements and are therefore usually more generalizable. Improvement efforts in the areas of high context dependency should on the other hand take into consideration that the results might vary considerably between printer setups, geometries, materials and process parameters. According to the theory of *Design of Experiments* [36]—in addition to including more contextual factors—interactions between the different factors is also very common. The number of interactions will grow exponentially with the number of factors, and rigorous generalization across different materials, printers and process parameters would often become difficult.
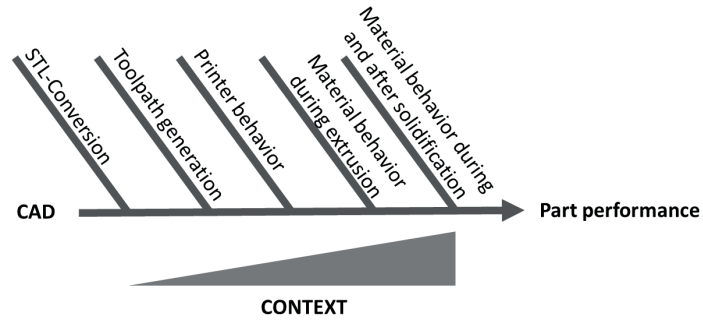
Figure 3-8: Illustration of context dependency for the FDM process. Toolpath generation also includes all parameter definitions in the G-code, as speed/acceleration parameters and flow calibration.

4. Key drivers for dimensional accuracy of FDM

4.1. Relation of dimensional accuracy to prototyping applicability

Excluding the STL file conversion, the dimensional accuracy of FDM fundamentally depends on how accurately one can place lines of molten material, and to which extent one can control its cross section in terms of size and shape. The main aspects can be broken down into the following 5 categories, with examples given in Figure 4-1:

1. layer sampling;
2. printing fundament (the structure of which the molten material is extruded onto);
3. accuracy of machine positioning and travel;
4. accuracy of material extrusion;
5. residual strain (due to thermal expansion/contraction of material).
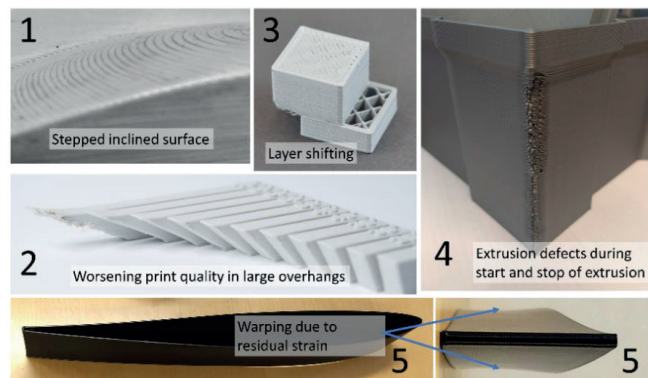
Figure 4-1: Examples of defects due to 1) layer sampling (reproduced from appended Paper1, 2) lack of printing fundament (reproduced from [37]), 3) inaccuracies during positioning (reproduced from [38]), 4) inaccuracies during extrusion, and 5) residual strain.

This thesis' work on dimensional accuracy is aimed at exploring 1) the defects due to layer sampling and 4) accuracy of material extrusion. Both categories were found to be key issues during the prototyping activities encountered. The former is one of the main reasons for the incompatible threads in the motivational example, and was targeted by developing a method that would be equivalent to a *'digital thread gauge',* as seen in Figure 4-2. Details and results from this research are provided in Chapter 6.1., and appended Paper 1.

Figure 4-2: Comparison of ideal and measured (photographed) thread silhouette, from Paper 1 in Part 2 of this thesis.

Inaccuracy of material extrusion was, through our prototyping activities, found to create difficulties for press fits and other applications requiring high dimensional accuracy, as sharp corners were often disfigured as seen in Figure 4-3. The most popular FDM-system firmware, *Marlin* [39]*,* had recently incorporated a method for compensation of such defects, while the theoretical basis for this method was lacking in literature, and actual performance was uncertain. This research is provided in Chapter 6.2. and appended Paper 2.

Figure 4-3: Disfigured corner due to inaccuracy during material extrusion, also called corner blob*.*

As it is not trivial to what extent each category of printing defects affects the dimensional accuracy, nor how they are reduced or solved, this chapter will go through the foundation of each of these aspects and present existing research and practices. At last it will sum up the challenges for dimensional accuracy of the FDM process and explain why material extrusion and layer sampling are key aspects in that regard. Questions posed by these inaccuracies from a *redesign-for-FDM* perspective would, for instance, be:

- What redesign is needed to achieve sufficient accuracy and printability?
- What is the optimal build orientation?
- What are the optimal process parameters?

While from a *calibration-of-results* perspective, the questions would be e.g.:

- Is the result representative for the proposed manufacturing method in terms of dimensional accuracy?
- If not representative, how far apart is the realized performance from desired performance?

4.2. Layer height and sampling

As with other layer-by-layer approaches, the resolution of a part is highly dependent on layer height. Any vertical surface would display a repeated pattern of the lines of material, and inclined surface would result in a stepped profile, and a horizontal or vertical surface would display regular grooves, as illustrated in Figure 4-4.
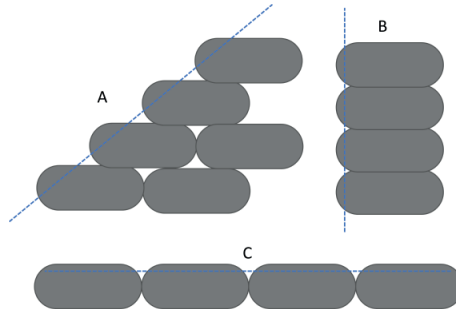
Figure 4-4: Approximate surface profile for A) inclined surfaces, B) vertical surfaces and C) horizontal surfaces.

The roughness of FDM components have been investigated by different sources [33,34,40–43]. Ahn et al. [40] and Pandey et al. [34] have developed analytic solutions for the surface roughness based on elliptic and parabolic cross sections, respectively, which is found to correspond well with experimental results across a wide range of inclinations. The circular-ends assumption, as elaborated on in appended Paper 2, is the most used by slicers to calculate the volumetric flow for a certain line width and height. An important aspect from the slicing procedure is that most slicers only apply mid layer sampling, where the geometry is only sampled in the middle of each discrete slice of the part along the height direction. Using this approach, there is a high risk for any geometry lower in height than the layer height would be lost in the sampling. An example from appended Paper 1, of how the geometry is sampled with different layer heights, is shown in Figure 4-5. Other slicing procedures have been proposed [44], but is not included in common slicing firmware.
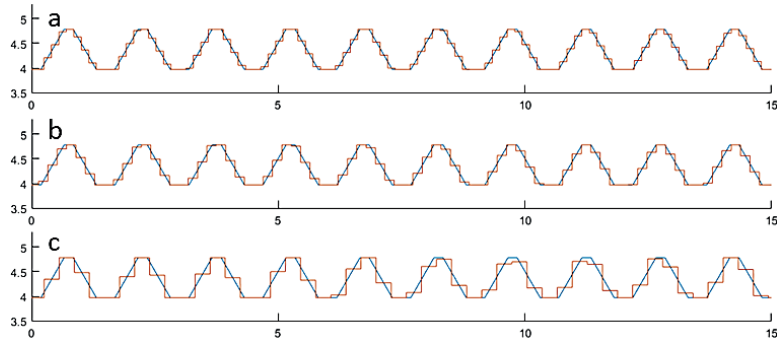
Figure 4-5: Discrete sampling of a M10x1.5 thread profile with layer heights of approximately a) 0.15 mm, b) 0.19 mm and c) 0.30mm. Vertical direction is shown horizontally for convenience. Blue lines show prescribed geometry by CAD, while the red line shows the discrete sampling. Dimensions in mm. Image from appended Paper 1.

The resulting shape of the extruded plastic is a difficult-to-control variable, as it is dependent on the rheological properties combined with the external and internal forces of the melt, after it leaves the nozzle. Due to the mid layer sampling combined with the normal cross section of the extruded filament lines, the resulting outline of an inclined or overhanging geometry fluctuates between being on the inside and on the outside of the prescribed geometry. This must therefore be considered when estimating tolerances for FDM parts with surfaces that are neither vertical or horizontal, since it creates an offset between the part maxima and the prescribed CAD geometry, as seen in Figure 4-6. The magnitude and implications of this offset are not explored prior to this project and is found to be significant for fine-tolerance applications, in appended Paper 1.
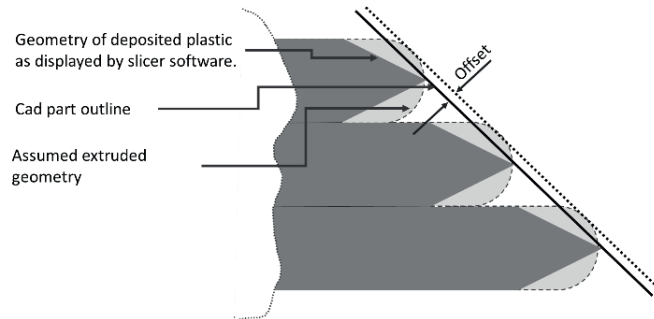
Figure 4-6: Difference between CAD outline, deposited plastic and slicer visualization. Image from Paper 1.

The most obvious way of tackling the challenges posed by the layer-by-layer manufacturing method is by reducing the layer height. As layer height and lead time are inversely related, such a strategy obviously would come at a price of increased lead time. However, these two methods are often introduced to minimize impact on dimensional accuracy:

- reducing layer height only in the areas of fine visual details or slightly inclined surfaces;
- printing outlines, often with fine tolerance requirements, at a lower layer height than infill.

Another method shown by Walter [45] is intra-layer variable layer height. With this method, curved or inclining surfaces could be made without solely adhering to the uniform layer height approach, but rather adjusting the layer height within each layer. This has not yet been implemented in any CAM software and will therefore require post processing of G-codes. However, the results look very promising and will probably be implemented in slicers in the future, which would expand the possible geometries printable with FDM.

Figure 4-7: Intra-layer variable layer height, limiting the stepped surface, and hence improving the surface finish and dimensional accuracy of an airfoil profile, from Walter [45].

What is lacking in knowledge to fully utilize the potential of these variable height approaches, is how the they affect the other aspects influencing dimensional accuracy (interactions). Examples considered in this thesis is the relation between layer height and *advance* parameters (in the appended Paper 2), and deflection of the structure (in next chapter and briefly treated in the appended Paper 1), which affects the requirements for the structure on which printing is done.

4.3. Printing fundament and support structures

A significant difference that might compromise the accuracy of FDM parts compared with other additive technologies, are the forces involved. Whereas other methods require only jetting of small drops of binder, melting and solidifying of powder or curing of UV-reactive resin, FDM requires pressurizing molten plastic to enable extruding it through a small orifice before shaping it into the desired shape. This sets requirements for the geometry one extrudes upon, where the preferred is extruding onto a perfectly flat and infinitely stiff surface, this being the bed or the workpiece. A flexible surface would be pushed down, resulting the line of printed material to be higher and slimmer than prescribed.

A common region where flexible fundaments play a role is when printing overhangs, where the last portion on the edge of the geometry is weak and susceptible to bending. On such overhangs, one is also required to print with only partially having a fundament to deposit the material onto, which creates a difficult-to-control shape as seen in Figure 4-8 [42]. The same would be true for bridge-type configurations, as these are free hanging lines of building material supported on two sides, or horizontal overhangs. Due to the lack of a fundament to squeeze material onto, the free hanging lines of building material will not exhibit the same compressed cross section as those segments extruded against a solid fundament. Such problems can often be avoided by changing the orientation of the part on the print bed and eliminating overhangs and bridges. Xu et al. [46] have investigated methods of analysis for finding impact of printing orientation on the amount of support structure and accuracy. As will be discussed later in the thesis, the printing orientation also affects mechanical properties, which needs to be considered when manufacturing

parts by FDM. The most common alternative approach is building support structures to act as a fundament, as seen in Figure 4-9.
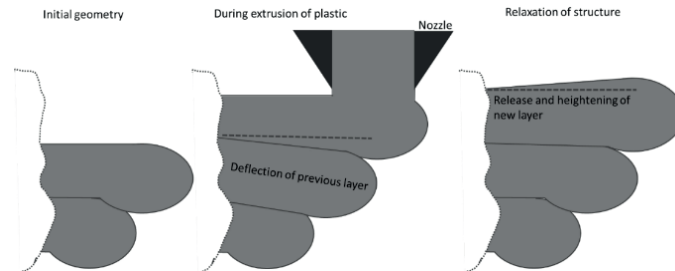
Figure 4-8: Defects due to deflection of edges. Illustration from the appended Paper 3.
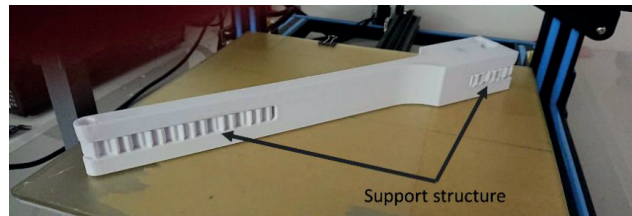
Figure 4-9: Support structure allowing for printing of a split-end rod.

Good design practices for additive manufacturing, in general, aim to eliminate such support structures as it adds time and waste material, as well as often compromises the surface finish of the part [47,48]. However, as one usually prototype designs made for other types of manufacturing, altering the design to optimize for FDM could be non-desirable. Consequently, for prototyping purposes, there is a significant upside in investigating methods for generating and optimizing such structures, as this might help developers get closer to the ideal prototype form and function.

4.4. Accuracy during positioning and travel

The positional resolution of FDM printers is mainly dependent on the hardware and electronics used in the machine setup. Desktop FDM printers mostly use stepper motors with a fixed minimum rotational resolution, which combined with other hardware as pulleys and gears, determine the resolution of the positioning. There are; however, systemic stationary errors that either require fine tuning of the setup, replacement of components, or compensation through firmware. This could be e.g. inaccuracy of belts, pulleys, ball-screws, alignment of axes, bed shape, shape of feed shafts, stepper steps-to-distance conversion, backlash in gears etc.

Within the area of dynamic behavior of digitally-controlled machines, there are numerous methods for stabilizing machine dynamics. Many of these are based on methods applied for general numerically controlled machinery, as CNC mills. A drawback directly related to the workflow for desktop FDM that makes trajectory planning difficult, is the

conversion of geometry into the tessellated STL file format. This implies that all moves within the G-code are linear, and for curved surfaces they are often very short. Conventional CAM software for, e.g., milling or turning use either direct CAD models from the modeling software, or the ISO-standard file format STEP. This allows for extracting curved surfaces using the more accurate *NURBS* (non-uniform rationale b-spline) geometric formulation [49]. In addition to being more accurate, using such curves also eases dynamic stabilization as one applies longer defined line segments for each G-code command, rather than splitting it up into many linear segments. No open source slicer has support for converting step files into NURBS segments. However, the most used printer firmware, *Marlin,* has incorporated functions for following circular arcs and a somewhat constrained subset of NURBS called *b-splines* (basis splines) [50]. An example where trajectory planning is used for FDM without having to define long segments is shown by Duan et al. [51], whose tuning method is capable of improving the printing results for a poorly constructed desktop FDM machine. This method first analyzes the system response to dynamic movements and then finds the system's frequency response function and uses this information for error compensation during printing. Results with and without this tracking control can be seen in Figure 4-10.

47% (1:53 h) time saving using conservative accelerations for both Baseline and FBS					
Acceleration Limit	1 m/s^2	3 m/s^2	5 m/s^2	7 m/s^2	10 m/s^2	30 m/s^2
Printing Time	3:59 h	2:41 h	2:21h	2:12 h	2:06 h	1:50 h
Baseline (No FBS)						N/A
FBS						

> 31% (0:51 h) time saving using aggressive accelerations for both Baseline and FBS
(It is unclear at which acceleration FBS fails)
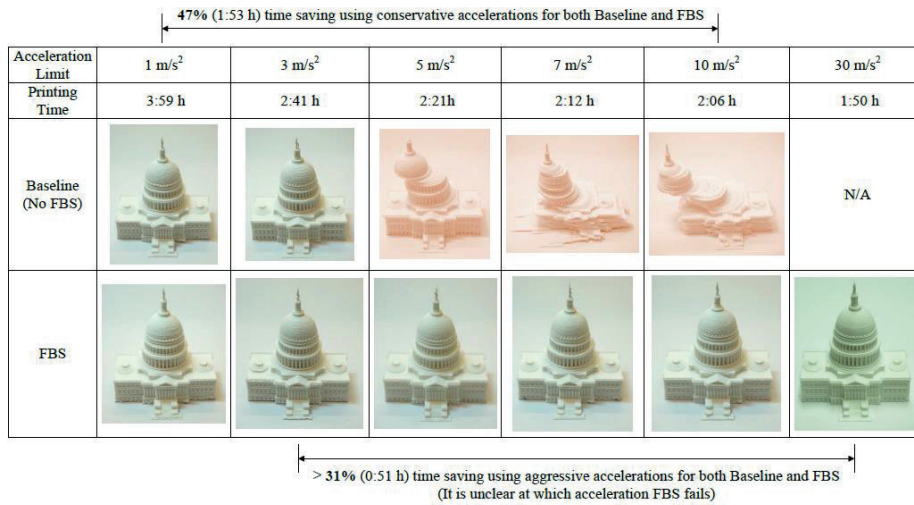
Figure 4-10: Effects of using a dynamic tracking control (filtered B-spline) to compensate for unwanted dynamic effects. Image reproduced from [52].

As desktop FDM machines use stepper motors for positioning, there is normally no positional feedback, and limits the possible tools for improving machine dynamics. Using motors with positional feedback could also have prevented the skewing seen from the baseline sample in Figure 4-10 (displacing the geometry to the left), without incorporating tracking control of any kind.

4.5. Extrusion accuracy

As with layer height being the main driver for vertical resolution, the nozzle diameter is the main parameter constraining in-printing-plane resolution. As it is difficult to constrain the material flow to only partially cover the nozzle orifice, it would be nearly impossible to extrude a line of material that is slimmer than the diameter of the nozzle, and at the same time achieve a decent bonding with the previous layer (it would be possible if the line of material should not bond to the previous layer, as it could be stretched in free air). The minimum linewidth achievable with a circular nozzle, while ensuring bonding with the previous layer, is slightly wider than the diameter of the nozzle, due to a phenomenon of polymer rheology called 'die swelling'. This phenomenon makes the cross section of the extruded material expand after leaving the nozzle [53,54], as seen in Figure 4-11. Therefore, these two aspects limit the minimum wall thicknesses and hence level of detail achievable using FDM.
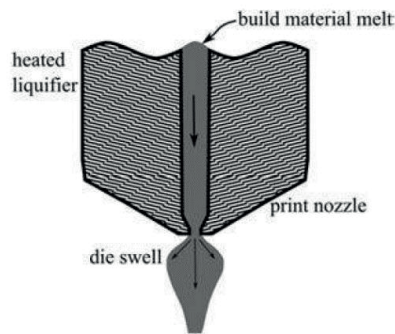
Figure 4-11: Illustration of die swelling. Figure reproduced from Turner et al.[53].

The nozzle diameter also affects how thick layers one can print, since achieving a taller layer height than nozzle diameter plus eventual die swelling is also found difficult. Many manufacturers of FDM printers therefore recommends a layer height of maximum 80% of the nozzle diameter. As layer height and nozzle size are directly related, and the relation between layer height and time is directly proportional to the print time, printing with larger nozzles at the expense of detail is a common strategy for lowering printing time. Some printers therefore have dual extruders with varying nozzle sizes to achieve both accuracy and speed. Printing with larger nozzle and hence larger line widths also increases overall strength for the same print time, as this results in thicker walls and higher relative density. Another constraint imposed by the diameter is how it affects the external corner radii. From an analytical perspective, the theoretical minimum possible radius would be the same as the nozzle radius.
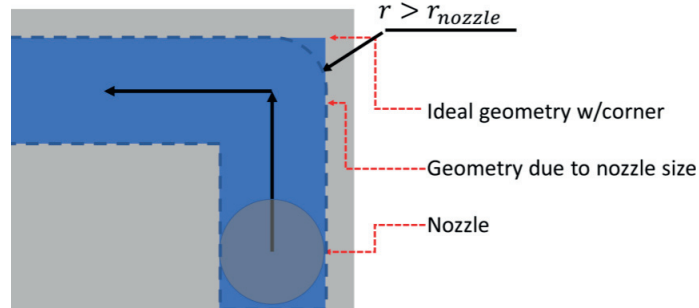
Figure 4-12: Illustration of corner geometry altering due to nozzle diameter.

A less pronounced constraint affecting extrusion resolution, is the chosen components for driving material into the extruder. Most often, this mechanism consists of a stepper motor coupled to a hobbed drive wheel, which grips the filament using a pinch mechanism. The relation between the rotational resolution and resolution of raw material extrusion can be found through (using relations from Bellini and Güçeri [55]):

$$\Delta f = \Delta\theta r g$$

where Δf is the resolution of extruded raw material in terms of raw filament length, $\Delta\theta$ is the angular resolution of the stepper, r is the radius of the drive wheel and g is the gearing ratio in case of a geared connection. Due to slippage and deformation of the raw filament, this is however only approximate. Bellini and Güçeri found a steady state error of approximately 12% less material extruded than requested on a Stratasys printer using ABS [55]. Go et al. [56] show how this slippage increases with speed and being a major limit to the printing speed. Tuning this rotation-to-volume parameter is therefore an important aspect of setting up the printer. Any deviation in roundness of the drive wheel or gear would also introduce extrusion errors. Additional noise could stem from the raw-material filament tolerances or moist content. High water content in the filament would result in gaseous bubbles inside the melt, expanding the filament, which would result in higher material volume in some areas, or material seeping out of the nozzle during travel moves.

Compared with dynamic control of positioning, which is well established within the field of numerical controlled machinery, extrusion dynamics for FDM printing is a less explored field of research. A challenge identified through experimental work is under-extrusion (extruding less material than requested) while accelerating and over-extrusion (extruding more material than requested) when deaccelerating, as seen in Figure 4-13. These effects would be most prominent at corners, and at stop and start positions of extrusion as seen Figure 4-14
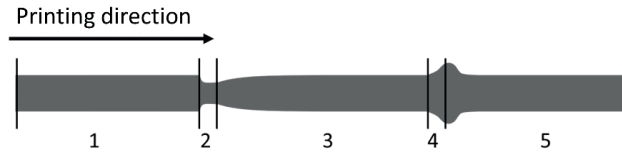
Figure 4-13: Typical printed shape while print acceleration/deacceleration. 1 – uniform extrusion at consistent slow speed, 2 – defects start during acceleration, 3 – returning to uniform extrusion at consistent high speed, 4 – defects start during deacceleration, and 5 – returning to uniform extrusion at slow speed. Reproduced from appended Paper 2.
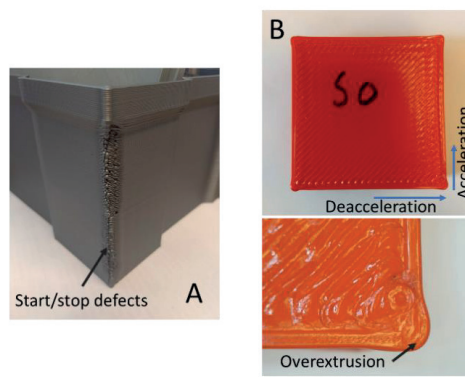
Figure 4-14: Picture of A) defects due to start and stop of extrusion and B) due to acceleration/deacceleration. Parts are printed using a large scale FDM printer from 3DPlatform. Pictures in B) are reproduced from Paper 2.

These defects have been investigated by Bellini et al. [55], seeing it as a heat transfer problem. However, the practitioner's community treats this as a result from deformation of filament or other parts between the nozzle and drive wheel, caused by the forces required to extrude material through the nozzle. Many FDM firmwares attempt to compensate for these effects through the approaches made by Roberts [57] and Kubicek [58]. The latter approach assumes that the deformation is proportional to the volume rate during extrusion, and is often implemented as parameters called *advance*, *linear advance* or *pressure advance*. The theory behind these algorithms is only justified in terms of quite coarse estimates on pressure loss in the nozzle due to friction and acceleration of material. This thesis contribution within this aspect is listed in the appended Paper 2, and is a compilation of historic aspects, theoretical and experimental investigation of such algorithms. An illustration of this algorithms' performance during acceleration and deacceleration of the printer is shown in Figure 4-15.

Low speed	Acceleration	High speed	Deacceleration	Low speed
20 mm/s	1000 mm/s^2	80 mm/s	-1000 mm/s^2	20mm/s
30 mm		40mm		30mm

Figure 4-15: Extrusion width consistency during acceleration deacceleration with and without advance algorithms *for compensation of pressure variations. Data from appended Paper 2.*

4.6. Residual stress due to thermal shrinkage

Residual stresses and strains in fused deposition modeling are mostly known for reducing accuracy by warping the geometry to such an extent that it dismounts from the build plate. In addition, residual stresses could also warp thin shelled, curved parts in the horizontal plane. As such parts have no internal structure to keep dimensional stability, they could easily deform due to thermal shrinkage, as previously illustrated in Figure 4-1.

Residual stresses are present in most methods of manufacturing. Especially additive and welding processes where one deposits high-temperature molten material on a relatively cold, solid material. Both the phase shift from molten to solid form, and the cooling contributes to thermal shrinkage, and any new string of material added will have some degree of tension after cooling. For every new layer added, the she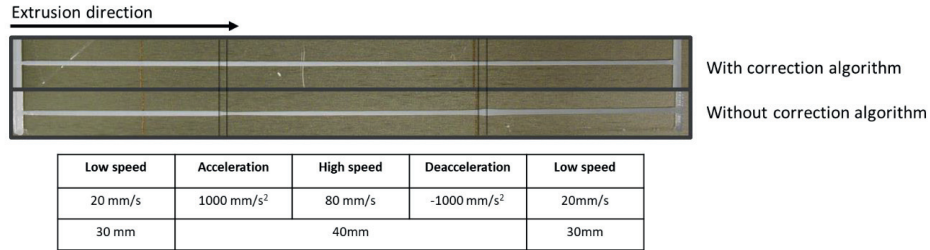ar forces on the previous layers increase, and the resulting gradient of residual stress would seek equilibrium and thereby curve the part. The main problem for dimensional accuracy is therefore not the residual stress itself, but relaxation of residual stress, as this is what alters the geometry.

Residual strains and stresses in FDM components have been investigated and measured by various researchers [59–66]. Davis et al. [63] investigate through-thickness measurements of strain during printing of FDM parts. Furthermore, analytic solutions and numerical simulations on residual strains can be found from Wang et al. and Xia et al. [64,65]. Xinhua et al. [66] investigate warping of thin-plated parts in a physical experiment simulating a fully detached bed.

There are mainly three methods of reducing the deformations caused by residual stress: (1) improving the adhesion to the bed and hence reducing the ability for the structure to relax/curve; (2) reducing the difference between the hot and cold layers employing either a heated build chamber or a heated bed; or (3) predict the deformations based on process parameters and thereby compensate for them. However, (3) is rarely done due to the following:

- o uncertain material structure (will be further discussed in Chapter 5);
- o uncertain temperature-to-stiffness relation;
- o uncertain temperature-to-coefficient of thermal expansion relation;

37

o complex heat transfer problem (one-to-three sources of heat, and dissipation by radiation and convection to air through a domain of varying size and shape).

As a result, improving bed adhesion and reducing thermally induced stresses by increasing the workpiece temperature are the most common methods for coping with the deformations caused by residual stress.

Most printers nowadays include a heated bed, which normally can achieve a temperature of 60-110° Celsius. However, the effect of heated beds diminish with increasing height of the part, as the heat dissipates to the surrounding air. To cope with this, industrial FDM printers from Stratasys Inc. have an additional heated build chamber, achieving temperatures in the range of 70 to 90° Celsius for the whole part. Stratasys Inc. hold a key patent [67] which limits its application on low-cost FDM systems. This patent will expire summer 2019, thereby allowing for industry-wide adoption of this technique.

Improving bed adhesion is a frequently discussed topic, especially among practitioners. Hairspray, painters' tape, glue stick, polyimide (PI) or polyetherimide (PEI) covered print beds all are common methods of improving adhesion. Some research on the topic does exist, such as Spoerk et al. [68], who investigate the effect of bed temperature and effect of using glass or PI on the adhesive forces while printing with PLA and ABS. They find that a high bed temperature plays a key role for both materials, while bed material is only crucial for ABS where PI beds exhibit much better adhesion. From practical experience, printing with a small flange as seen in Figure 3-7, minimize the problems with warping prints for some materials. It must also be noted that for some geometries and materials, the difficulty of removing the print from the bed is a larger challenge than making the workpiece stick to the bed.

4.7. Key challenges of dimensional accuracy for further investigation

The key challenges and current *state of the art* identified and presented in prior research, together with the identified needs within each subject can be summarized as follows:

1. **Layer sampling:** The stepped construction of FDM parts is inherent to the nature of the process, constrained by layer height. Layer sampling is currently implemented as mid-layer sampling only.

   Current state of the art: Recent methods use variable layer heights (both within each layer and between layers) for increased accuracy in key areas.

   Need 1: Implementation of intra-layer varying layer height in CAM software.

   Need 2: Prediction of the related inaccuracies *a priori*, and hence predict the areas in need of lowered layer height.

2. **Printing fundament stiffness and geometry:** Lack of, or insufficient stiffness of substrate to deposit the material onto, is reducing the accuracy of parts.

   Current state of the art: Partially solved by printing support structures. This does however increase the processing time and material consumption, and at the same

time degrade the surface quality. Designing and orientating the parts to minimize overhangs and bridges will also reduce defects.

Need: Prediction of the defects *a priori*, and hence be able to estimate the requirements for support.

3. **Accuracy of machine positioning and travel:** Static and dynamic effects during machine movements compromise the dimensional accuracy. This is constrained by machine positioning resolution and construction, as well as the linear representation of geometry (STL file) used by the slicer software.

Current state of the art: Dynamic effects are partially solved by using techniques from CNC trajectory planning.

Need 3.1: Implementation of trajectory planning techniques in openly available firmware.

Need 3.2: Implementation of STEP file format for geometry representation, developing CAM software and printer firmware handling these formats and create non-straight segments (B-splines or NURBS).

4. **Accuracy of material extrusion:** The resolution of material extrusion is constrained by nozzle radius, die swelling, and machine construction. Dynamic effects create defects during printer movements.

Current state of the art: Pressure advance algorithms are used to partially compensate for dynamic effects.

Need 4: Finding the behavior of these algorithms, and potential interactions with other parameters.

5. **Residual stress:** The fundamental characteristic of the process, melting and solidifying strings of material segment by segment, creates residual stresses, which warp the part geometry.

Current state of the art: Maintaining adhesion between the workpiece and the bed is essential for reducing deformations. This can be enhanced by using various bed materials or coatings. Residual strain can also be reduced by using heated beds and heated build chambers.

Need 5.1: Identification and compensation of deformations *a priori*.

Need 5.2: Improvement bed adhesion for certain materials (very material dependent)

These can again conveniently be split into implementation and research tasks as seen in Table 4-1.

Table 4-1: Implementation and research tasks for improving the prototyping applicability of fused deposition modelling.

Implementation tasks	Research tasks
1.1 – Implementation of intra-layer varying layer height in CAM software	1.2 – Prediction and compensation of dimensional inaccuracies due to layer sampling
3.1 – Implementation of improved trajectory planning in FDM firmware	2 – Prediction and compensation of defects due to insufficient printing fundament
3.2 – Implementation of non-linear geometry in CAM software and FDM firmware	4 – Investigate behavior of pressure advance algorithms and dependency on other process parameters.
	5.1 – Prediction and compensation of deformations due to residual strain
	5.2 – Find methods and techniques to improve bed adhesion

Research Tasks 2 and *5.1* are highly complex problems that would need advances of the knowledge on other areas such as thermal and mechanical properties of FDM structures. Some of these challenges will be targeted in *Chapter 5*, but not enough to predict residual stresses or deflections while printing. The problem in *Research Task 5.2* is common, but most combinations of structures and materials can be printed without large difficulties and is therefore omitted in this thesis. As briefly mentioned, *Research Tasks 1.2.* and *4* were therefore chosen for further investigation in this thesis, provided in Paper 1 and 2.

5. Structural integrity of FDM parts

5.1. The complexity of structural integrity of FDM parts

The integrity of a structure, its ability to carry loads, is dependent on two essential aspects; 1) the geometry of the structure, and 2) the material characteristics. In contrast to dimensional accuracy, which depends heavily on the capability of the manufacturing method's capability to produce external surfaces, structural integrity relies on the capability of also manufacturing internal, load-bearing members. In the case of structural integrity, the term *mesostructure* is essential. Mesostructure is the geometry with a scale between the macroscale (global geometry) and the microscale, as illustrated in Figure 5-1, and for FDM specifically, this would mostly refer to the shape and size of the infill. For conventional FDM printer setups, the *mesoscale* range would both cover the minimum and maximum size of geometries possible to deposit. The layer height would normally be in the range of 0.05 to 0.80mm, while the line width would normally be in the range of 0.2 to 1.0mm. Hence, smaller cross sections than 0.05×0.2mm would rarely be possible to deposit without non-standard modifications to the hardware. On the other hand, larger cross sections than 0.8×1.0mm would not be possible without stacking strings of material, hence introducing voids/porosities into the structure as shown earlier in Figure 3-4.
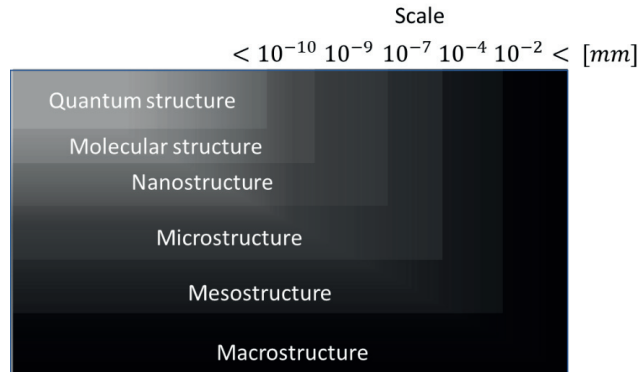
Figure 5-1: Quantum to macro scale structure dimensions. Boundaries vary slightly from source to source.

The behavior of a structure at microscale and lower is often pooled into the broad term *material behavior*, while in the case of including the behavior of the mesoscale structure this would often be rephrased into *cellular material behavior.* The difference between the behavior of the raw material (assessed through tensile testing of filament or injection molded dog-bones) and the cellular material behavior of FDM manufactured parts can be significant, according to Ahn et al. [40]. The large difference between assessing structural integrity of FDM parts compared to 'ideal parts', which are often considered using hand calculations or FEA, is illustrated in Figure 5-2. Uncertainty in mechanical performance

of FDM parts complicates using FDM for applications where strength and stiffness parameters are crucial. This implies that, when testing the performance of prototypes, using material stiffness and strength parameters to assess the difference between the prototype and its' to-be-manufactured counterpart would be difficult.

Figure 5-2: Illustration of the complexity of the structural capacity of FDM parts compared to ideal parts.

Mechanical performance of FDM parts is on high-end of contextual dependency, as illustrated in Figure 5-3. Finding any predictive method to go from process parameters, bulk material constants, and toolpaths, to stiffness and strength is therefore highly difficult. That is why most research on FDM parts strength ends up as very isolated experimental c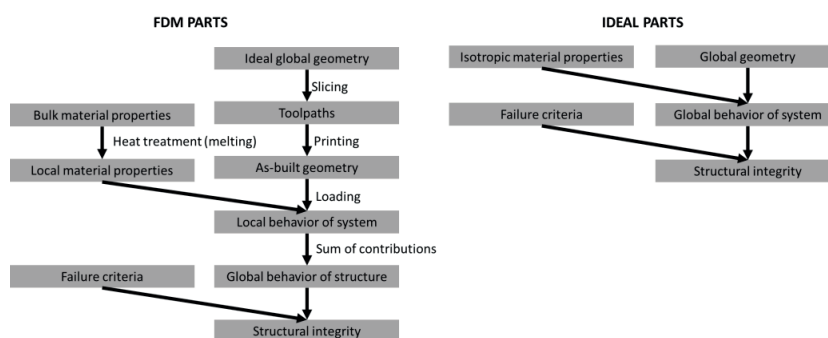ases of mechanical performance-to-process parameter relations, only applicable for one geometry, one printer, one material and a small variation in toolpaths and process parameters. Before many of the crucial FDM patents expired in the late 2000s, finding generalizable knowledge through experimental data was easier. In this era, Stratasys Inc. was the only supplier of machines, using a narrow range of materials, also providing proprietary slicers with a very limited range of infill geometries and process parameters. This limited the degrees of freedom substantially and ensured low variation between different machines and prints. With the wide range of printer manufacturers, slicing procedures, and the poor reliability and repeatability of these printers, such results have now low value in terms of generalization. Modern slicers also have a higher number of control parameters, to allow for tuning and perfecting the prints for each machine and material setup.

A more generalizable approach than to predict strength and stiffness directly from machine input would be to: 1) find the relation between the process parameters and the mesostructured; and 2) try to assess mechanical performance parameters based on mesostructure and material data, as illustrated in Figure 5-3. By using such an approach, one could ultimately quantify to what extent the inferior structural integrity of FDM parts is caused by the mesostructure or other effects.
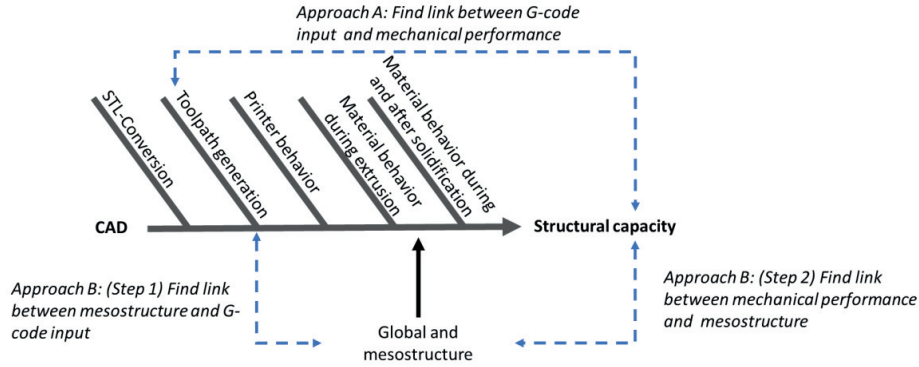
Figure 5-3: The classical approach (Approach A), and the more generalizable approach (Approach B) for research on structural integrity of FDM.

This thesis' research on structural integrity is focused towards such a two-step approach, where the second step is investigated in appended Paper 3, introducing statistical elements to predict failure loads/anisotropy based on the mesostructure as seen in Figure 5-4.
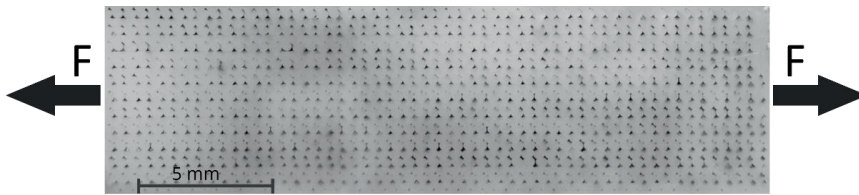
Figure 5-4: Image of the transverse cross section of a dogbone specimen with load direction indication, analyzed for the purpose of prediction of failure loads. Details provided in appended Paper 3.

Appended Paper 4 goes more into detail on the relation between the input parameters and the mesostructure, and contrary to research Paper 3 which use 2D-data, explores 3D-data of the geometry using results from X-ray computed tomography (CT). Through-thickness averages of relative density for a small cubic specimen from this research, is illustrated in Figure 5-5.
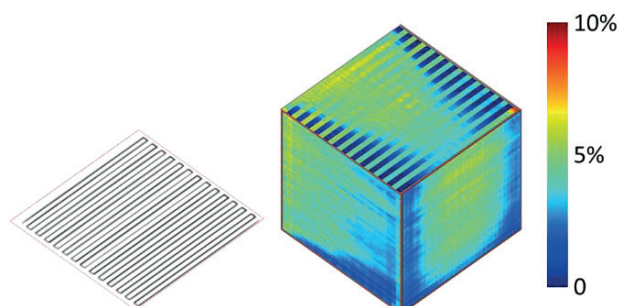
Figure 5-5: Through thickness averages of relative density (each value represents the average throughout the specimen normal to the plane), together with the toolpaths. Toolpaths start in the leftmost corner. Adapted from appended Paper 4.

5.2. Existing research on structural integrity of fused deposition modeling in brief

The mechanical performance of FDM parts has been widely discussed in the FDM literature since the commercialization of the method. Common for this research is that it often tries to achieve as-strong-as-possible, near-dense parts, and often compares this with bulk material properties. This touches upon a crucial element of FDM parts' mechanical performance; the performance of the cellular material made by the process is inferior to the bulk material in terms of strength and stiffness [69–72]. Utilizing FDM to prototype designs supposed to be made by the same material, or calibrated by comparing bulk material stiffness or strength parameters, would therefore give results on the conservative side if high strength and stiffness are desirable. Although a slightly conservative prototype performance is often better than non-conservative; overly underperforming prototype performance could result in non-optimal designs. Therefore, optimizing the process to achieve the highest strength and stiffness possible—and/or finding estimates of how conservative the performance is—would increase the final part's performance by eliminating material waste.

Parts made by FDM are anisotropic in terms of strength and stiffness, and researchers have generally explored this anisotropy as a result of toolpath alignments, infill and build orientations. Coogan and Kazmer have investigated tensile strength of specimens cut out from shell-like structures [69], while most others are investigating as-printed near-dense (relative density higher than 85%) infilled specimens [70–74]. For specimens with some type of infill, the general findings are that the ultimate tensile strength is higher when the printing direction of the infill is in the direction of loading, while there is substantially lower strength for transverse or vertical loading. Another important aspect is that the planes of failure for these different load cases are perpendicular to the direction of loading, running along the boundaries of the fused lines of material [70,71], as illustrated in Figure 5-6. The cross section and material properties along these interfaces are therefore crucial for deciding the overall load-carrying capacity of the specimens. In this thesis' research on structural integrity, the focus has been placed on investigating the

voids that are formed in the intersection between four adjacent lines of material, attempting to assess to what extent the anisotropic behavior can be explained the size of these.
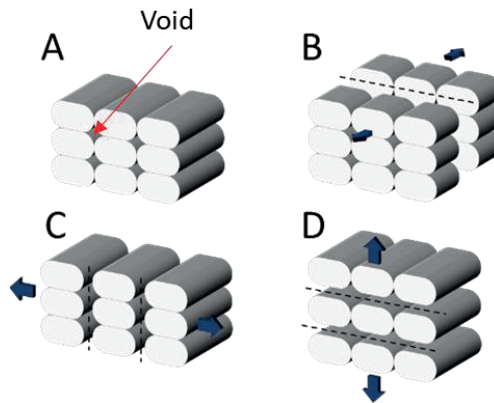
Figure 5-6: A) Virgin linearly printed sample B) Failure pattern for longitudinal loading, C) failure pattern for transverse loading running along the voids in the vertical direction, and D) failure pattern from vertical loading running along the voids in the horizontal direction.

For high relative-density specimens, common cellular configurations of the infill, as e.g. honeycomb, where the infill is printed in multiple directions in each layer is difficult and therefore seldom applied. For such specimens the most used infill configuration is called *linear raster.* In such configurations, the infill within each layer is unidirectional and equally spaced, while the direction can be altered from layer to layer. Drawing the analogy from composite manufacturing, the configuration of infill direction would be synonymous to the term *lay-up,* most often described by stating the raster angle relative to the dominant loading direction. An example could be the configuration *[0, 90, 45, - 45]^n*, which denotes a repeating pattern of longitudinal, transverse and both diagonal directions as illustrated in Figure 5-7. This thesis' contributions on structural integrity, provided in appended Paper 3 and 4, also investigate such high-relative-density and uniaxial infill configurations. This, because it generates the least complex structure, and to be in-line with prior research.

Figure 5-7: 45° (diagonal), 90° (transverse) and 0° (longitudinal) raster patterns.

The similarity of linearly rastered FDM structures to laminated fiber-polymer composites has been explored by multiple researchers, especially for elastic properties and strength assessments. The composite laminate specific Tsai-Wu failure criterion [75] is found capable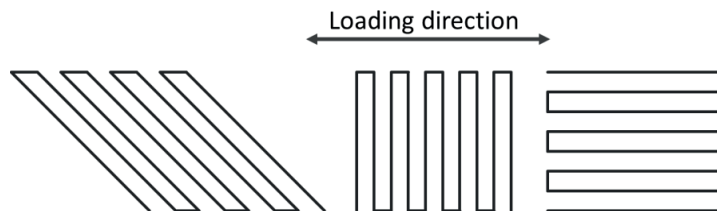 of predicting strength properties of alternating raster FDM structures according to Ahn et al. [76] and Rodriguez et al. [74]. However, these methods are in general based on extrapolation of uniaxial and shear tests of unidirectionally printed specimens into more complex load cases and lay-ups, hence requiring several experimental tests to be performed. These tests, therefore, have a limited value in terms of generalization as they would need to be performed for each printer/material setup.

Casavola et al. [71] and Li et al. [77] have predicted elastic properties in non-unidirectional layups based on unidirectional layer properties, using methods from classical laminate theory. In these methods, unidirectional layer properties can be based on either experimental tests, or analytical models or *representative volume element* (RVE) models [71,72,77], where experimental tests are superior.

The reason why analytical predictive methods of strength and stiffness based on input material and process parameters is not well established for FDM, can be attributed to the following:

- lack of an accurate model of the mesostructure;
- difficult to assess the local mechanical properties of the bond between the adjacent lines of material, due to a complex temperature history;
- lack of knowledge on and control of residual stress (which would need knowledge and control over the two former aspects).

Some work on residual stress is provided in the previous chapter, while no research connects residual stress to mechanical performance for FDM parts.

Li et al. [77] developed an analytical method for assessing the mesostructure of unidirectionally-printed specimens based on analysis of cross section, which resulted in relatively high discrepancies compared to experimental data. Li et al. [78] and Bellehumeur et al. [79] explored using polymer sintering models for assessing the mesostructure. Sun et al. [80] explored the applicability of these models for larger structures, and found them incapable of predicting the bonding area between extruded segments. It is thus concluded that there is a lack of suitable models for assessing the mesostructure, based on toolpaths and other process parameters for relatively dense FDM parts.

Coogan and Kazmer [69] explored the mechanical properties of bonds between adjacent lines in PLA based on microscopy pictures, as shown in Figure 5-8. They found that the area of contact could explain most of the variation in load-carrying capacity of specimens made from different manufacturing conditions. They also conclude that secondary parameters are considerable, though, including interdiffusion of polymer chains, fracture mechanics and non-homogenous material due to manufacturing method.
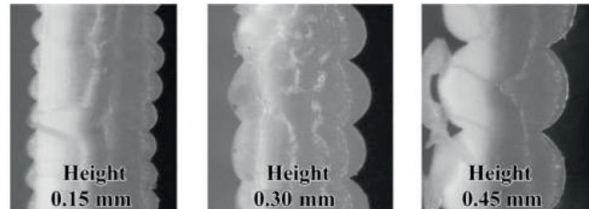
Figure 5-8: Illustration of mesostructure variations due to increased layer height, reproduced from Coogan and Kazmer [69].

What is found lacking in existing experimental research on geometry of FDM parts is statistical or through-thickness aspects. Most assessments of geometry of the mesostructure are based on very few measurements throughout the specimen. Here examples are given as Sun et al. [81] and single measurements in Coogan and Kazmer [69], using microscopy images.

5.3. Key challenges related to structural integrity for further investigation

Modelling of strength and stiffness directly from input parameters is an established field of research, yet mostly based on non-generalizable experimental results, where the dominant methods are Tsai-Wu and Classical Laminate theory. Deterministic and generalizable approaches remain to be established. As stated, this thesis instead focuses on a two-step approach. The first step would be to assess the geometry of the mesostructure based on input parameters, for then to combine this with material data and relate this to structural integrity. Deterministic models for assessing the geometry of the mesostructure of printed specimens do exist, but are as mentioned, found to have poor performance. To elaborate on such an approach without requiring deterministic analytical models for geometry assessment, this thesis investigates the behavior of the structure based on experimental measurements of the geometry, as illustrated in Figure 5-9.
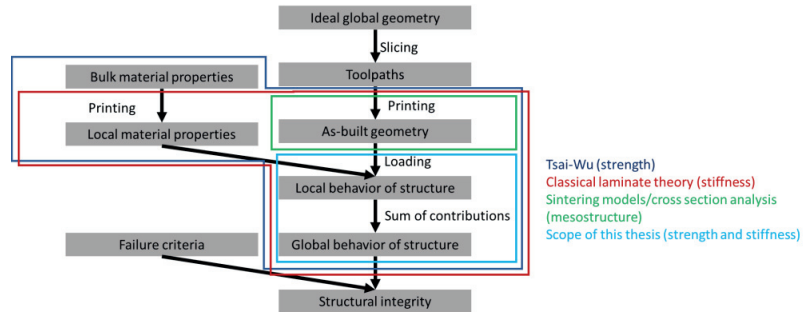
Figure 5-9: Modelling domain of Tsai-Wu [76], classical laminate theory (CLT)[77], geometry assessments as sintering models [78,79] and cross section analysis [77], and the modelling domain of this thesis scope.

As previous work describing structural behavior based on assessments of the geometry seems to lack both a statistical aspect and through-thickness overview of the structure, this thesis will target these specifically. This is done through the following work:

- investigation of the influence of the statistical *weakest link* effect for assessing the anisotropy of tensile specimens and the effect on strength, using data from microscopy (provided in the appended Paper 3);
- assessment the actual through-thickness geometry of the mesostructure using computed tomography, and investigate the elastic properties and strain energy density distributions based on the found geometry (discussed in the appended Paper 4).

6. Article overview

6.1. Paper 1

Tronvoll SA, Elverum CW, Welo T. Dimensional accuracy of threads manufactured by fused deposition modeling.

Status: Published in *Procedia Manufacturing* 2018; 26:763–73. DOI:10.1016/j.promfg.2018.07.088.

Research objective 1: Develop a method for analyzing the dimensional accuracy of threads.

Research objective 2: Investigate the root causes, and process variables contributing to the defects of fused deposition modeled threads.

Brief description: FDM is in some cases capable to generate dimensionally correct, or dimensionally *sufficient* prototypes, but certain design elements have a tendency to degrade the results. Large defects are often seen in geometries featuring small details, large overhangs or inclined planes. Threads, as in machine screws, are common mechanical elements which often suffer from flaws when replicated with FDM. This paper presents a developed method for estimating *dimensional accuracy* of threaded parts. Moreover, it investigates root causes and effects of dimensional flaws on threaded parts, finding that they can be attributed to the layer-by-layer manufacturing method, and the geometry sampling done by the CAM software.

Main results

- Mid layer sampling has a considerable effect on the dimensional accuracy and hence functional performance of FDM manufactured threads. It is identified as the dominant source of errors in the specific case investigated. The influence of mid-layer sampling is illustrated in Figure 6-1.
- Inductively, the findings can be expanded to dimensional accuracy of any overhanging or inclined surfaces manufactured by FDM.
- Reduction of layer height seems to reduce the impact of mid-layer sampling.
- The effect of mid-layer sampling can be reduced by prescribing a thread profile that is narrower than what would be standard, for parts made with low layer height to thread pitch values.
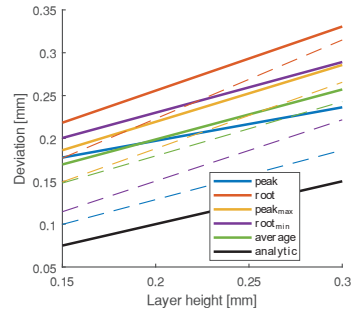
Figure 6-1: Various performance measures regression results of thread accuracy together with the analytical model. Details in Paper 1.

Relation to research questions

In the case considered, research question 1, *"What are the main drivers/factors influencing dimensional inaccuracy of FDM parts?",* can be answered as follows:

> Errors related to mid-layer sampling are significant factors for the dimensional accuracy in FDM manufactured threads, while aspects such as inadequate *printing fundament* due to printing overhanging structures, are secondary factors in the case considered.

Developed methods and tools:

- an analytical model for estimation of offset due to mid-layer sampling;
- a new method for creating a '*digital thread gauge*' based on image processing.

Reflections on contribution

The challenges covered in this paper aid manufacturing of threaded parts using FDM. The analytical model would serve as a baseline estimation of the extra radial clearance needed for such geometries, or conical geometries in general. As mentioned, this would be on the high end of contextual dependency, so there will be differences between setups and thread geometries but as a minimum required offset parameter*,* the analytical model will be adequate. As the method provided is a proof-of-concept prototype, it is not thoroughly explored in terms of accuracy.

Personal contribution to paper:

- development of thread analysis method;
- software coding for automated analysis;
- image taking;
- first author, leading the writing of article drafts and final version together with co-authors.

6.2. Paper 2

Tronvoll SA, Popp S, Elverum CW, Welo T. Investigating pressure advance algorithms for fused deposition modelling: Theory, practice and simulations

Status: Manuscript approved for publication in *Rapid Prototyping Journal*.

Research objective 1: Model and investigate the performance of dynamic pressure compensation methods for FDM, called *advance algorithms*.

Research objective 2: Investigate the process parameter dependency of these algorithms.

Brief description: So-called *pressure advance algorithms* are common methods for avoiding print defects in regions where the nozzle accelerates and deaccelerates upon printing. These defects are commonly known to result in dimensional variations and degradation of visual appearance in corners and start/stop regions. Compensation strategies are thus supposed to improve both the functionality and appearance of FDM parts, and hence the applicability of FDM for prototyping.

This paper gives an overview of the theories of the origin of these defects and the mathematical formulation of the algorithms. Further, it presents experiments where one algorithm is investigated, namely *linear advance v1.0* from the *Marlin* FDM machine firmware. The experiment investigates different calibration parameters for this algorithm, together with different layer heights. The article then presents the same experimental result alongside simulations using the *Simulink* software.

Main results

- Advance algorithms effectively reduce defects due to acceleration/de-acceleration of the printer.
- The mathematical formulation is only valid for uniform layer heights, as tuning parameters vary considerably between different layer heights.
- Severe overcompensation can happen if this algorithm is not tuned correctly.

Relations to research questions

Its relation to research question 1, *"What are the main drivers/factors influencing dimensional inaccuracy of FDM parts?",* can be answered as follows:

> For extrusion accuracy, the main cause of inaccuracies and deviations is the need of building up or release pressure in the nozzle during acceleration/deacceleration. These can effectively be reduced by advance algorithms. However, the effect is significantly dependent on layer height, and possibly other process parameters, which can lead to significant overcompensation.

Developed tools and methods:

- mathematical description of advance algorithms;
- simulation model for assessing the behavior of these algorithms.

Reflections on contribution

This paper's contribution to the body of knowledge is, in addition to the main results and methods, 1) thorough mathematical description; and 2) first investigation of these algorithms in academic literature. The outcomes could therefore be used as a reference for further investigation of algorithms.

The identified layer height dependency is an important aspect for further application, as variable layer-height methods are getting ever more popular. A new method for incorporating this algorithm into FDM-systems is therefore needed.

The proposed simulation method captures the behavior of these algorithms to a certain extent, but as no analytical method exists for relating flow rate to line width for low material flows, the performance of the algorithm in these areas is uncertain. This is also the case for rapid changes in material flow, as the flow pattern in these areas are uncertain.

Personal contribution to paper:

- most mathematical formulation, except from the key relation $v_{in} = K_{LA}\dot{v}_{in}^0 + v_{in}^0$;
- development of a simulation model;
- all experimental work;
- image taking;
- first author leading the writing of the article drafts and final version together with co-authors.

6.3. Paper 3

Tronvoll SA, Welo T, Elverum CW. The effects of voids on structural properties of fused deposition modelled parts: a probabilistic approach.

Status: Published in *International Journal of Advanced Manufacturing Technology* 2018; 97:3607–18. DOI:10.1007/s00170-018-2148-x.

Brief description: When making prototypes using FDM, it is useful to know the difference in structural strength between the prototype and parts made by production-intent tooling and methods. However, the mesostructure of FDM parts is anisotropic and their structural behavior is difficult to assess. The key reasons for the anisotropy are frequently debated in the literature, and significant efforts have been made into optimizing process parameters to improve the structural integrity FDM parts.

Rather than aiming to optimize performance parameters, this paper studies whether it is possible to predict this anisotropy from the mesostructure created by the FDM process. This problem is investigated using tensile testing, and comparing the results with cross sectional data extracted from microscopy pictures of the cellular material structure. The failure model used together with the mesostructure is based on cross-section considerations, and statistically predicting the smallest cross section (weakest link) in an FDM specimen.

Main results

- The findings indicate that by analyzing cellular material structure one is able to predict anisotropy.
- Findings suggests that the size of the voids in the mesostructure of FMD parts is the dominant driver for anisotropy.
- From this it can be argued that the failure load of transversely printed FDM parts should be taken as a weakest link problem, hence following a statistical Weibull distribution.
    - This also implies that the structural capacity of FDM parts is size dependent, making comparisons of results from different sample geometries rather difficult.

Relations to research questions

Its relation research to question 2; *"What are the main drivers/factors influencing structural integrity of FDM parts?",* this paper's contribution can answered as follows:

For structural integrity of near-dense FDM parts, the size of the voids introduced in the mesostructure is a key driver for the difference between the cellular material behavior and the bulk material behavior, especially anisotropic behavior. Other aspects as interdiffusion of polymer chains and fracture mechanics play a secondary role.

Developed tools and methods:

- method for predicting anisotropic failure loads based on the voids in the component's mesostructure.

Reflections on contribution

This article is the first to introduce stochastic perspectives into failure load prediction of FDM parts. The results obtained suggest that the weakest link effect could be considerable due to significant variations in void sizes.

The method of assessment employed does not take into account fracture mechanical effects or interdiffusion of polymer chains, though. The approach was therefore expected to predict a higher failure load than the one showed in the experimental results. However, the prediction turned out to estimate a significantly lower failure load than the one observed in the experiments. This somewhat surprising result is possibly attributed to premature failure of longitudinally-printed specimens, or alternatively, that the method of analyzing the cross-sectional configuration was conservative. Investigating the latter, by assessing the actual 3D-configuration of the mesostructure was therefore the background for Paper 4. The insights revealed from paper 4 questions the method of analysis in Paper 3, as the spatial variation in void sizes is not uniform throughout their length.

Personal contribution to paper:

- mathematical formulation;
- software coding for automatic measuring of voids from microscopy images;
- executing all the experimental work;
- first author writing the article drafts and final version together with co-authors.

6.4.   Paper 4

Tronvoll SA, Vedvik NP, Elverum CW, Welo T. A new method for assessing anisotropy in fused deposition modelling: Analysis of computed tomography data

Status: Manuscript submitted for publication in *International Journal of Advanced Manufacturing Technology (under review as of April 28th, 2019)*

Research objective 1: Establish a method for characterizing through thickness-properties of the cellular structure of FDM parts.

Research objective 2: Develop a multiscale method to assess the structure's response due to mechanical loading.

Brief description: Due to the questions surrounding the method of analyzing the cross section, presented in Paper 3, it was decided to establish a suitable method to assess the volumetric geometric properties of the cellular mesostructure of FDM parts. This was done using computed tomography data of small cubic specimens. However, extracting valuable information from such vast amounts of data requires a suitable method of analysis to be developed. Such a method is presented and demonstrated in this paper. The results from applying the method indicates that the void sizes have a clear spatial dependency. Therefore, it is argued that using data from cut and polished samples, as used in most research in the literature, can be misleading.

The effect of altering the two process parameters *flow rate* and *pressure advance,* on the mesostructure is also investigated. In that regard, the findings show that a relative under-extrusion of 10% compared with what is thought as optimal, significantly alters the void sizes and more than doubles their height and width. Using the advance parameter recommended by the printer manufacturer does not significantly alter the mesostructure.

As a first step towards using this data for stiffness and strength assessments, a multiscale approach based on the geometrical data is created. The proposed multiscale method uses the CT-scan data to generate a linear elastic model, which is used to assess the force-displacement relationship for the global structure, and the energy density distribution throughout the geometry. This was achieved using a 1st order homogenization finite element analysis approach. As with the voids, the energy density distribution has a strong spatial dependency, as well as dependency of the direction of loading.

Main results

- The void sizes in near-dense FDM parts have a large spatial dependency.

- Altering the flow rate has a significant effect on void sizes.
- The voids introduce significant softening of the material, mainly in the transverse and vertical directions compared with the stiffness of the bulk material.
- The strain energy density distribution in near-dense FDM parts have a large spatial and load direction dependency.
  - Most energy dense regions appear near the edges, implying considerable edge effects in the failure mechanisms.
  - Edge effects imply high size dependency of the specimens.
  - Much higher energy densities for FDM samples than for bulk material (10-40% higher for the highest unit-cell averages, dependent on loading).

Developed tools and methods:

- a new method for assessing the geometry of voids in FDM specimens by analysis of FDM data;
- a finite element-based multiscale simulation method, utilizing the identified void geometries to assess the linear elastic properties of the structure.

Relations to research questions

Its relation to research question 2; *"What are the main drivers/factors influencing structural integrity of FDM parts?",* this paper's contribution can be explained followingly:

For structural integrity of near-dense FDM parts, the voids in the mesostructure considerably soften the structure while increasing the strain energy density in the structure. This implies significantly lower failure loads than those for the bulk material. Due to the complex strain energy density distribution, no conclusions on magnitude could be made in this study.

Reflections on contribution

The insights from this paper is believed to have large implications on all prior research on near-dense, unidirectionally rastered structures, which is one of the more conventional test specimen configurations in academic literature. The void sizes decrease throughout each layer, and significantly in vicinity of the turning points of the toolpaths. This spatial dependency has implications on the strain energy density, as seen in Figure 6-2: Factor of increase in strain energy density due to the voids in the structure, for loading in x-direction. Figure 6-2, and hence the failure loads of FDM specimens.
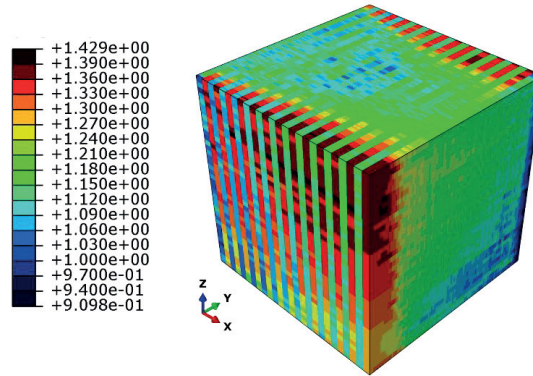
Figure 6-2: Factor of increase in strain energy density due to the voids in the structure, for loading in x-direction. Toolpaths as in Figure 5-5.

As the regions of the higher energy density arise on the specimen boundaries, it implies that any crack formation would most possibly start in this region. This makes the magnitude of failure loads of such FDM specimens affected by edge effects, which implies a significant size dependency. Using cut-out tensile samples, removing the edge regions, could increase generalizability of the results. There is also spatial variation not related to edges, as densification towards the end of each layer, that would still persist.

The analysis method developed is; however, quite time consuming, and presently limited to a somewhat narrow span of geometries. Therefore, the method is less applicable in a real-world prototyping activity.

Personal contribution to paper:

- mathematical formulation of void analysis method;
- coding for automatic measuring of voids from microscopy images;
- all CT-scans;
- development and coding of multiscale simulation method together with the 2nd author, Nils Petter Vedvik;
- first author writing the article drafts and final version together with co-authors.

6.5. Supporting paper

Tronvoll SA, Elverum CW, Welo T. Prototype Experiments: Strategies and Trade-offs.

Status: Published in *Procedia CIRP* 2017; 60:554–9.

DOI:10.1016/j.procir.2017.01.049

Research objective 1: Identification of the different dimensions of a prototype experiment in product development.

Research objective 2: Identification of different modes of development and experimentation.

Brief description: In this conceptual study, efforts have been made to categorize prototype experiments according to what attributes are valued when conducting these; hence, what *trade-offs* are committed. In addition, different modes of experimentation and development to mitigate uncertainty, is also categorized by a compilation of prior art on the topic. Both these trade-offs and modes are exemplified through four practical prototyping cases from an industrial-academic innovation project *Systemflomvern-2020*.

Main results

Six different dimensions of prototype experiments were proposed:

- iteration cost;
- iteration time;
- approximation level;
- user level;
- result presentation;
- experiment flexibility.

Furthermore, four different modes of development were identified, namely:

1. *Point-based design* – Create and test the most promising design (redo if it fails).
2. *Set-based solution array* – Create and test multiple solutions and proceed with those performing above a required performance threshold.
3. *Performance-set investigation* – Scope out the most promising design and investigate performance thoroughly on a conceptual level and converge into more detailed designs only when design choices are needed.
4. *Flexible design* – Design the most promising solution in a way, so that if the design fails, potential changes needed are easier to incorporate (e.g. by modularity or use of flexible platforms).

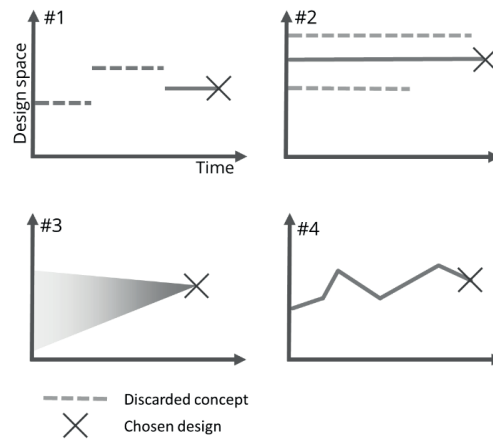These four modes are illustrated in Figure 6-3.

Figure 6-3. Different strategies for development and experimenting illustrated in a design space/time diagram.

Reflections on contributions: In the context of this thesis, the present paper mostly serves as literature to establish a relation between prototyping in general and prototyping by FDM. In a more general scope, the framework proposed enables investigating prototypes and prototype experiments beyond the established categorization methods provided by e.g. Ulrich and Eppinger [17] (analytical – physical, and focused – comprehensive axes) and Schrage [28] (formal – informal, risk-management – opportunity, and internal – external axes). The dimensions found are more closely related to performance measures of a development process, including *cost*, *time*, *total product quality* [82], and are hence easier to analyze in the context of product development performance. The synthesis of different modes of development also clarifies some key aspects around what is known as *set-based concurrent engineering*, and how this particular development strategy relates to other forms of development.

6.6. Other research items

The PhD candidate has also taken part in the two following papers, that are not included in this thesis:

Elverum CW, Welo T, Tronvoll S. Prototyping in New Product Development: Strategy Considerations. Procedia CIRP 2016;50:117–22. doi:10.1016/j.procir.2016.05.010.

Tronvoll SA, Elverum CW, Welo T. Test Environments in Engineering Design: A conceptual study. DS 85-1: Proceedings of NordDesign 2016, Volume 1, Trondheim, Norway, 10th-12th August 2016 2016.

7.   Conclusions, reflections and further work

7.1.   Research findings and contributions

Two research questions were posed as the fundament of this thesis work. This following section will answer these research questions, and in addition provide related contributions.

> **RQ1:** *What are the main drivers/factors influencing dimensional inaccuracy of FDM parts?*

The thesis' compilation of prior art and practices targets the known drivers for dimensional inaccuracy. Together with new and novel insights this have provided a thorough overview of the factors driving dimensional inaccuracy for FDM parts. These drivers can be categorized into 6 pools as illustrated in Figure 7-1.
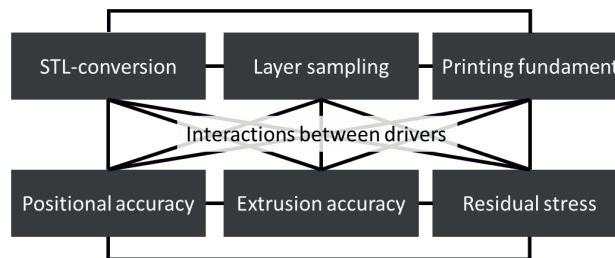

Figure 7-1: Key drivers and interactions for dimensional inaccuracy

Through this work, the effect of two previously unexplored aspects have been investigated and quantified, namely mid-layer sampling and pressure advance algorithms.

The new insights into dimensional accuracy can be listed as follows:
- Mid-layer sampling has a considerable effect on the dimensional accuracy and hence functional performance on FDM manufactured threads.
  - Inductively this can be expanded to dimensional accuracy of all overhanging and inclined surfaces manufactured by FDM.
  - Reduction of layer height reduces the impact of mid-layer sampling, and findings suggests that it is the dominant source of errors.
  - For low layer heights the accuracy could be improved by altering the thread profile.
- Advance algorithms can improve the dimensional accuracy of FDM parts.
  - This is significantly impacted by layer height.
  - Defects from overcompensation could be more severe than original defects.

To answer these questions, the following new methods and tools have been developed:

- method for assessment of dimensional accuracy of threads by analysis of digital images;
- analytical model for deviations introduced by mid-layer sampling;
- simulation models for advance algorithms;
- generalized mathematical framework for applying advance algorithms is formalized.

RQ2: *What are the main drivers/factors influencing structural integrity of FDM parts?*

For the structures investigated in this thesis, the mesostructure of near-dense, linear rastered parts is found to be a key driver for the inferior performance of FDM parts compared with bulk material. This includes both stiffness and strength aspects. As the multiscale approach presented is not yet coupled with failure models, no firm conclusion to magnitude of the mesostructure influence on mechanical strength aspects is given. The increased strain energy density does however suggest that it is significant.

New insights into the structural integrity of FDM parts can be summarized as follows:
- The weakest link effect should be considered when assessing the strength of FDM parts;
  - implies a clear size dependency of FDM parts, making longer parts statistically weaker than shorter ones.
- The geometry of voids in near-dense FDM parts of PLA is highly spatially dependent, with variations in both transverse, longitudinal and vertical directions;
  - implies high size dependency due to effects near turning points of toolpaths and accumulation of material throughout each layer;
  - severely dependent on extrusion multiplier/flow rate;
  - would be dependent on geometry and size of the specimens.
- The parts investigated have a non-uniform strain energy density distribution;
  - dependent on spatial coordinates and direction of loading;
  - variations in the range of 40% from least to highest energy density regions;
  - strain energy density is clearly higher for vertical and transversal loading than for longitudinal loading of same magnitude.

To obtain these new insights, new methods related to the structural integrity of FDM parts have been developed, including:
- a framework for weakest link assessment of transversely rastered parts based on microscopy pictures of mid-section of specimen;
  - This framework is based on uniform through-thickness variation of geometry, which was later found to be incorrect.
- a framework for assessing through-thickness parameters of void geometries from CT-scan data;

60

- a method for using CT-scan data on a multiscale, finite element-based simulation approach for stiffness and energy density distribution.
    - o This utilize the knowledge of the as-built geometry rather than statistical representative elements (as in representative volume elements approaches).

7.2. Reflections on implications for academia

For academia, the major contribution on dimensional accuracy are the new methods and frameworks introduced. The mathematical description of the advance algorithm would especially be an important contribution, as the topic of advance algorithms have become very popular among practitioners, while having lacked attention in the academic sphere. Having a description of the current as-is situation of these algorithms would be the first step towards researching, evolving and improving these methods. This algorithm would also be important for research on many other process parameters, as it would possibly need to be tuned for each temperature, material, layer height and other related parameters. As an example, research on temperature vs. accuracy aspects would be compromised, when failing to implement some form of tuning sequence of the advance parameter. This would also be the case for our early research on dimensional accuracy of threads, as this experiment was not conducted using such an algorithm. The method of analysis of thread accuracy can be further used to investigate the influence of other process parameters on dimensional accuracy.

Considering understanding of structural integrity, the investigation using CT-scan data revealed critical flaws with current research on structural integrity of FDM parts. The performance of near-dense parts is expected to be significantly influenced by:

- specimen geometry;
- specimen size;
- wall effects;
- raster direction (in addition to angle).

The strain energy density throughout such specimens is heavily non-uniform, which must be thoroughly considered when designing experiments for strength and stiffness testing. Different loading direction gives different strain energy density distribution, and results from e.g. anisotropy assessments would hence have an unclear interpretation, and would be very difficult to generalize. The multi-scale method of analysis is proposed to serve as a framework for further exploring these effects.

7.3. Reflections on implications for industry and practitioners

For dimensional accuracy, the advance algorithms dependency on layer height is an important aspect for practitioners, as different tuning parameters for each layer-height used are required. For the popular variable layer height approaches, one should ideally alter the tuning parameters to optimize for each layer height. Currently, this would need to be done manually, but it would be relatively easy to incorporate tabular values of advance parameters into slicing software and correct them automatically. The analytical

model and experimental data of the influence of layer-heights on the dimensional accuracy of threads can be used as a starting point for trying out the extra radial clearance needed to successfully manufacture threads with FDM.

For prototyping application specifically, knowledge presented in this thesis regarding dimensional accuracy will improve the chance of manufacturing FDM prototypes with adequate results the first time, without adding substantial lead time or cost. This could lead to less iterations around *design for FDM* activities for tolerance critical parts; hence reducing prototyping lead time and cost.

The research on structural integrity emphasizes the importance of well-tuned flow rates, as this is important for the configuration of the mesostructure. The increased bonding and stiffness in regions near the turning-points of the toolpath, are particularly important for designing parts subjected to bending, as e.g. snap fits and other spring type components. An anisotropic strain energy density distribution implies significant anisotropic effects, which is in accordance with literature. The key challenges for using the method of analysis on actual industrial parts are that it is quite extensive and developed for one geometry and one type of lay-up (uniaxial). These aspects must be improved upon before it can be used for real-world industrial application.

For prototyping application specifically, knowledge presented in this thesis regarding structural integrity gives some important insights into what to expect from FDM manufactured parts, related to how the mesostructure changes throughout a part, and how that would affect the mechanical performance of some geometries. On the other hand, the generalizability of this knowledge is restricted. The largest contribution of this thesis is, therefore, considered to be the development of the multiscale simulation method. This method has a potential to become the starting point for developing and investigating multiscale simulation methods, which can further be developed to simulate strength and stiffness aspects of generic FDM parts. Such methods would then enable generating links for the structural integrity between FDM prototypes and the potential end product, improving the possible knowledge generated through physically testing FDM prototypes.

7.4. Concluding remarks and further work

The objective of thesis reads:

Objective: *To improve the applicability of fused deposition modeling as a prototyping method by reducing the uncertainty in part performance, by building knowledge and establishing methods for assessing and improving their dimensional accuracy and structural integrity.*

Relating this to the thesis contributions, the work has given key insights and knowledge of assessing the dimensional accuracy and structural integrity of FDM parts, mainly related to the following aspects: 1) layer sampling, 2) extrusion dynamics, 3) mesostructure. In all these three aspects, the contributions are believed novel, providing new information of the performance of the process and the parts. Some of the concepts presented have industrial/practitioner implications and would improve the prototyping

applicability by having established methods for assessing and improving the performance, and thus improving the design for FDM activities.

Knowledge in-brief:

- Dimensional accuracy of threads is related to the layer height. The results obtained herein suggest that this follows the trend of an analytical solution plus a baseline error.
- Optimal advance parameters are dependent on the layer height.
- Structural integrity of near-dense FDM parts have multiple non-material related dependencies due to the mesostructure configuration (part size, part geometry, wall effects, raster direction).

Methods in-brief:

- dimensional accuracy estimation by image analysis and analytical methods;
- methods of assessing the mesostructure of FDM parts;
- multiscale method of analyzing the mechanical behavior of the mesostructure;
- simulation model for extrusion dynamics.

This has expanded the knowledge of the FDM process performance in general and given new tools for further exploring its qualities and drawbacks. Further work on dimensional accuracy should mainly be focused around implementation details. From this thesis work, this could be implementing 1) a layer-height dependent advance algorithm in printer firmware, and 2) thread-identification and offset compensation in slicer software.

There are other techniques in need of implementation that are mentioned in Chapter 4.7 but is not specifically targeted in this thesis, where the most obvious aspect would be implementing non-linear toolpath generation in slicer software. This would also require CAM software to handle non-linear file formats.

Further work on structural integrity related to this thesis should attempt to couple the multiscale approach to failure assessments of FDM parts, or further develop the approach to handle other geometries and layups.

Finally, it is pointed out that the activity and progress of desktop FDM is dominated by the open source community. For anyone researching desktop FDM, a tight collaboration with developers of machines, software or firmware would increase the potential for integration of ideas and concepts into existing systems. It is also important to give recognition to the community that have made low-cost additive manufacturing systems available.

8.   References

[1]   Kennedy BM, Sobek DK, Kennedy MN. Reducing Rework by Applying Set-Based Practices Early in the Systems Engineering Process. Syst Eng 2014;17:278–96.

[2]   Frobes BC. Why do so many men never amount to anything? Am Mag 1921:10–1, 85–9.

[3]   Ullman DG, Dietterich TA. Mechanical design methodology: Implications on future developments of Computer-Aided Design and Knowledge-Based Systems. Eng Comput n.d.;2:21–9.

[4]   Haskins C, Forsberg K, Krueger M, Walden D, Hamelin D. Systems engineering handbook. INCOSE, 2006.

[5]   Roy ER, Kerr C. Decision Engineering Report Series. Cost Eng 2003:45.

[6]   Fabrycky WJ, Blanchard BS. Life-Cycle Cost and Economic Analysis. 1st ed. Englewood Cliffs, N.J: Prentice-Hall; 1991.

[7]   Kockler F, Withers T, Poodiack J, Gierman M. Systems Engineering Management Guide. Defence Systems Management, Coll Fort, Belvoir VA; 1990.

[8]   Thomke S. Enlightened experimentation: The new imperative for innovation. Harv Bus Rev 2001;79:66–75.

[9]   Smith PG. The business of rapid prototyping. Rapid Prototyp J 1999;5:179–86.

[10] Wohlers T, Campbell I, Diegel O, Kowen J. Wohlers Report 2018. Wohlers Associates, Inc; 2018.

[11] Camille Bosqué. What are you printing? Ambivalent emancipation by 3D printing. Rapid Prototyp J 2015;21:572–81.

[12] Kim GD, Oh YT. A benchmark study on rapid prototyping processes and machines: Quantitative comparisons of mechanical properties, accuracy, roughness, speed, and material cost. Proc Inst Mech Eng Part B J Eng Manuf 2008;222:201–15.

[13] Bikas H, Stavropoulos P, Chryssolouris G. Additive manufacturing methods and modelling approaches: a critical review. Int J Adv Manuf Technol 2016;83:389–405.

[14] Shah P, Racasan R, Bills P. Comparison of different additive manufacturing methods using computed tomography. Case Stud Nondestruct Test Eval 2016;6:69–78.

[15] Pham DT, Gault RS. A comparison of rapid prototyping technologies. Int J Mach Tools Manuf 1998;38:1257–87.

[16] Dixon JR, Duffey MR. The Neglect Of Engineering Design. Calif Manag Rev Berkeley 1990;32:9.

[17] Ulrich KT, Eppinger SD. Product design and development. 5th ed. McGraw-Hill; 2012.

[18] Laplante PA, Neill CJ. The Demise of the Waterfall Model Is Imminent. Queue 2004;1:10–15.

[19] Royce WW. Managing the development of large software systems: concepts and techniques. Proc. 9th Int. Conf. Softw. Eng., IEEE Computer Society Press; 1987, p. 328–338.

[20] Sobek DK, Ward AC, Liker JK. Toyota's Principles of Set-Based Concurrent Engineering. Sloan Manage Rev 1999;40:67–83.

[21] Thomke S, Reinertsen D. Agile Product Development: Managing development flexibility in uncertain environment. Calif Manage Rev 1998;41:8–30.

[22] Simon HA. The sciences of the artificial. Cambridge, Mass.: MIT Press; 1969.

[23] Clark KB, Fujimoto T. Lead time in automobile product development explaining the Japanese advantage. J Eng Technol Manag 1989;6:25–58.

[24] Thomke SH. Simulation, learning and R&D performance: Evidence from automotive development. Res Policy 1998;27:55–74.

[25] Tronvoll SA, Elverum CW, Welo T. Test Environments in Engineering Design: A conceptual study. 85-1 Proc Nord 2016 Vol 1, Trondheim; 2016:134-43.

[26] Liker JK, Pereira RM. Virtual and Physical Prototyping Practices: Finding the Right Fidelity Starts With Understanding the Product. IEEE Eng Manag Rev 2018;46:71–85.

[27] Elverum CW, Welo T, Tronvoll S. Prototyping in New Product Development: Strategy Considerations. Procedia CIRP 2016;50:117–22.

[28] Schrage M. The culture (s) of prototyping. Des Manag J Former Ser 1993;4:55–65.

[29] Smith PG. Flexible product development: building agility for changing markets. John Wiley & Sons; 2007.

[30] Thomke S, Fujimoto T. The Effect of "Front-Loading" Problem-Solving on Product Development Performance. J Prod Innov Manag 2000;17:128–42.

[31] Crump SS. Apparatus and method for creating three-dimensional objects. US5121329 A, 1992.

[32] Bradshaw S, Bowyer A, Haufe P. The intellectual property implications of low-cost 3D printing. ScriptEd 2010;7:5.

[33] Ahn DK, Kim HC, Lee SH. Determination of fabrication direction to minimize post-machining in FDM by prediction of non-linear roughness characteristics. J Mech Sci Technol 2005;19:144–55.

[34] Pandey PM, Venkata Reddy N, Dhande SG. Improvement of surface finish by staircase machining in fused deposition modeling. J Mater Process Technol 2003;132:323–31.

[35] Wang J, Xie H, Weng Z, Senthil T, Wu L. A novel approach to improve mechanical properties of parts fabricated by fused deposition modeling. Mater Des 2016;105:152–9.

[36] Montgomery DC. Design and Analysis of Experiments. John Wiley & Sons; 2008.

[37] How to design parts for FDM 3D Printing, 3D Hubs n.d. https://www.3dhubs.com/knowledge-base/how-design-parts-fdm-3d-printing (accessed November 29, 2018).

[38] Print Quality Troubleshooting Guide, Simplify3D Software n.d. www.simplify3d.com/support/print-quality-troubleshooting/ (accessed November 14, 2018).

[39] MarlinFirmware. Marlin Firmware n.d. http://marlinfw.org/ (accessed February 2, 2019).

[40] Ahn D, Kweon J-H, Kwon S, Song J, Lee S. Representation of surface roughness in fused deposition modeling. J Mater Process Technol 2009;209:5593–600.

[41] Anitha R, Arunachalam S, Radhakrishnan P. Critical parameters influencing the quality of prototypes in fused deposition modelling. J Mater Process Technol 2001;118:385–8.

[42] Thrimurthulu K, Pandey PM, Venkata Reddy N. Optimum part deposition orientation in fused deposition modeling. Int J Mach Tools Manuf 2004;44:585–94.

[43] Rahmati S, Vahabli E. Evaluation of analytical modeling for improvement of surface roughness of FDM test part using measurement results. Int J Adv Manuf Technol 2015;79:823–9.

[44] Ma W, But W-C, He P. NURBS-based adaptive slicing for efficient rapid prototyping. Comput-Aided Des 2004;36:1309–25.

[45] By. 3D Printering: Non-Planar Layer FDM. Hackaday 2016. https://hackaday.com/2016/07/27/3d-printering-non-planar-layer-fdm/ (accessed October 26, 2018).

[46] Xu F, Loh H t., Wong Y s. Considerations and selection of optimal orientation for different rapid prototyping systems. Rapid Prototyp J 1999;5:54–60.

[47] Mirzendehdel AM, Suresh K. Support structure constrained topology optimization for additive manufacturing. Comput-Aided Des 2016;81:1–13.

[48] Leary M, Merli L, Torti F, Mazur M, Brandt M. Optimal topology for additive manufacture: A method for enabling additive manufacture of support-free optimal structures. Mater Des 2014;63:678–90.

[49] Gilman CR, Rock SJ. The Use of STEP to Integrate Design and Solid Freeform Fabrication, Solid Freeform Fabrication Symposium 1995: 213-20.

[50] Latheine S. Bézier cubic spline. Marlin Firmware 2018. http://marlinfw.org/docs/gcode/G005.html (accessed November 7, 2018).

[51] Duan M, Yoon D, Okwudire CE. A limited-preview filtered B-spline approach to tracking control – With application to vibration-induced error compensation of a 3D printer. Mechatronics 2017.

[52] How to cut FFF 3D print times in half by the University of Michigan. 3D Print Ind 2017. https://3dprintingindustry.com/news/cut-fff-3d-print-times-half-university-michigan-123158/ (accessed February 2, 2019).

[53] Turner BN, Strong R, Gold SA. A review of melt extrusion additive manufacturing processes: I. Process design and modeling. Rapid Prototyp J 2014;20:192–204.

[54] Miller JC. Swelling behavior in extrusion. Polym Eng Sci 1963;3:134–7.

[55] Bellini A, Güçeri S, Bertoldi M. Liquefier Dynamics in Fused Deposition. J Manuf Sci Eng 2004;126:237.

[56] Go J, Schiffres SN, Stevens AG, Hart AJ. Rate limits of additive manufacturing by fused filament fabrication and guidelines for high-throughput system design. Addit Manuf 2017;16:1–11.

[57] Roberts M. Mattroberts' Firmware n.d. https://reprap.org/wiki/Mattroberts'_Firmware (accessed July 19, 2018).

[58] Kubicek B. Another acceleration-extrusion compensation for repraps n.d. http://bernhardkubicek.soup.io/post/168776124/Another-acceleration-extrusion-compensation-for-repraps (accessed June 7, 2018).

[59] Casavola C, Cazzato A, Moramarco V, Pappalettera G. Preliminary Study on Residual Stress in FDM Parts. Residual Stress Thermomechanics Infrared Imaging Hybrid Tech. Inverse Probl. Vol. 9, Springer, Cham; 2017, p. 91–6.

[60] Casavola C, Cazzato A, Moramarco V, Pappalettera G. Residual stress measurement in Fused Deposition Modelling parts. Polym Test 2017;58:249–55.

[61] Kantaros A, Karalekas D. Fiber Bragg grating based investigation of residual strains in ABS parts fabricated by fused deposition modeling process. Mater Des 2013;50:44–50.

[62] Fitzharris ER, Watanabe N, Rosen DW, Shofner ML. Effects of material properties on warpage in fused deposition modeling parts. Int J Adv Manuf Technol 2018;95:2059–70.

[63] Davis M, Middendorf J, Garg N, Ohanian OJ. Additively Manufactured Components With Embedded Instrumentation. Vol. 2 Adv. Manuf., Phoenix, Arizona, USA: ASME; 2016.

[64] Wang T-M, Xi J-T, Jin Y. A model research for prototype warp deformation in the FDM process. Int J Adv Manuf Technol 2007;33:1087–96.

[65] Xia H, Lu J, Dabiri S, Tryggvason G. Fully resolved numerical simulations of fused deposition modeling. Part I: fluid flow. Rapid Prototyp J 2018;24:463–76.

[66] Xinhua L, Shengpeng L, Zhou L, Xianhua Z, Xiaohu C, Zhongbin W. An investigation on distortion of PLA thin-plate part in the FDM process. Int J Adv Manuf Technol 2015;79:1117–26.

[67] Swanson WJ, Turley PW, Leavitt PJ, Karwoski PJ, LaBossiere JE, Skubic RL. High temperature modeling apparatus. US6722872B1, 2004.

[68] Spoerk M, Gonzalez-Gutierrez J, Sapkota J, Schuschnigg S, Holzer C. Effect of the printing bed temperature on the adhesion of parts produced by fused filament fabrication. Plast Rubber Compos 2018;47:17–24.

[69] Coogan TJ, Kazmer DO. Bond and part strength in fused deposition modeling. Rapid Prototyp J 2017;23:414–22.

[70] Ahn S, Montero M, Odell D, Roundy S, Wright PK. Anisotropic material properties of fused deposition modeling ABS. Rapid Prototyp J 2002;8:248–57.

[71] Casavola C, Cazzato A, Moramarco V, Pappalettere C. Orthotropic mechanical properties of fused deposition modelling parts described by classical laminate theory. Mater Des 2016;90:453–8.

[72] Rodríguez JF, Thomas JP, Renaud JE. Mechanical behavior of acrylonitrile butadiene styrene (ABS) fused deposition materials. Experimental investigation. Rapid Prototyp J 2001;7:148–58.

[73] Montero M, Roundy S, Odell D, Ahn S-H, Wright PK. Material characterization of fused deposition modeling (FDM) ABS by designed experiments. Soc Manuf Eng 2001;10:1-24.

[74] Rodríguez JF, Thomas JP, Renaud JE. Mechanical behavior of acrylonitrile butadiene styrene fused deposition materials modeling. Rapid Prototyp J 2003;9:219–30.

[75] Tsai SW, Wu EM. A General Theory of Strength for Anisotropic Materials. J Compos Mater 1971;5:58–80.

[76] Sung Hoon Ahn, Changil Baek, Sunyoung Lee, In Shup Ahn. Anisotropic Tensile Failure Model of Rapid Prototyping Parts - Fused Deposition Modeling (FDM). Int J Mod Phys B Condens Matter Phys Stat Phys Appl Phys 2003;17:1510-16.

[77] Li L, Sun Q, Bellehumeur C, Gu P. Composite Modeling and Analysis for Fabrication of FDM Prototypes with Locally Controlled Properties. J Manuf Process 2002;4:129–41.

[78] Li L, Sun Q, Bellehumeur C, Gu P. Investigation of Bond Formation in FDM Process. Solid Freeform Fabrication Symposium 2007:400-7.

[79] Bellehumeur C, Li L, Sun Q, Gu P. Modeling of Bond Formation Between Polymer Filaments in the Fused Deposition Modeling Process. J Manuf Process 2004;6:170–8.

[80] Sun Q, Rizvi GM, Bellehumeur CT, Gu P. Experimental Study of the Cooling Characteristics of Polymer Filaments in FDM and Impact on the Mesostructures and Properties of Prototypes n.d.:11.

[81] Q. Sun, G.M. Rizvi, C.T. Bellehumeur, P. Gu. Effect of processing conditions on the bonding quality of FDM polymer filaments. Rapid Prototyp J 2008;14:72–80.

[82] Clark KB, Fujimoto T. Product Development Performance: Strategy, Organization, and Management in the World Auto Industry. Harvard Business Press; 1991.

Part 2: The appended papers
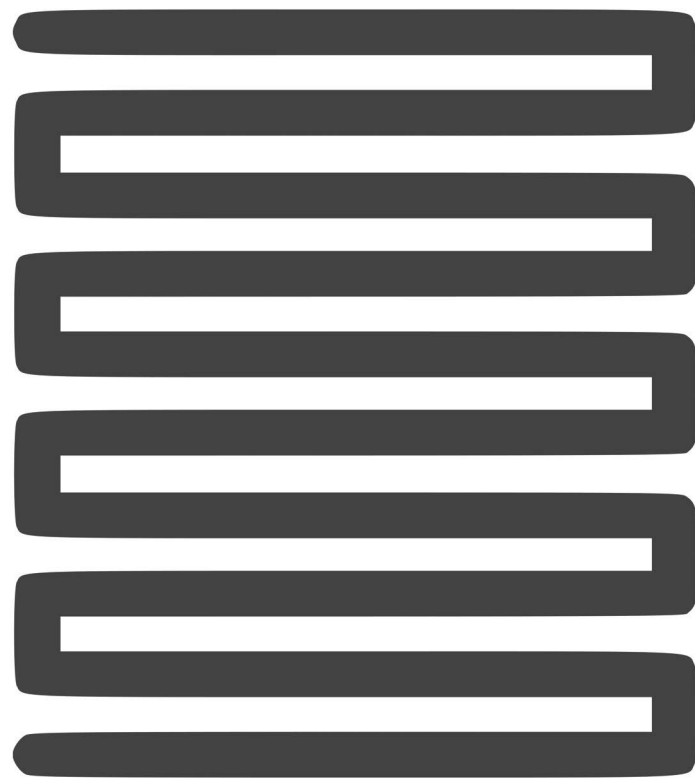
46th SME North American Manufacturing Research Conference, NAMRC 46, Texas, USA

Dimensional accuracy of threads manufactured by fused deposition modeling

Sigmund A. Tronvoll*, Christer W. Elverum, Torgeir Welo

NTNU – Norwegian University of Science and Technology, Department of Mechanical and Industrial Engineering.
Richard Birkelands vei 2B, 7491 Trondheim, Norway.

* Corresponding author. Tel.: +47-905-20-107 .
  E-mail address: sigmund.tronvoll@ntnu.no

Abstract

For parts manufactured by fused deposition modeling (FDM), helical threads drawn in accordance with normal standards (e.g. ISO 68-1), tend to end up deformed when manufactured. These dimensional imperfections typically include violation of radial tolerances and often distorted thread profile. Therefore, making successful threaded connections using FDM would often require looser tolerances than standard ones, unless the nominal threaded sections are in the very loose end of their tolerance band. As a proof-of-concept, this paper aims to characterize such dimensional inaccuracies through image analysis. It also investigates the implications of the defects and partially compensate for the defects by using a strategy of narrowing the thread profiles. In addition, an analytical model for defects on printed inclined planes is presented and verified experimentally by manufacturing three M10x1.5 screws using layer heights corresponding to approximately 10, 8 and 5 layers per pitch. The results show that a lower layer height significantly reduces the defects. However, there is a significant nominal targeting error independent of layer height. On most performance measures, the results show that narrowing the thread profiles with $1/16^{th}$ of the pitch has only an effect on specimens modelled with 10 layers per pitch. The coarser samples did show improvement in some measures, yet leaving others unchanged. In addition to the quantitative results, key points for investigating threads by microscopy is highlighted in this study.

© 2018 The Authors. Published by Elsevier B.V.
Peer-review under responsibility of the scientific committee of the 4th International Conference on System-Integrated Intelligence.

Keywords: additive manufacturing; fused deposition modeling; threads; design for additive manufacturing

1. Introduction

Using *Fused Deposition Modeling* (FDM) for generating small detailed structures and features with large overhangs tends to generate undesirable defects in terms of dimensional inaccuracies. Helical threads are commonly used for assembling components that includes both small features and large overhangs, with details in the sub-millimeter scale and overhangs of 60 degrees. By experience, attempting to achieve a

clearance fit for threads manufactured by FDM, violation of radial tolerances for major (screw) or minor (nut) diameters is often required. The defects are usually so large that they are visible to the naked eye, and this does not only include the discrete layer stepping inherent by the process, but also a certain saw toothed (asymmetrical) thread profile, as seen in Fig. 1.
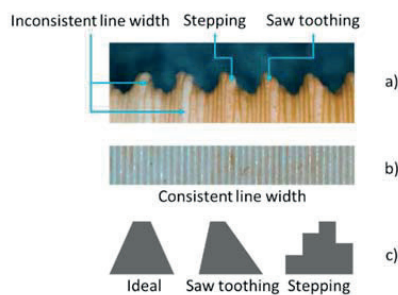

Fig. 1. Illustration of a) common defects on a thread printed with the FDM process (z-print direction from right to left), b) reference line width for a non-overhanging structure, and c) conceptual illustration of ideal profile, "saw-toothed" profile, and stepped profile. Dye penetrant used for contrast enhancing.

It is common to use the term *free form fabrication* to describe additive manufacturing. Although some additive manufacturing technologies might be the best free form tools currently available, there are also many limitations. As with most manufacturing processes, results suffer with increasing geometric complexity, as in the case of manufacturing threads. For such a fine detailed and overhanging structure, the dimensional quality of a 3D-printed component would easily be outperformed by conventional methods as rolling or cutting. However, due to the ease of 3D-printing, many threaded components are made by FDM, even if the dimensional quality is in some cases subpar.

Some researchers argue that additive manufacturing opens the possibility of creating highly optimized structures, e.g. by using topology optimization. However, an increase in the complexity would often increase uncertainty regarding both dimensional accuracy and structural integrity, ultimately resulting in a marginally optimized structure with uncertain dimensions and uncertain metamaterial performance. For utilizing the full potential of the geometrical flexibility of additive manufacturing, control and prediction of the metamaterial and structural defects

would be crucial for successful application on complex geometries and critical components.

As *computer aided manufacturing* (CAM) software for fused deposition modeling (*slicers*) are getting more and more capable of identifying the different troublesome elements of the design, they would eventually be capable of partially compensating for the nominal defects normally seen on geometries, such as overhangs or small details.

As a starting point to investigate how this compensation should be implemented, we are in this paper proposing a novel process for measuring the defects on threads by using a single macro image, which is analyzed through brightness thresholding and compared with an ideal profile. Processing the data from this approach enables investigating how dimensional accuracy is affected by the layer height. In addition, an analytical model of layer height dependency is presented and evaluated against the experimental results.

Finally, a concept of narrowing the thread profiles with a fixed offset as a possible compensation method for dimensional imperfections is proposed and investigated. The presented method is an easy-to-implement solution, to compensate for the errors introduced during exterior sampling of the geometry while generating toolpaths.

2. Threads by fused deposition modeling

Investigation of dimensional capability of FDM machines and the influence of geometrical accuracy based on process parameters is currently done by many researchers and practitioners. In fact, printing to tune the printer or printing quality is found to be one of the most common reasons for printing among self-claimed expert users [1]. Multiple benchmarking objects that have been promoted for quantitative research do also exist [2,3]. However, the trend is that the more complex the geometry, the more difficult it is to quantify the defects. Therefore, it is more common to use qualitative benchmark objects (as e.g. the well-known *Benchy* artefact [4]).

Many would argue that the problem of large manufacturing defects is solved easily by changing to a more accurate process, such as *stereolithography* (SLA), *digital light processing* (DLP), or *selective laser sintering* (SLS) [3]. However, most of the industry use FDM. It is believed that price is the main reason for this, but availability, size and simplicity of the process might also play a role. The FDM process is

inexpensive, both in purchase (machine and software) and usage (materials) compared to other processes [5]. Some manufacturers have however started making SLA/DLP printers for the consumer segment (e.g., currently the DLP printer *Wanhao Duplicator 7* is sold for 500$). It is reported that a large share of the consumer to prosumer grade 3D printer (mainly FDM) market is driven by industrial companies buying these instead of industrial grade printers [5].

2.1. Printing process, errors and characteristics

The path from design to a printed physical part consists of three main steps: *computer aided design* (CAD), slicing, and printing as seen in Fig. 2. To make a digital input, the design would need to be modelled in a CAD model, which in turn must be exported into a *stereolithography* file (referred to as STL), which is the normal format for input to the slicers. In short, this is a linearization of the possible curvatures of a CAD part, where the position of the geometry is sampled at points along the edges of the part and connected with plane triangular facets.
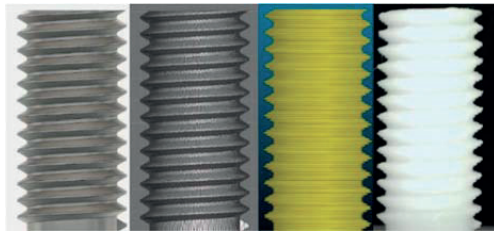
Fig. 2. The CAD model, the facets in the STL file, the toolpaths from the slicer, and the printed part respectively.

Poor sampling or distribution of these discrete points could give tolerance violations, as seen in Fig. 3. However, with decent resolution and an appropriate algorithm, this step should not give significant errors.
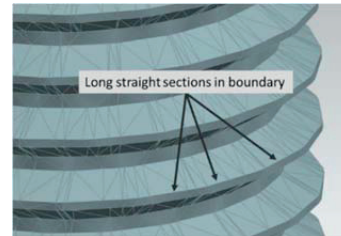

Fig. 3. Linearization of geometry from a CAD drawing to a STL file could lead to straight sections in the boundary.

The next step, the slicing, also introduces discretization errors. In the software, the plane facets are sampled at intervals along the height, which dictates the outlines of the final printed part. The coordinates of the printer nozzle travel, and the material extrusion rate are then calculated with the objective that the outer edges of the extruded material would follow these outlines, encircling a domain. Then, the encircled domain would be filled with some type of infill geometry. These instructions are then transferred to the printer through some type of *gcode* standard. As the *x-y* coordinates are decided by the extruder nozzle motions, the resolution of the actuators governing these movements would dictate their linear resolution. The theoretical resolution for the nozzle motions based on a normal consumer grade setup (200 steps per revolution stepper motors, 16 step micro stepping, and a 9.5 diameter belt drive gear) is approximately 10 µm. However, machine dynamics due to acceleration/retardation, slack in drivetrain and less-than-perfect alignment in the setup would increase the inaccuracy. The extrusion of material is an even more complex task as it would depend on the behaviour of a non-Newtonian flow at temperatures just above the melting temperature. This may be the reason why extrusion related control parameters, as flow rate, line width, retraction, coasting, nozzle temperature, bed temperature and cooling are often debated. However, in-plane travel and extrusion combined are found to result in an resolution of ±0.1 mm for most purposes [6].

As the sampling of the geometry is identical to the STL facets in the *x-y* direction, while discretely in the *z* direction (layer-by-layer), as seen in Fig. 4, inclined geometries are expected to have lower accuracy than in-plane geometries [6].

Fig. 4. Layering effect of a printed inclined plane.

Commonly used slicer software (*Slic3r, Cura, Simplify3D, and KISSLICER*) samples the geometry outline in mid-layer position and attempts to match this outline with the nozzle tool paths and the prescribed plastic line width. As the outline maxima are result of the material flow and solidification during extrusion of plastic—and not shaped according to the STL geometry—the maxima of an inclined printed surface would have an offset compared to the CAD-part, as seen in Fig. 5.
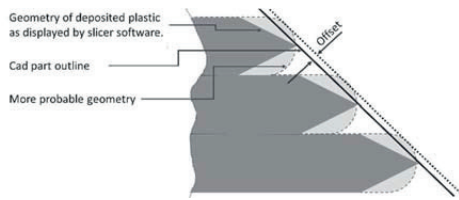
Fig. 5. Silhouette of offset between an inclined ideal and printed geometry due to mid-layer sampling.

Earlier research assumes everything from elliptical to circular or sharp ends of the cross section of the filament lines [2,7–9]. Based on experience with the machine used in our experiment (Creality 3D CR-10), the cross section tends to have near circular ends. Assuming perfect positioning in the mid layer position (see Fig. 6), the offsets have the following analytical solution:

$$O_p = h \cdot \frac{1 - \sin(\alpha)}{2} \tag{1}$$

$$O_h = \frac{O_p}{\cos(\frac{\pi}{4} - \alpha)} \tag{2}$$

$$O_v = \frac{O_p}{\cos(\alpha)} \tag{3}$$

with values as calculated in Table 1.
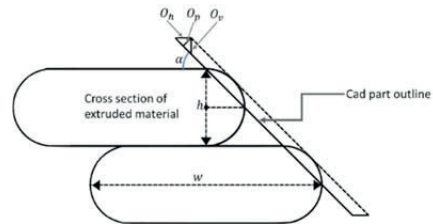
Fig. 6. Cross section of filament lines alongside offset between CAD and printed part.

Table 1. Ideal to printed geometry offset, in fractions of layer height for different inclinations.

Inclination [°]	O_p [h]	O_h [h]	O_v [h]
60	0.067	0.077	0.134
55	0.090	0.110	0.158
50	0.117	0.153	0.182
45	0.146	0.207	0.207
40	0.179	0.278	0.233
35	0.213	0.372	0.260
30	0.250	0.500	0.289
25	0.289	0.683	0.319

This layering effect and the resulting off-sets are somewhat predictable for inclined planes, where the plastic material is extruded onto a solid base. For overhangs, however, the effect is more unpredictable as plastic is extruded partially on a solid base and partially into the air, as seen in Fig. 7.

Printing of overhanging structures generates more and larger errors than non-overhanging structures [10,11], and an example of the difference in performance is displayed in Fig. 8. Some researchers mention 45° as a threshold [12], claiming that printing larger angle this will imply that less than 50% of the filament will be extruded onto a solid base. However, this is only true for layer heights of exactly half the dimension of the extrusion width (e.g., *h*=0.2, *w*=0.4), which is commonly used but not necessarily the case.
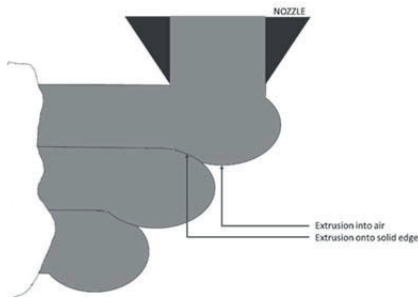
Fig. 7. Printing of overhanging edges.

One could go into the fallacy of assuming that these errors come from merely the extrusion into free air, but the reality is somewhat more complex. If this is the fact, the errors would increase with a decrease in nozzle-to-previous layer-overlap, and hence increase with layer height. However, as displayed in Fig. 8, there are additional root causes for these defects, as increasing the layer height could improve the results.
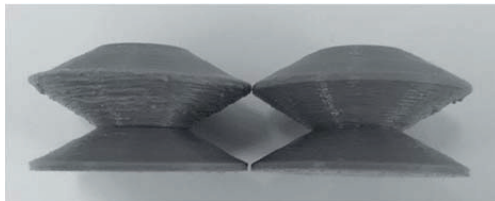

Fig. 8. 30° inclined plane, and 60° overhang printed with 0.15 (left) and 0.3 (right) mm layer height.

This suggests that there are additional sources for these defects, and following effects are proposed:

- Phase shift and thermal shrinkage;
- Nozzle-trailing-melt viscoelasticity (the nozzle motions affects the already extruded material before it solidifies);
- Deflection of structure during printing.

Due to the saw-tooth shaped thread profile distortion, we suspect that the last one (deflections of structure) would be most influential for steep overhanging prints. The effect from this is that the previous layer would deform under the hydraulic pressure from the nozzle, creating an abnormally thick layer in those regions, and then bounces back to its

original state after the nozzle has passed (Fig. 9). This will create an outer perimeter of the geometry that is levelled higher than the firmly supported regions. This heightening would further increase the nozzle pressure in those regions the next time the nozzle passes by, accumulating in size for each new layer that is added to the overhang (see Fig. 8, how the quality worsens the further out in the overhang). Moreover, as pressure increases with decreased layer height [13], this effect would increase.
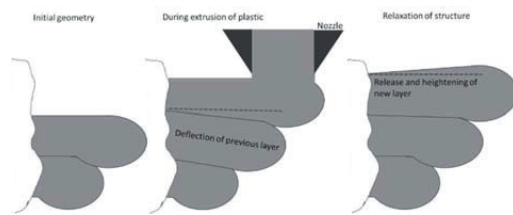

Fig. 9: Deflection and heightening due to hydraulic pressure during extrusion.

2.2. Printing threads

The most used international standard for metric threads, is the ISO 68-1, which dictates the geometry based on the thread pitch (P), and nominal diameter (D) [14]. The basic geometry is seen in Fig. 10.
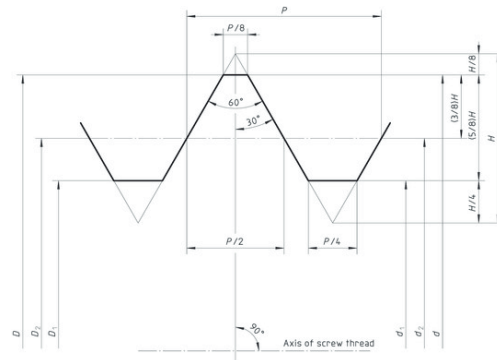

Fig. 10. ISO 68-1 definition of thread geometry. The parameter P and H are related by $H = \sqrt{3} \cdot P \div 2$.

The only way to achieve a satisfying dimensional result, is by printing the threads in a standing configuration, which implies printing inclined planes at 30° and overhangs of 60°. In the case considered

herein, these will be printed using three different layer heights corresponding to 10, 8 and 5 layers per pitch, which results in 0.15, 0.1875 and 0.30 mm layer heights. According to Table 1, this would result in a radial offset of the inclined surfaces of at least $O_r = h/2$, which corresponds to 0.075, 0.09375 and 0.15 mm, respectively.

As a compensation method, this research seeks to test the effect of narrowing the threads with 1/16 of the pitch as seen in Fig. 11. This should reduce the offset with approximately 0.08 mm, estimated using basic trigonometry.
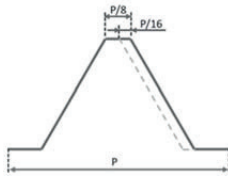
Fig. 11. Proposed method of compensating for the defects by narrowing the thread profile, based on thread pitch P.

When printing a thread with a layer height h, where the pitch, P is a multiple of h, one would get create a periodically identical discretized thread along the height, as seen in Fig. 12. However, as the thread goes through different discretizations as they coil around the center axis, we would like to capture a wider range.
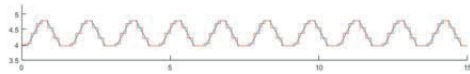

Fig. 12: Cross section of an ideal M10x1.5 thread, discretised with layer height of 0.1875 mm, resulting in a repeating identical discretization. Units in millimetres.

Therefore, these layer heights are altered to go through 10 different discretizations during 10 thread profiles (one layer shift in ten pitches). This altered layer height h_{alt} can be calculated as:

$$h_{alt} = \frac{P \cdot 10}{\frac{P \cdot 10}{h} - 1} \qquad (4)$$

which corresponds to layer heights of 0.1515, 0.18984375 and 0.306 mm, displayed in Fig. 13. As seen, this range of layer heights results in a selection of discretizations ranging from something near an isosceles trapezoid for the 0.15mm layer height

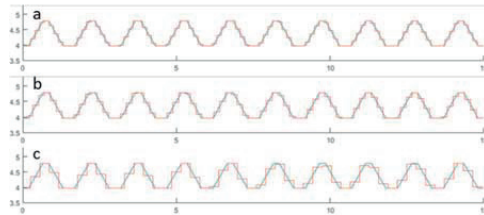specimens, to clearly "stepped towers" for the 0.3 mm layer height specimens.

Fig. 13. Discretization of a M10x1.5 thread with layer heights of a) 0.1515, b) 0.18984375 and c) 0.306 mm, alongside the ideal profiles. This combination of layer height vs. pitch creates an altering thread profile. Units in millimetres.

To be able to capture flat sections in the profile (the thread peaks and bottoms), the layer height must at maximum be equal to the size of these sections. In the case of an ISO-thread, these are 1/8th (peak) and 1/4th (root) of the pitch P, which corresponds to 0.1875 mm and 0.375 for a 1.5 mm pitch. This means that slicing with layer heights above these thresholds will sometimes miss the roots and peaks of these threads; see e.g., at x≈10 mm in Fig. 13 c.

For the set of screws manufactured with narrower-than-standard threads, the flat thread peak section reduces to 1/16 of the pitch, which corresponds to 0.09375 mm. This implies that all printed specimens with this profile will to some degree miss the position of these peaks. Hence, these specimens will in average have a smaller thread height than the ideal profile.

3. Method

The method consists of three different steps:

1. Generate and measure the visible geometry of the printed specimens;
2. Generate the visible geometry of an ideal counterpart;
3. Find their optimal position relatively that possess maximum engagement, and no interference between these geometries.

An overview of the different steps can be seen in Fig. 14. This method does not measure the diameter of the screw, which should be included if the goal is to conduct an absolute error estimation. However, this is

beyond the scope of this article as the focus is placed on the discrepancies between the thread profiles.
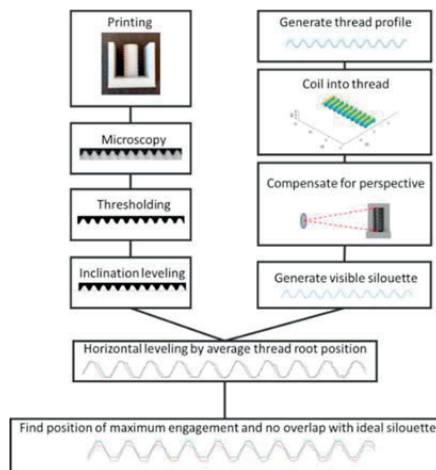

Fig. 14. Method for comparing the physical parts to the geometry of ideal counterparts.

The use of imaging for analyzing threads has been investigated earlier by Gadelmawla [15]—a method that relies on multiple pictures using a *Nikon-10 measurescope*. It uses the imaging and analysis procedure proposed by He et al. [16], which relies on a small pitch-to-diameter factor (as in tube threads), and imaging along the ridge of the thread (requires a pitch-to-diameter dependent angle on the viewing axis of the camera). In addition, the method would not be applicable for viewing more than 2-3 threads at a time, making it difficult to use the results to find a position of maximum engagement for a longer thread.

3.1. Printing, microscope, and thresholding

All specimens were printed with a Creality 3D CR-10 consumer grade printer in the sub 500$ class. The geometry was sliced using the software Simplify 3D. This software allows all specimens to be printed at the same time, ensuring similar process parameters other than layer height. Flashforge Finder white PLA filament in 1.75 mm diameter was used based on experience of achieved satisfying results with this filament.

All threads were photographed using a microscope with 640x480 resolution, using a black background

and a rather large object-to lens distance of 115mm to minimize distortions. In total 4 pictures were taken of each thread, to give some statistical rigor to the thread profile.

Then, the pictures were processed using a brightness threshold, separating the pixels at a brightness of 50 (from a scale from black to white of 0 to 255) using the image analysis software ImageJ. A sensitivity study using threshold levels of 40 to 120 gives no effect on the results.

Then, the picture was imported into the numerics software MATLAB, where the position of the border between the regions was extracted and scaled according to a reference pixel/length ratio (found by using a picture displaying a checkerboard grid with 10 mm boxes). The image also had to be levelled, which was done by running linear regression on the minimum thread root positions, and linearly compensating for the discrepancy.

3.2. Generating the ideal silhouette of a screw thread

First, as the silhouette and thread profile are not identical, the silhouette based on the profile (M10x1.5) and distortions due to viewpoint had to be created. The prescribed ISO thread profile is fundamentally the shape of the cross section of a screw, when cut along a plane running through the center axis. The coiling of the thread would make the silhouette wider than the thread profile, as the section of the thread both behind and in front of the center plane is only partially visible. In addition, the perspective from the microscope lens warps the image, so that sections to the far sides would either run more along the axis of the thread's inclination or with a higher angle, as seen in Fig. 15 and Fig. 16.
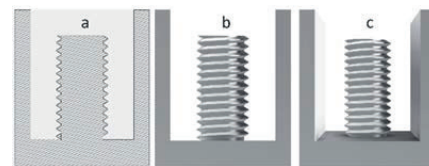

Fig. 15: Drawings of a) thread profile, b) orthographic projection and c) perspective projection.
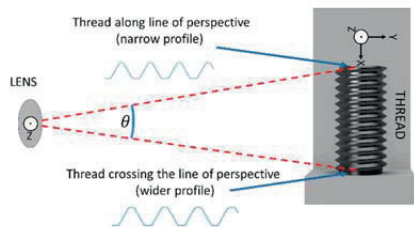
Fig. 16. Lens-object-distance influence the silhouette of the thread due to angle of perspective.

Generation of the ideal thread silhouette was done by initially constructing a general ISO-thread profile repeating 10 times, represented as a vector, and then coiling this into a thread section of $\pm 25°$ degrees with a pitch of 1.5 mm per 360° of revolution (Fig. 17). This surface was then transformed into a cylindrical coordinate system, oriented with z-axis and angle θ as indicated in Fig. 16 (lens position). Then, for each angle in this coordinate system, the maximum z-coordinate was found. This vector of maximum z-coordinates was then transformed back to the original Cartesian system for comparison with the experimental results. As expected, this results in a wider silhouette in the lower part of the thread, compared with the upper, due to the perspective.
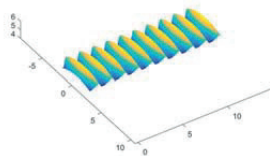

Fig. 17. The thread section used for analysis.

3.3. Comparison and Analysis

Then the position of maximum engagement (the position where the two silhouettes are closest, without overlapping) was found. To achieve this, an algorithm searched through the graph, moving them x-direction maximum $\pm P/2$, to find the position with the minimum largest overlap value between the two graphs, after which this value was subtracted as seen in Fig. 18.
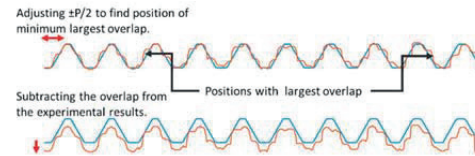

Fig. 18. Procedure for finding the position of maximum engagement.

Different performance measures were then drawn from the data, as seen in Fig. 19, including average radial distance between the thread peak maxima, between the root minima, in the peak and root regions, and between all points over the whole silhouette.
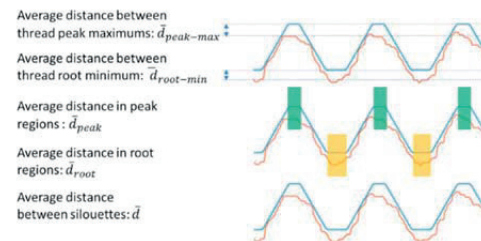

Fig. 19. Performance measures for analysis

The average over root/peak regions were expected to exhibit lower standard deviations, and hence better as performance measures, while the max values are better for relating the measures to real applications as they are possible to measure. The minimum values will be important for further using the method for estimating mechanical performance as they dictate the minimum cross sections.

Assuming normal distribution of the data, these results were then analyzed by three-by-two-way *analysis of variance* (*ANOVA*) to investigate significance of improvement in the results, based on reducing the layer height (three groups) and using the narrow thread profile (two groups). The data were analyzed for violations against the assumption of normality using Shapiro-Wilks, which does not reject the assumption (using confidence level $p = 0.05$), but the test is less certain due to the low number of samples for each group (four pictures for each thread).

4. Results and discussion

All distributions are shown in Fig. 20 to Fig. 24. 4 pictures from different locations on each screw were used for analysis.
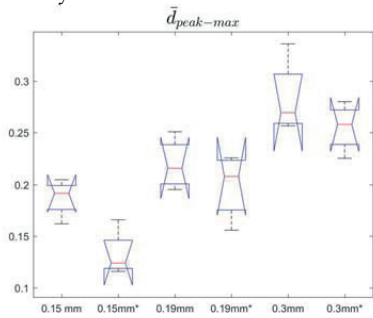

Fig. 20. Average radial distance between the silhouettes of the peak maximums. Samples marked with an asterixis denotes an altered (narrower) thread profile.
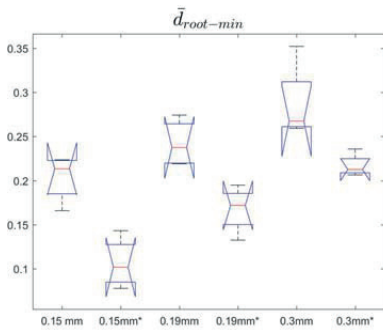

Fig. 21. Average radial distance between the silhouettes of the thread root minimums. Samples marked with an asterix denotes an altered (narrower) thread profile.
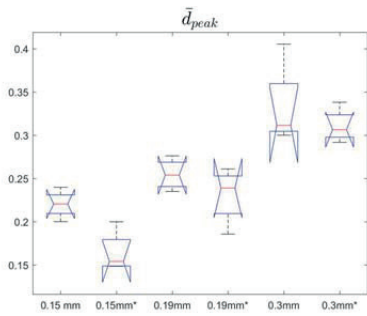

Fig. 22. Average radial distance between the silhouettes of the profiles in the peak regions. Samples marked with an asterix denotes an altered (narrower) thread profile.
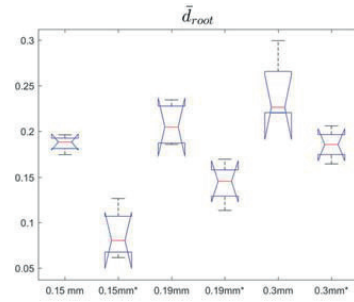

Fig. 23. Average radial distance between the silhouettes of the thread profiles in the root regions. Samples marked with an asterix denotes an altered (narrower) thread profile.
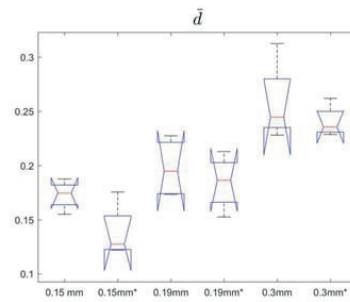

Fig. 24. Average radial distance between the silhouettes of the profiles.

Table 2: Overview of which methods which resulted in a significant improvement in the various performance measures. Significance indicates a P-value lower than 0.05, found through ANOVA analysis. *Decrease in layer height* denotes an decrease from 0.3 to 0.15 mm.

| Method | Measure | | | | |
	$\overline{d}_{p-m}$	$\overline{d}_{r-m}$	$\overline{d}_p$	$\overline{d}_r$	$\overline{d}$
Decrease layer height	Yes	Yes	Yes	Yes	Yes
Narrower thread	0.15	All	0.15	0.15 and 0.3	0.15

The results in Table 1 show that lowering the layer height from 0.3 mm to 0.15 mm increases the performance for all the groups. The average distance

from thread to ideal curve decreases from 0.26 to 0.17 mm, and the maximum peak distance decreases from 0.28 to 0.18mm. Although not directly linked, this implies that when using a standard M10x1.5 screw/nut, with a minimum internal thread major diameter of 10mm, the major diameter of the screw must be printed with a diameter less than 9.72 mm for 0.3 mm layers and 9.82 for 0.15 mm layers to obtain a clearance fit.

Using a narrower-than-standard thread profile (1/16th of the pitch of 1.5 mm) would further improve this situation, as it has an average maximum peak distance of only 0.13 mm. However, this statement is only valid when using the minor, 0.15 mm layers. Distance between root minimums is the only performance measure that is significantly improved, across all layer heights when using a narrower thread profile. The reason why none of the other measures are improved is possibly due to reduced size of the flat region of the thread peaks, causing the slicer to miss it when discretizing/sampling the edge. This reduces the average thread height with 0.0518 mm in average among all narrow thread samples, compared with the normal profiles.
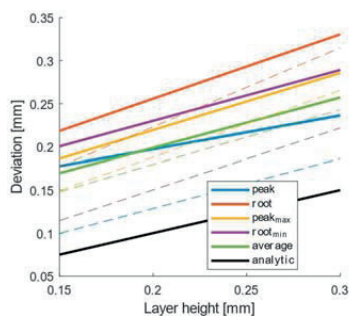

Fig. 25. Linear regression of all performance measures together with the analytic solution. Dotted lines show the performance measures for the narrow profile counterparts.

Using linear regression, all performance measures show a slope like the analytical model for the normal-profile-threads, but as displayed in Fig. 25 there is an extra substantial baseline deviation for all specimens. The narrow threads seem to be more affected by layer height, as earlier explained by poorer sampling of smaller details for high layer heights. For low layer heights, the reduction seems to correspond well with the analytical solution, that predicts approximately 0.08 mm less deviation.

5. Conclusions and outlook

The presented framework is possible to use for analyzing thread geometry. For our chosen performance measures, layer height and defects seems to have relationship corresponding well to the analytical model presented. For the layer heights investigated, however, there is a substantial nominal baseline error. Although the numerical values would differ from machine to machine, we believe that the trend would be similar for the FDM process in general (baseline error in addition to layer dependent error).

Narrowing the thread profiles does increase the performance for threads printed with a relatively small layer height compared with thread pitch (0.15 layer height to a pitch of 1.5 in this case). However, this effect does diminish with increased layer height due to finer geometries that would be insufficiently sampled during slicing. The methods of improving the dimensional accuracy of threads proposed herein are easily implemented in either CAD or slicer software.

Moreover, we believe that there is value in investigating such performance parameters, generating analytical models and relationships from experimental values that can aid practitioners and software developers in the field of Design For Additive Manufacturing (DfAM). Further work in this specific project would include developing guidelines for dimensioning of screws produced by FDM, based on additional process characteristics (in addition to layer height), and potentially estimating the implications on mechanical performance.

The image processing framework for investigating defects on threads would be applicable to all forms of threads, and not only those produced by FDM.

Acknowledgements

References

[1]   Camille Bosqué. What are you printing? Ambivalent emancipation by 3D printing. Rapid Prototyping Journal 2015;21:572–81.

[2]   Byun H-S, Lee KH. Design of a New Test Part for Benchmarking the Accuracy and Surface Finish of Rapid Prototyping Processes. Computational Science and Its Applications — ICCSA 2003, Springer, Berlin, Heidelberg; 2003, p. 731–40.

[3]   Shah P, Racasan R, Bills P. Comparison of different additive manufacturing methods using computed tomography. Case Studies in Nondestructive Testing and Evaluation 2016;6:69–78.

[4]   #3DBenchy. #3DBenchy n.d. http://www.3dbenchy.com/ (accessed October 27, 2017).

[5]   Wohlers T. Wohlers report 2016. Wohlers Associates, Inc; 2016.

[6]   Etesami F, Griffin T. Characterizing the Accuracy of FDM Rapid Prototyping Machines for Machine Design Applications. ASME 2013 International Mechanical Engineering Congress and Exposition, American Society of Mechanical Engineers; 2013.

[5]   Ahn D, Kweon J-H, Kwon S, Song J, Lee S. Representation of surface roughness in fused deposition modeling. Journal of Materials Processing Technology 2009;209:5593–600.

[6]   Pandey PM, Venkata Reddy N, Dhande SG. Improvement of surface finish by staircase machining in fused deposition modeling. Journal of Materials Processing Technology 2003;132:323–31.

[7]   Jonathan Torres, Matthew Cole, Allen Owji, Zachary DeMastry, Ali P. Gordon. An approach for mechanical property optimization of fused deposition modeling with polylactic acid via design of experiments. Rapid Prototyping Journal 2016;22:387–404.

[8]   Armillotta A, Bianchi S, Cavallaro M, Minnella S. Edge quality in fused deposition modeling: II. experimental verification. Rapid Prototyping Journal 2017;23:686–95.

[9]   Johnson WM, Rowell M, Deason B, Eubanks M. Comparative evaluation of an open-source FDM system. Rapid Prototyping Journal 2014;20:205–14.

[12]   Montero M, Roundy S, Odell D, Ahn S-H, Wright PK. Material characterization of fused deposition modeling (FDM) ABS by designed experiments. Society of Manufacturing Engineers 2001;10.

[11]   Tian X, Liu T, Yang C, Wang Q, Li D. Interface and performance of 3D printed continuous carbon fiber reinforced PLA composites. Composites Part A: Applied Science and Manufacturing 2016;88:198–205.

[12]   ISO 68-1:1998 n.d.

[13]   Gadelmawla ES. A novel system for automatic measurement and inspection of parallel screw threads. Proceedings of the Institution of Mechanical Engineers, Part B: Journal of Engineering Manufacture 2004;218:545–56.

[14]   He F, Cui X, Zhang Y, Huang Z. Non-contact measurement of oil tube thread and the application. vol. 5058, International Society for Optics and Photonics; 2003, p. 661–6.

Investigating pressure advance algorithms for filament-based melt extrusion additive manufacturing: Theory, practice and simulations

Sigmund A. Tronvoll, Sebastian Popp, Christer W. Elverum and Torgeir Welo

Structured abstract

Purpose: This paper aims to present the mathematical foundation of so-called *advance algorithms,* developed to compensate for defects during acceleration and deacceleration of the print head in *filament-based melt extrusion additive processes*. It then investigates the validity of the mathematical foundation, it's performance on a low-cost system, and the effect of changing layer height on the algorithm's associated process parameter.

Design/Methodology/Approach: This study starts with a compilation and review of literature associated with *advance algorithms,* then elaborate on its mathematical foundation and methods of implementation. Then an experiment displaying the performance of the algorithm implemented in *Marlin* machine firmware, *linear advance 1.0,* is performed using 3 different layer heights. The results are then compared with simulations of the system using *Simulink*.

Findings: Findings suggests that advance algorithms following the presented approach, is capable of eliminating defects due to acceleration and deacceleration of the print head. The results indicate a layer height dependency on the associated process parameter, requiring higher compensation values for lower layer heights. It also shows higher compensation values for acceleration than deacceleration. Results from the simulated mathematical model corresponds well with the experimental results, but predicts some rapid variations in flow rate that is not reflected in the experimental results.

Limitations: As there are large variations in printer design and materials, deviation between different setups must be expected.

Originality: First article to describe and investigate *advance algorithms* in academic literature.

Keywords: fused deposition modelling, FDM, melt extrusion additive manufacturing, advance, flow control

Article Classification: research article

Nomenclature

A_{in} – Cross section of filament
A_{out} – Cross section of annular section of nozzle
A_{print} – Cross section of deposited material

d_{out} – Diameter of annular section of nozzle

d_{in} – Diameter of filament

F_{dw} – Forces exerted on the filament by the drive-wheels

F_n – Forces exerted on the filament by pressure loss in the nozzle

F_f – Forces due to pressure loss caused by friction

F_a – Forces due to pressure loss caused by acceleration of material

h – Layer height

H – Transfer function of input to output speed

k – Compliance of system

K – Lag factor of system

K_{LA} – Correction parameter for linear advance

l – length of filament inside extruder

L – Length of nozzle outlet

μ – Friction coefficient

ΔP_a – Pressure loss in nozzle caused by acceleration of material

ΔP_f – Pressure loss in nozzle outlet caused by friction

Q_{in} – Ingoing material volume flow

Q_{out} – Outgoing material volume flow

R – Flow rate (v_{out}^*/v_{in}^0)

s – Complex domain variable for Laplace transforms

v_{in} – Ingoing extrusion speed

v_{in}^0 – Ingoing prescribed extrusion speed

V_{in} – Laplace transform of v_{in}

v_{out} – Outgoing extrusion speed

v_{out}^* – Q_{out}/A_{in}

V_{out}^* – Laplace transform of v_{out}^*

v_{print} – Printing speed

w – Line width

ω_{dw} – Rotational speed of the drive wheels

Introduction

For the development of *filament-based melt extrusion additive manufacturing*, the activity level of the open source and practitioner community has resulted in a multitude of practical techniques and tools being available before they are described and analyzed in academic research. One such widely used aspect, yet less described, is the compensation of defects due to undesirable extrusion dynamics occurring while accelerating and deaccelerating the print-head—known as *advance algorithms*. These algorithms have the potential to substantially enhance the print quality, but they can also impact the performance negatively if they are not correctly configured. There is also uncertain how these algorithms are affected by different process characteristics such as layer height, material, temperature and nozzle geometry.

To be able to investigate these aspects thoroughly we will first present the algorithms' background and develop its theoretical foundation, both in terms of mathematical

description and graphical block-system design. This would hopefully aid further research on the matter and ease the understanding of the algorithms for practitioners. As most of the work on this subject is done by the open source community, the previous work is rarely published, and therefore consists of sources outside of the academic sphere.

As a start of investigating the algorithm's dependency of process parameters we will perform an experimental procedure focusing on dependency of layer height and whether the acceleration is positive or negative. These results will then be compared with simulation results of the process using *Simulink*, which can determine the model validity.

Although a trademarked by Stratasys Inc., filament-based melt extrusion additive manufacturing is commonly referred to as *fused deposition modeling* (FDM), which will be used throughout the article.

Background and objectives

A typical area for defects is in regions of high acceleration or deacceleration of the print head. The most common display of these effects is shown in terms of over-extrusions on corners when printing with a fast pace, as seen in Figure 1.
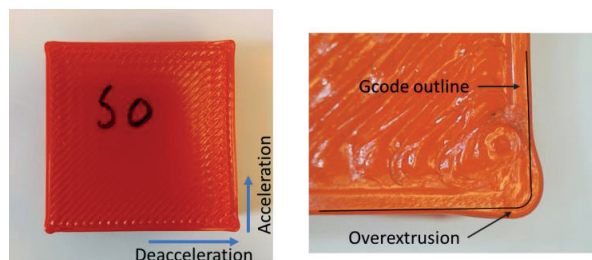

Figure 1: Over-extrusion in corners due to deacceleration.

Generally, the extruder tends to extrude too much material while deaccelerating, and too little while accelerating (referred to as over-extrusion and under-extrusion, respectively) as illustrated in Figure 2.
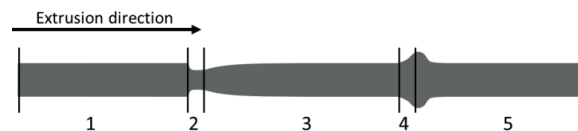

Figure 2: Typical printed shape while print acceleration/deacceleration. 1 – uniform extrusion at consistent slow speed, 2 – defects start during acceleration, 3 – returning to uniform extrusion at consistent high speed, 4 – defects start during deacceleration, and 5 – returning to uniform extrusion at slow speed.

As these defects will severely impact the tolerances at corners, manufacturing fine tolerance clearances or press fits would often require post processing of the parts by sanding or machining, for removing excess material.

There is a shortage of academic work on extrusion dynamics related to fused deposition modeling, with the exception of Bellini, Guceri & Bertoldi (Bellini et al., 2004) who made a thorough exploration of extrusion dynamics using Stratasys equipment, working towards strategies for flow control. They did however have a focus on the electronic circuit, assuming the heat transfer, rate and temperature dependent characteristics to be the root cause of the dynamics.

The first applied open source algorithm attempting to calibrate for the defects shown in Figure 1, was through an algorithm called simply *advance,* developed by Matt Roberts (n.d.). This was later implemented in the widely used *Marlin* firmware. The algorithm assumed that the root cause of the error was the compression of filament in the extruder combined with the pressure loss in the nozzle due to acceleration of material. Influenced by this work, Bernard Kubicek pointed out that the pressure loss in the nozzle was dominated by friction forces, rather than forces due to acceleration (Kubicek, n.d.). An algorithm incorporating these ideas was then implemented in the *Sailfish* firmware by Jetty, Kubiceck and Newman, and hence called *JKN-advance* ("Jetty Firmware Manual," n.d.). This progress led many firmware developers to develop their own version of this algorithm, and different versions is now implemented in many other firmwares, e.g. *Marlin*, *RepRap* and *Klipper* ("G-code," n.d.; Kevin O. Connor, 2018; Sineos, 2018)

Building on the same physical principals of JKN-advance, the developers of Marlin created an algorithm named *linear (pressure) advance*, which due to *Marlin*'s popularity is now possibly the most adopted version. The algorithm was developed and implemented by Sebastian Popp, improved by multiple GitHub users including Scott Latheine, and documented by Sineos (2018). As there might be slight differences of the implementational details for different firmwares, we will be referring to the *Marlin* implementation, if not stated otherwise.

Mathematical formulation

Some of the most promising explanations for potential contributions to these deformities are:

- Deflection of the drive wheel position relative to the nozzle
- Compression/deformation of the filament between the drive wheels and nozzle
- Deflection/elongation of the guide tube (in case of Bowden type extruders, using extruder drive wheel mechanism placed apart from the heating assembly, connected by a polymer tube)
- Load dependent phase lag in the extruder stepper motor

Together with a pressure loss in the molten plastic throughout the nozzle, which increases with material velocity, any of these causes could possibly reproduce the same phenomena.

In the compensation procedure to be described here, the assumed root causes are all modelled as linearly dependent on the rate of the filament extrusion, and hence pooled

into one single system. The easiest way to describe the mechanism would be using the compression of filament analogy, as seen in Figure 3.
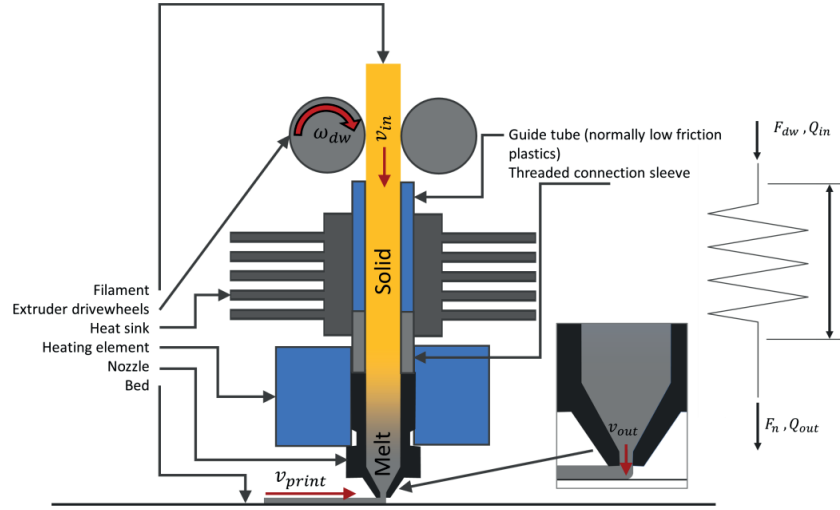

Figure 3: Direct drive extruder assembly, together with simplified physical model. Forces at nozzle F_n, the length of the filament section inside extruder l, drive wheel forces F_{dw}, and incoming/outgouing material volume flow, Q_{in} and Q_{out}, together with incoming/outgoing extrusion speed v_{in} and v_{out}, printing speed v_{print} and rotational speed of the extruder drive wheel ω_{dw}.

Based on Sineos and Kubicek (n.d.; 2018), the following procedure could describe a compensation procedure for this type of system. The system is assumed quasi-static, so that forces due to acceleration of solid material is assumed negligible. This means that the forces exerted by the drive wheel are equal to those arising from the pressure drop in the nozzle:

$$F_{dw} = - F_n \tag{1}$$

Explanation for the symbols are shown in Figure 3. Moreover, the compression or possibly buckling deformations of the filament inside the extruder is assumed linearly dependent on the forces in the following way:

$$\Delta l = k F_n \tag{2}$$

where k is a constant and $\Delta l = l - l_0$, where l_0 is the initial (unloaded) length of the filament section between the nozzle and drive wheel. The counteracting forces are assumed to be caused by pressure loss in the nozzle or nozzle outlet. There might also be friction stemming from along the rest of the path from drive wheel to nozzle, but as the filament normally has a diametral clearance of 0.15 - 0.25 mm to the walls that are mostly covered with low friction Teflon or Nylon tubing, this contribution is assumed low. The

remaining question is then the relation between velocity and forces in the nozzle, where we have both a contribution from the acceleration of material, for which the contribution can be found through the Bernoulli equation, and frictional forces.

As a rough estimate of magnitude of these forces, we would use an example with an standard E3D nozzle (Younge, 2014), with 0.4 mm diameter nozzle (d_{out}), 0.6 mm outlet length (L), used for 1.75 mm filament diameter (d_{in}), and at an relatively high extrusion speed of 100 mm/s (v_{out}). We would choose to use polylactic acid (PLA) data as it is the most common material for FDM. PLA is found to exhibit low shear thinning and is therefore assumed Newtonian. We assume a density of 1250 kg/m3 ρ, and a viscosity of approximately 200 to 1000 Pa·s (μ) at 220-190°Celsius (Zhou et al., 2006). The forces on the filament due to acceleration of material, named F_a, would be calculated as:

$$F_a = \Delta P_a A_{in} = \frac{\rho(v_{out}^2 - v_{in}^2)}{8} \pi d_{in}^2 = \frac{\rho v_{out}^2 \left(1 - \frac{d_{out}^4}{d_{in}^4}\right)}{8} \pi d_{in}^2 \approx 1.37 \cdot 10^{-5} \, N \quad (2)$$

where ΔP_a is the pressure loss in the nozzle. Using the Hagen Poiseuille equation, assuming laminar flow, the friction contribution of the force from the nozzle outlet only, named F_f, can be found as:

$$F_f = \Delta P_f A_{out} = \pi 8 \mu L v_{out} \approx 0.28 \text{ to } 1.4 \, N \quad (3)$$

where ΔP_f is the pressure loss due to friction. The friction forces from the conical section are harder to assess, as this is a region where the material goes from solid to melt, and its rheological properties would therefore be very difficult to include. However, the friction forces from the nozzle outlet only, are larger than the acceleration contribution by a magnitude of $3.5 \cdot 10^4$, and hence clearly the dominating force. The relation between velocity and forces from the nozzle are therefore assumed linear. This leads to a relation between the velocity and the compression of the filament that is also linear, related by a constant K, which we call the *lag factor*, by the following convention:

$$\Delta d = K \frac{Q_{out}}{A_{in}} \quad (4)$$

The older *advance* created by Matt Roberts assumed that the Bernoulli pressure drop to be the dominant term, and hence defined:

$$-\Delta d = K Q_{out}^2 \quad (5)$$

As shown, there are many factors influencing the pressure loss, and results from one FDM printer setup (machine, material, temperature) might therefore not be the same in another setup.

The ratio between the extruder speed and printing speed is dictated by the slicer, based on the assumed geometry of the printed filament. The output geometry assumed by slicers are most often rectangular, with semicircular ends, as seen in Figure 4, which is however only defined for width less than the layer height. Much work has been done on microgeometry of FDM parts, for relating the process parameters to surface roughness. Most notable is the elliptical cross sections model by Ahn et al. (2009), and the parabolic

model by Pandey, Reddy and Dhande (2003). These have limitations in practical implementations due to being based on experimental observations.
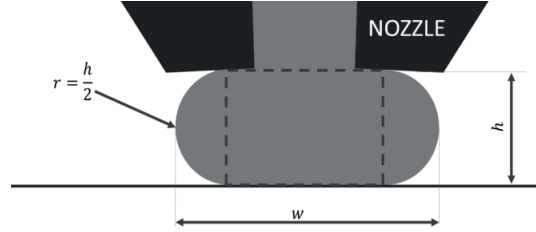

Figure 4: Assumed geometry of extruded filament for slicer implementation. Out of plane printing movement.

Relating the geometric measures to the output geometry gives (Gary et al., n.d.):

$$A_{print} = wh - \left(1 - \frac{\pi}{4}\right)h^2 \tag{6}$$

For accelerating/deaccelerating, Equation 3 gives:

$$\frac{d}{dt}\Delta d_f = K\frac{d}{dt}\frac{Q_{out}}{A_{in}} \tag{7}$$

$$\frac{Q_{in} - Q_{out}}{A_{in}} = K\frac{\dot{Q}_{out}}{A_{in}} \tag{8}$$

$$v_{in} = K\frac{\dot{Q}_{out}}{A_{in}} + \frac{Q_{out}}{A_{in}} \tag{9}$$

Solving for $\frac{Q_{out}}{A_{in}}$ gives:

$$v_{in} - K\frac{\dot{Q}_{out}}{A_{in}} = \frac{Q_{out}}{A_{in}} \tag{10}$$

In the advance algorithms, one simply corrects v_{in} to be equal to $K_{LA}\dot{v}_{in}^0 + v_{in}^0$, where v_{in}^0 is the required extrusion speed, as defined by the G-code. This gives

$$v_{in}^0 + K_{LA}\dot{v}_{in}^0 - K\frac{\dot{Q}_{out}}{A_{in}} = \frac{Q_{out}}{A_{in}} \tag{11}$$

$$v_{in}^0 + K_{LA}\frac{\dot{Q}_{out}^0}{A_{in}} - K\frac{\dot{Q}_{out}}{A_{in}} = \frac{Q_{out}}{A_{in}} \tag{12}$$

Which for $K = K_{LA}$ would give $Q_{out}/A_{in} = v_{in}^0$, as required for a correct extrusion width. The reason for having the $1/A_{in}$ factor is due to *G-code* conventions for most FDM firmware. For a printing move the G-code prescribes the required length of raw-filament needed to extract the correct amount of material as prescribed by the computer aided manufacturing software, as illustrated in Figure 5.
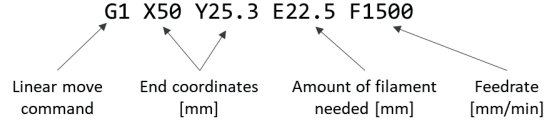
```
G1 X50 Y25.3 E22.5 F1500
```

| Linear move command | End coordinates [mm] | Amount of filament needed [mm] | Feedrate [mm/min] |

Figure 5: General entries in a printing move, using the G1 G-code command.

As FDM-printers are most often driven by stepper motors, that are advancing in discrete time/length intervals, this could be implemented in each of these intervals. Calculating the required length of filament at interval n, ΔD_n, with time step Δt_n, as a function of the requested extruded filament segment ΔD_n^0 in each time step, can be done as follows:

$$\frac{\Delta D_n}{\Delta t_n} = K_{LA}\left(\frac{\frac{\Delta D_n^0}{\Delta t_n} - \frac{\Delta D_{n-1}^0}{\Delta t_{n-1}}}{\Delta t_n}\right) + \frac{D_n^0}{\Delta t_n} \tag{13}$$

$$\Delta D_n = K_{LA}\left(\frac{\Delta D_n^0}{\Delta t_n} - \frac{\Delta D_{n-1}^0}{\Delta t_{n-1}}\right) + \frac{D_n^0}{\Delta t_n} \tag{14}$$

The *K*-factor is in units of seconds, and its magnitude is found experimentally, typically seen in range of 0.1 – 0.3 for direct drive extruders, and in range 2.0–3.0 for Bowden type extruders (Sineos, 2018). The presented framework represents most advance algorithms, but some have a scaling factor for K, which for the *linear advance 1.0* from the *Marlin* firmware is 512.

It is debatable whether the volume flow is a valid independent variable for this compensation. The material from the nozzle is deposited on a bed perpendicular to the extrusion direction, and there is contact between the nozzle and melt both inside and outside of the nozzle, as seen in Figure 6. This would create a layer height dependent pressure drop, but the magnitude is difficult to assess due to a complex flow pattern with combined open, moving and stationary boundaries. As lower layer heights are associated with a higher pressure loss (Coogan and Kazmer, 2017), it is expected that lower layer heights also requires higher compensation parameters.
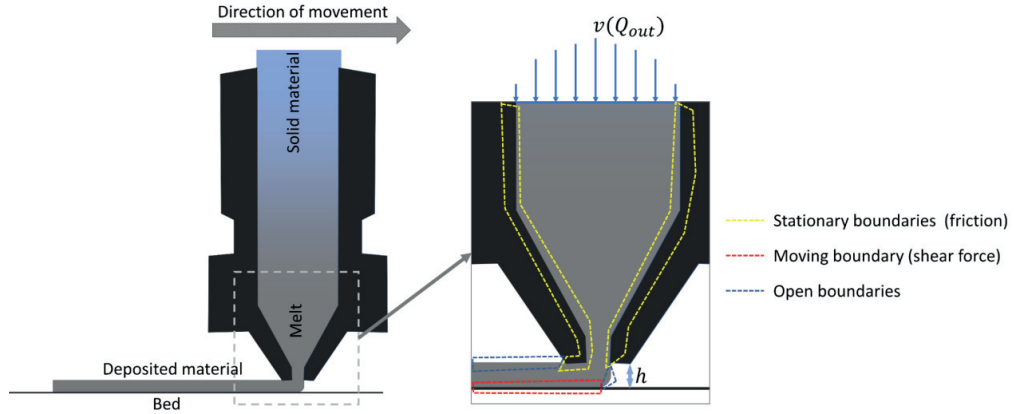
Figure 6: Overview of the different boundary types in the nozzle. Stationary boundaries would increase the pressure drop, while the pressure drop due to open and moving boundaries has a more uncertain influence.

For simulation purposes, the solution of equation 7 could be found using Laplace transformation, where the solution of this first order ODE is:

$$V_{in}(s) = V_{out}^*(s)(Ks + 1) \tag{15}$$

And the transfer function $H(s)$ would be written as:

$$H(s) = \frac{V_{out}^*(s)}{V_{in}(s)} = \frac{1}{1 + Ks} \tag{16}$$

where Q_{out}/A_{in} is called v_{out}^* for simplicity, and it's Laplace transform is called V_{out}^*. This transfer function is very similar to what Bellini et al. found in their research (Bellini et al., 2004), where the only difference is a time-delay function and a gain. The gain is the link between the theoretical extrusion speed of the drive wheel and the real extrusion speed of the filament. These values would have a discrepancy due to for example, slip between the drive wheel and filament, and deformation in the filament. For printing applications, it is assumed constant and usually tuned on the printer through the parameter *extruder steps per mm*, and in the G-code through the parameter called *flow rate, flow* or *extrusion multiplier*. This is however omitted in this article, as these parameters are tuned in advance. The resulting system is the solution of the system seen in Figure 7.
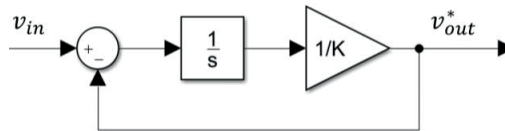

Figure 7: Resulting extruder system from equation 14.

Although less important for uncorrected flow, for special cases as e.g. overcompensation, v_{out}^* might become negative. This would empty the nozzle for material instead of dragging material from the print bed into the nozzle again. During negative v_{out}^* the velocity dependent friction is assumed neglectable as no material is moving through the nozzle, and the following correction of the system for negative speeds in Figure 8 is therefore applied.
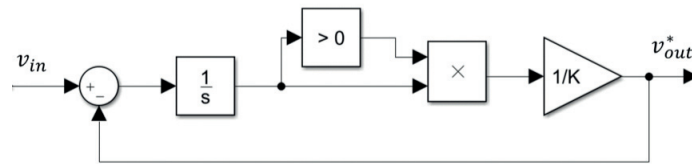

Figure 8: Corrected extruder system eliminating backflow of material.

The combined system of the extruder and the pre-processing of the speeds using linear advance, is seen in Figure 9.
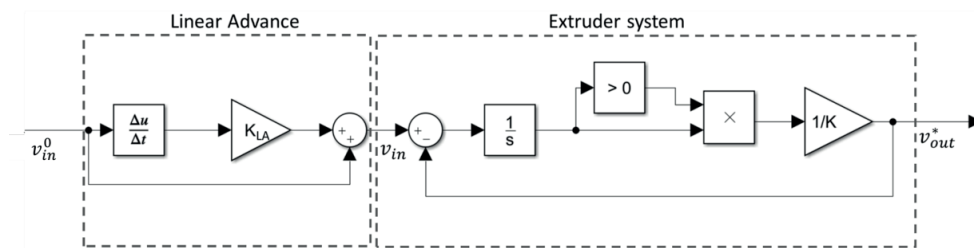

Figure 9: Model for processing the input speed using linear advance, altering the G-code input speed v_{in}^0 based on the acceleration to calibrate the extruder speed.

All these models assume that the mechanical/mechatronic system is flawless and that the method of discretization is irrelevant, and will be used in the Simulink simulation software.

Experimental setup

Using an Original Prusa i3 MK2.5 desktop FDM printer, a controlled experimental test for different linear advance values and different layer heights was performed. The test was generated from the test template provided in the *Marlin* documentation (MarlinFirmware, 2018), and consists of an acceleration from low speed to high speed at values for K_{LA} from 0 to 0.2. Key process parameters are listed in Table 1 and Figure 10, and simulated results are seen in Figure 11 and Figure 13. The test is only performed for deposition onto the bed, and the geometry and stiffness of the substrate would possibly affect the result.

Table 1: Process parameters for experimental tests

Layer height	0.10 mm, 0.20 mm and 0.30 mm

K_{LA}-values	0 - 0.2 s in 0.01 s increments
Line width	0.48 mm
Nozzle size	0.40 mm
Material	Generic polylactic acid
Nozzle temperature	215º Celsius

Extrusion direction

	1	2	3	4	5

Low speed	Acceleration	High speed	Deacceleration	Low speed
20 mm/s	1000 mm/s^2	80 mm/s	-1000 mm/s^2	20mm/s
30 mm	40mm			30mm
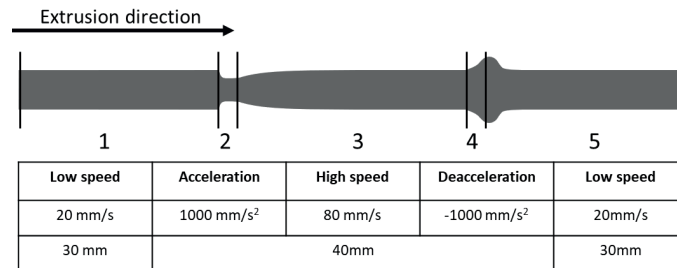
Figure 10: Test line speeds, accelerations and lengths.

Figure 11 shows the simulated output extrusion speed v^*_{out} for different K values of the system, when linear advance is not applied. Dividing $v(K)$ by $v(K = 0)$ would give the flow rate for the different positions along the test line as shown in Figure 13. This would to some extend reflect the changes in extrusion width but neglects the geometry of the filament line and extrusion dynamics after the melt leaves the nozzle. This implies that e.g. the peaks in the flow rate will not be reflected in the extrusion width, as they will be smoothed out by flow dynamics pushing material forwards and backwards from the nozzle, establishing the path of least resistance. To include these effects would possibly require highly non-linear simulations by e.g. finite element analysis using mixed Eulerian-Lagrangian formulation and hard-to-obtain rheological properties, and is in this study omitted due to complexity. The implications of displaying flow rate compared to the cross-section model implemented in the slicers (Figure 4) is shown in Figure 12. As

the results from Figure 13 shows, the defects should be easily identifiable, already at a value of 0.02 s.
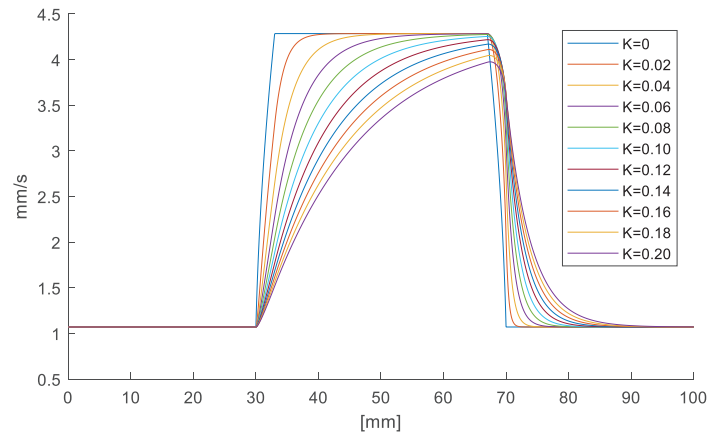

Figure 11: Simulated, non-calibrated output speed v_{out}^* from extruder for different K values, printing with 0.2 mm layer height along the test line.
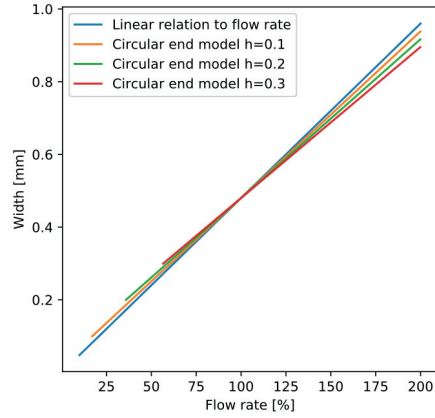

Figure 12: Difference in flow rate-to-line width relation between slicer implemented model with circular ends and using a linear relation to the flow rate as used for visualization of simulation results. Note that the slicer implemented model is ill-defined for widths lower than layer height.
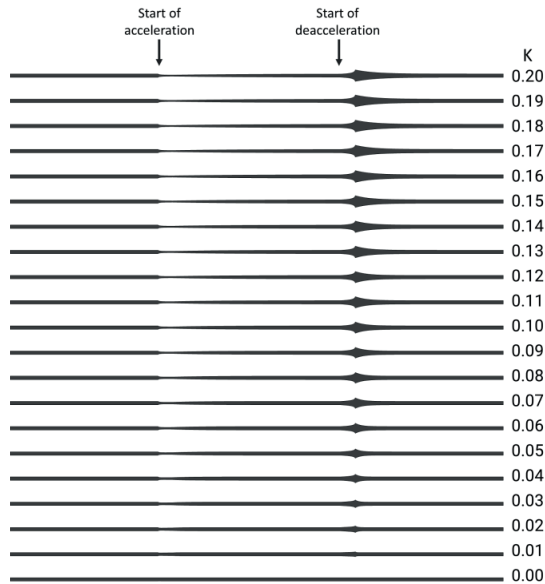
Figure 13: Simulated non-calibrated flow rates R for different values of K, where R = v(K)/v(K = 0). Start width indicates the ideal flow rate (R = 100%).

Results and discussion

First, we will present the combined results from the tests. Then the results from each layer height alongside a simulation will be presented. Figure 14 displays the results for all layer heights and all correction factors combined, along with a marking that shows the lines that are estimated to have the smallest defects, and hence the more optimal correction factor.
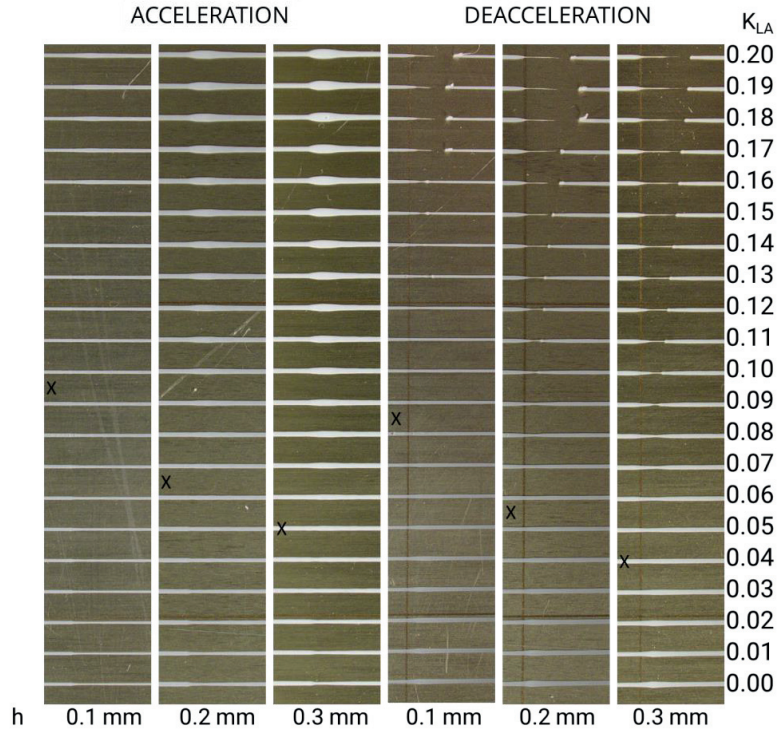
Figure 14: Defects for different layer heights, and K *values for linear advance calibration.* X *marks the line with least defects, or between if similar.*

Table 2 summarizes the findings from the figure. The identification of this correction factor is done by visual estimation only, placing the ideal correction factor half way between the test lines displaying visible defects. As a quantitative result, an accuracy on ideal K_{LA} of less than 0.01 s cannot be guaranteed. Due to defects in the glued-on polyetherimide (PEI) print surface as well as tolerances of the filament cross section of about ±2 %, any higher accuracy would anyways be difficult to achieve.

Table 2: Ideal correction factors for different layer heights

Layer height	K_{LA} for acceleration [s]	K_{LA} for deacceleration [s]	Average [s]
0.1	0.095	0.085	0.9
0.2	0.065	0.055	0.06
0.3	0.05	0.04	0.045

As seen in Figure 14, the defects get smaller for increasing K_{LA} until a value of around 0.04 to 0.95 for the different layer heights. Using a K_{LA} value of more than twice the optimal one, will result in severe overcompensation to an extent that results in no extruded material when deaccelerating. The experimental study shows that there is approximately 0.01 s^{-1} in difference between the optimal K-values for acceleration and deacceleration.

This is however within the range of the accuracy of our method. It must be emphasized that these values are only valid for our specific setup, as this will possibly be affected by many different parameters.

As hypothesized, there is also evidence for a layer dependency. The ideal compensation parameter is approximately twice as high for a layer height of 0.1 mm than for the layer height of 0.3 mm. This indicates that thin layers generate a significantly higher pressure-loss, which is suggested in literature (Coogan and Kazmer, 2017). However, due to the number of different nozzle geometries, it could be challenging to develop a universally valid layer height compensation function. As this test is quite easy to perform, the results could instead easily be implemented as tabular values in the slicer software.

Figure 15 to 17 shows the full test lines, alongside a simulation using the system shown in Figure 9, applying the identified average optimal K_{LA} value of the system for each layer height, to display whether the proposed model can replicate the experimental results. The simulation results are only displayed in terms of extrusion flow rate, $R = v_{out}^*/v_{in}^0$, and scaled so that the simulated flow rate is equal in width to the experimental results sampled between the start of the line and start of the acceleration phase, which indicates ideal flow rate ($R = 100\%$). Sample line for $h = 0.2$ and $K_{LA} = 0.06$ used as reference.
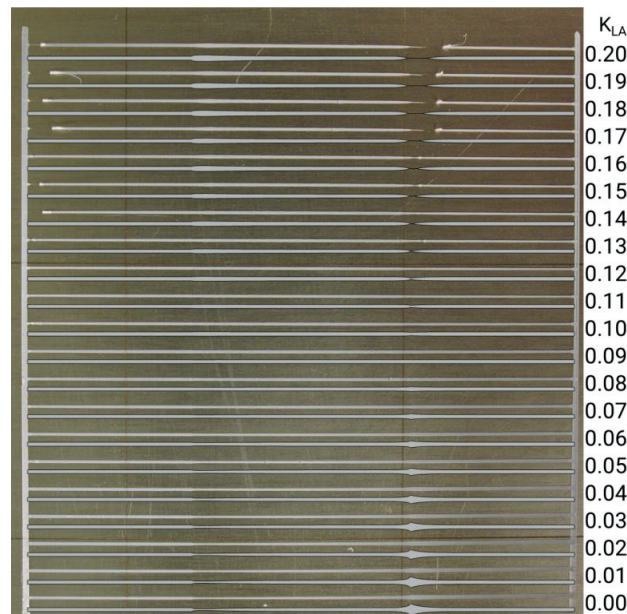

Figure 15: Experimental results for 0.1mm layer height, alongside simulation results for ideal K=0.09s

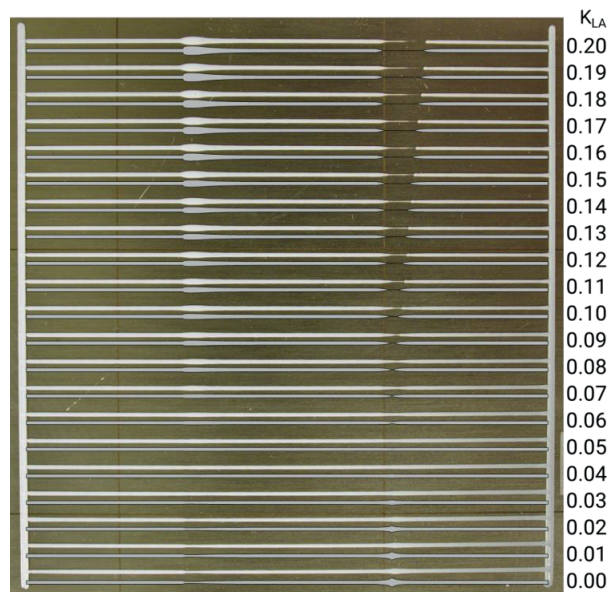*Figure 16: Experimental results for 0.2 mm layer height alongside simulation results for ideal K = 0.06s*

Figure 17: Experimental results for 0.3 mm layer height alongside simulation results for ideal K = 0.045s

For 0.3 mm layer height, the model fits very good to the experimental data, with approximately the same variations in the acceleration zone, and the same length of section

where there is no extrusion of material. For the lower layer heights, the length of the section with no extrusion is less reflected in the experimental data, as there seems to be a difficulty to make the plastic stick to the print bed while restarting the extrusion.

Comparing the simulation results for flow rate with the experimental results for filament width, they are very similar where there are no large variations/spikes in flow rate. For large variations, the experimental results are smoothened out compared with the simulation results, as illustrated in Figure 18. This discrepancy could be from dynamics of the melt after it leaves the nozzle. It is also possible that the discrepancy is due to high stepper motor load, resulting in skipped steps, as this compensation uses large and discrete velocity jumps when it starts an acceleration. Another reason for the discrepancy could be due to deflection between the nozzle and print bed, due to higher volume flow and hence higher pressure, increasing the layer height in those areas.

Figure 18: Illustration of experimental width (top) and simulation of flow rate (bottom) results for 0.3 mm layer height, and A) acceleration region for $K_{LA} = 0.2$ and B) deacceleration region for $K_{LA} = 0$. Edges traced using the software Inkscape *for image clarity.*

When the flow rate is relatively low, the experimental samples are somewhat wider, as illustrated in Figure 19. This is expected, as in this region the assumed extrusion width is less than the layer height. Having such a low flow rate would result in an uncertain shape of the extruded line, as they will not be sufficiently squeezed down onto the print bed.

Figure 19: Illustration of experimental (top) width and simulation (bottom) of flow rate from results for 0.3 mm layer height, and A) acceleration region for $K_{LA} = 0$ and B) deacceleration region for $K_{LA} = 0.0$. Edges traced using the software Inkscape *for image clarity.*

Summary and further work

The mathematical framework for the so-called *advance algorithms* is presented, and its effectiveness in compensating for defects due to extrusion dynamics is demonstrated. The algorithm *linear advance 1.0* from the *Marlin* firmware is shown to effectively compensate for irregularities in extrusion widths during acceleration and deacceleration of the nozzle. As hypothesized, the required correction parameters are layer dependent, and will therefore need to be tuned for each layer height used in a print. There is also possibly a small difference in optimal correction parameter for whether the acceleration is positive or negative. The mathematical model is through simulations with Simulink and comparison with the experimental data, shown to be quite accurate for smooth

variations in flow rate. When there are rapid variations in flow rate, the extrusion width seems to be smoothened out in the experimental results compared with the simulations.

As the algorithm enables printing a sufficiently uniform extrusion width for practical purposes, and the mathematical model can replicate that, we believe further work should focus on three areas:

- Investigate implications for printing 3D geometry
    - Non-linear extruder movements
    - Substrate stiffness and geometry
- Investigate dependency of more process parameters e.g.:
    - Material
    - Temperature
    - Specified extrusion width
    - Nozzle diameter
- Develop solutions and standards for implementing the process parameter dependency in the printer firmware

Acknowledgements

References

Ahn, D., Kweon, J.-H., Kwon, S., Song, J., Lee, S., 2009. Representation of surface roughness in fused deposition modeling. Journal of Materials Processing Technology 209, 5593–5600. https://doi.org/10.1016/j.jmatprotec.2009.05.016

Bellini, A., Güçeri, S., Bertoldi, M., 2004. Liquefier Dynamics in Fused Deposition. Journal of Manufacturing Science and Engineering 126, 237.

Coogan, T.J., Kazmer, D.O., 2017. Bond and part strength in fused deposition modeling. Rapid Prototyping Journal 23, 414–422.

Gary, H., Ranellucci, A., Moe, J., n.d. Slic3r Manual - Flow Math [WWW Document]. URL http://manual.slic3r.org/advanced/flow-math (accessed 4.10.18).

G-code [WWW Document], n.d. URL https://reprap.org/wiki/G-code (accessed 9.12.18).

Jetty Firmware Manual [WWW Document], n.d. URL http://makerbot.wikidot.com/jetty-firmware#toc46 (accessed 6.14.18).

Kevin O. Connor, 2018. Klipper Firmware [WWW Document]. URL https://github.com/KevinOConnor/klipper (accessed 9.12.18).

Kubicek, B., n.d. Another acceleration-extrusion compensation for repraps [WWW Document]. URL http://bernhardkubicek.soup.io/post/168776124/Another-acceleration-extrusion-compensation-for-repraps (accessed 6.7.18).

MarlinFirmware, 2018. Linear Advance Calibration Pattern [WWW Document]. Marlin Firmware. URL http://marlinfw.org/tools/lin_advance/k-factor.html (accessed 7.4.18).

Pandey, P.M., Venkata Reddy, N., Dhande, S.G., 2003. Improvement of surface finish by staircase machining in fused deposition modeling. Journal of Materials Processing Technology 132, 323–331. https://doi.org/10.1016/S0924-0136(02)00953-6

Mattroberts' Firmware - RepRap n.d. https://reprap.org/wiki/Mattroberts%27_Firmware (accessed July 19, 2018).

Sineos, S., 2018. Linear Advance [WWW Document]. Marlin Firmware. URL http://marlinfw.org//docs/features/lin_advance.html (accessed 3.7.18).

Younge, R., 2014. Drawing of E3D-v6 Nozzle series rev.8. [WWW Document]. URL https://e3d-online.dozuki.com/Document/rWuaQCQsJTlRdB1k/.pdf (accessed 10.12.2018).

Zhou, H., Green, T.B., Joo, Y.L., 2006. The thermal effects on electrospinning of polylactic acid melts. Polymer 47, 7497–7505.

ORIGINAL ARTICLE

CrossMark

The effects of voids on structural properties of fused deposition modelled parts: a probabilistic approach

Sigmund A. Tronvoll[1] · Torgeir Welo[1] · Christer W. Elverum[1]

Abstract

In the search to understand the functional capabilities and limitations of fused deposition modelling (FDM) manufactured components, control over their structural behaviour is crucial. For example, voids introduced during the production phase are a large contributor to anisotropy, yet the magnitude of this contribution remains unquantified. As a baseline model for quantifying strength reduction due to process-induced voids, a statistical method for evaluation of the minimum residual (net) cross section is proposed and tested. Our new method serves to predict the reduction in ultimate tensile strength of transversely printed specimens relative to solid or longitudinally printed specimens, based on void sizes identified from microscopy images of the centre plane of a tensile specimen. *ImageJ* is used to identify void sizes from the microscopy images, and residual cross sections are determined using a bit counting *MATLAB* script. From the distribution of residual cross sections, the weakest link for a given sample size is estimated. The accuracy of the proposed method is determined through comparison with experimental test data for samples of polylactic acid (PLA). The results reveal a close yet slightly under-predicted strength estimate, which for the case considered predicted approximately 5 MPa (12%) lower strength than observed in the experiments. Based on our findings, we have established evidence that the anisotropic behaviour of FDM specimens in PLA can to a large extent be explained by the reduction in residual cross section. This implies that other effects such as fracture mechanics and atomic diffusion of polymer chains play a secondary role for the phenomena observed.

1 Introduction

Creating and testing prototypes, as most other experimentation in product development, are mainly an endeavour to reduce uncertainty. How likely is it that the product works as expected? To draw valid conclusions from prototype testing, one would like the performance to be as close to the intended design as possible. This could require compatibility in multiple dimensions, and for physical products, these dimensions could be:

- Appearance
- Dimensions
- Stiffness
- Weight
- Strength

If there are ways in which the prototype performs different than the expected production model, one should at least be aware of the difference and able to estimate the potential deviation [1].
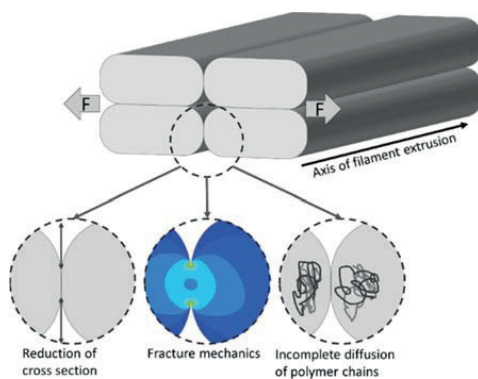
A major topic for prototyping processes over the past several years, probably boosted by the maker-movement, has been additive manufacturing (AM). Moreover, due to technology advances and patent expirations, AM has now become affordable for many hardware designers and engineers. For many cases, this technology has reduced the need of going

✉ Sigmund A. Tronvoll
sigmund.tronvoll@ntnu.no

1 Department of Mechanical and Industrial Engineering, NTNU - Norwegian University of Science and Technology, Richard Birkelands vei 2B, 7491 Trondheim, Norway

Springer

through production drawings and highly skilled labour to produce and hence test complex parts. Especially for production components such as injection moulded plastics, it is now possible to generate close-to-final quality-products by "hitting a button" and letting time do the work.
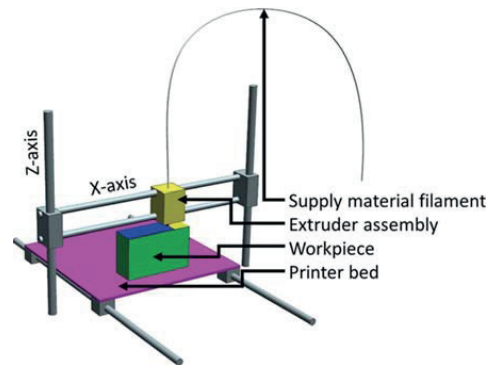
The industry surveying Wohlers Report shows that the volume of AM machines is largely driven by sales of consumer-directed machines, sold not only to consumers, but also to industrial customers. In 2015, an estimate of almost 280,000 desktop printers (sub 5000$) were sold worldwide, compared to approximately 13,000 units in the industrial price range [2]. Currently, the consumer segment is dominated by a single process type—namely the fused deposition modelling—in which lines of heated thermoplastic (called filament) are deposited, fused together and stacked in layers [3].

However, this filament fusing layer depositing method does create several compatibility issues. For the dimensions and appearance, one is restricted by the filament widths and layer heights, giving a minimum shell thickness and a clear "layered" look. While for the mechanical performance, one must tune the build strategy, process parameters and material to achieve the desired behaviour. Therefore, significant effort is put into investigating how these factors affect the mechanical performance.

The most apparent topic for investigation of mechanical strength of FDM parts is the change of tensile capacity for different build strategies, pioneered by the work of Ahn, Montero, Odell, Roudy and Wright [4, 5], as well as the investigation of the mesostructure by Rodríguez, Thomas and Renaud [6, 7]. The anisotropy arises from the fact that the load-bearing capacity of a filament along its axis of deposition differs from the capacity transversely of two filaments melted together (inter filament bonding). Optimization of process
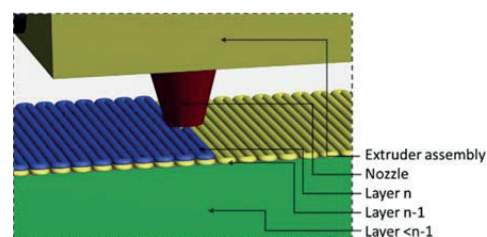

Fig. 2 3D printer axis and components

parameters and strategies to reduce this anisotropy—or generally increase the mechanical strength—has therefore been a major topic among researchers [8–15].

Our research started off likewise, aiming to reduce the anisotropy through annealing. This has proven to be effective for inter filament bonding in an earlier scientific study [8], but also been debated in different forums of the 3D printing community. The basic concept is that, when trying to melt together two lines of filament, one gets a reduction in strength compared to the bulk material due to incomplete diffusion of polymer chains, reduced cross section (introducing voids) and fracture mechanics type stress concentrations, as seen in Fig. 1. Annealing was therefore introduced to increase atomic diffusion. However, initial tests indicated no effect on the tensile specimens in polylactic acid (PLA). As a result, the following question was raised: What is the baseline reduction in strength due to each mechanism? There are numbers of papers seeking to improve the FDM process [8, 12–14, 16], yet, very few quantify the potential performance increase due to their proposed process enhancements.

To better understand the performance of 3D-printed parts, unlike process optimization where one seeks to find the optimal process parameters, we would therefore try to answer the

Fig. 1 The three main inter filament bonding strength reduction mechanisms. F denotes load direction

Fig. 3 Close-up of print paths with no perimeter. Colour for contrast only. Only two last layers shown, for convenience
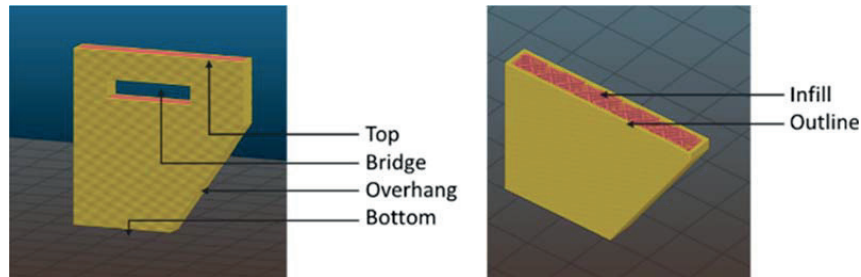
Fig. 4 Different area/volume domains of 3D-printed parts

following question: Just by visually inspecting the 3D-printed specimen, what can we expect of strength reduction due to the reduction in cross section, resulting from the characteristics of the process?

As a starting point, we propose a simple engineering method to estimate the nominal reduction in tensile strength due to voids. The method is meant to predict failure stress of transversely infilled tensile specimens, based on the statistical distributions of residual (remaining) cross sections. This will be achieved through the use of microscopy images processed through *ImageJ* for void identification, combined with a *MATLAB* script for size estimations to give statistical values for cross section reduction. Based on the identified size of voids, their statistical distribution and the sample size, an expected failure load distribution is created based on the size of the weakest link. The predicted distribution will then be compared with experimental tensile test data for parts in PLA to estimate the accuracy of the proposed method.

2 Theory and background of fused deposition modelling

The basic concept of FDM is manufacturing through deposition of materials in the form of small strips of filament.

Usually, this is done by using thermoplastics, which are heated up to above-melting temperature and extruded through a nozzle onto a table or the workpiece as seen in Fig. 2 and Fig. 3. The base material is either supplied as continuous filament through a rolling wheel feeder or as pellets using a hopper and a reciprocating screw. The material is deposited layer by layer in the *z*-direction, using a 2.5 axis CNC system.

As the material is deposited as lines—rather than melting or curing of volumetric pixels—the material characteristics are highly dependent on the strategy for producing these segments. In general, the resulting parts' structural integrity is governed by five characteristics:

- *Strategy*—How are the filament paths placed?
- *Material*—What are the characteristics of the extruded base material?
- *Geometry*—How are these lines shaped?
- *Accumulated strain*—What strains have been introduced to the part throughout the process?
- *Inter filament bonding characteristics*—How well do these lines stick to other lines?

The production strategy and material are preset control parameters, while the geometry of the lines of filament, their accumulated strains and their bonding are variables, resulting
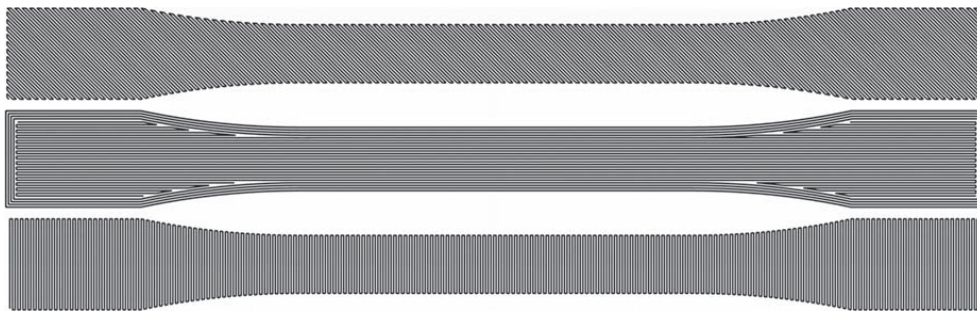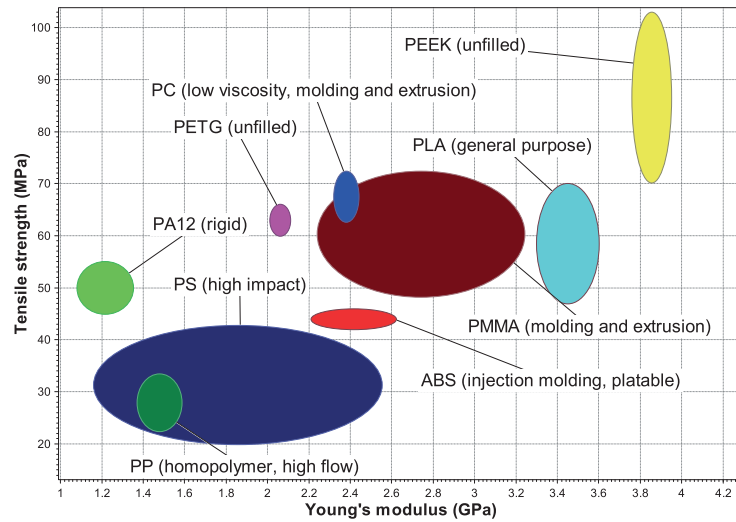

Fig. 5 45° (diagonal), 0° (longitudinal) and 90° (transverse) directed infill. 0° directed infill is shown printed with four outlines to reduce stress concentrations along the edges on the specimen exterior

✑ Springer

Fig. 6 Tensile strength vs. Young's modulus for already in-market FDM materials. Data from the software CES EduPack from Granta Design Limited


from the process parameters as layer height, nozzle temperature, bed temperature, extruder multiplier, overlap, material, etc. One would often need to choose a strategy both for creating exterior or interior (infill) of a part and what mechanical and aesthetic properties these domains should have. The exterior is divided into four sub categories: the outline (the in-plane outward facing domain), the bottom (domain in contact with build plate), the overhang or bridges (facing downwards into the air, or onto support structure), the top (facing out of *z*-plane upwards), as seen in Fig. 4.

To create a smooth outer surface, the outline is very often comprised of semi-continuous lines (lines that bite their tail), while the inner 2D domains are filled to their specified density. This can be achieved using different geometric patterns, e.g.,

Fig. 7 Fracture toughness vs. elongation to failure for already in-market FDM materials. Data from the software CES EduPack from Granta Design Limited
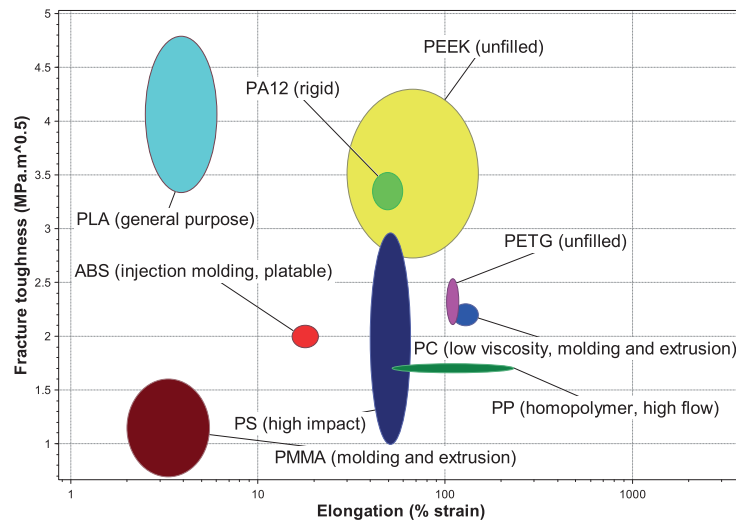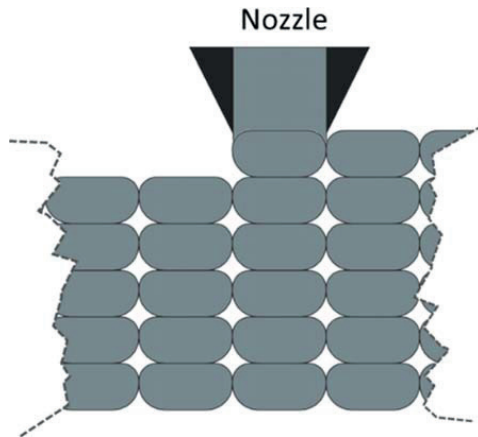
Fig. 8 Void formation between filaments

linear raster, honeycomb, Hilbert curve or concentric raster, to create a near solid, or a partially filled structure to reduce density/material and cost/build time.

The prior research on the subject of material mechanics is mainly done using linear raster infill [4–6, 10, 11, 17], where efforts have been made to find the optimal infill types and orientations, or use the results for classical laminate theory. The reasons for not using more complex infill could be that it would involve more complex analysis, or the fact that this was the standard method of filling before honeycomb and cubic infill became mainstream. The common findings are, however, that compressive strength is not severely affected by infill direction, unlike the tensile strength which is highly dependent. The most used tensile test specimens are 0° (longitudinal) infill, ±45° and 90° angled (transverse) infill compared to the axis of loading, shown in Fig. 5. Research on ABS shows that specimens with transverse infill have the
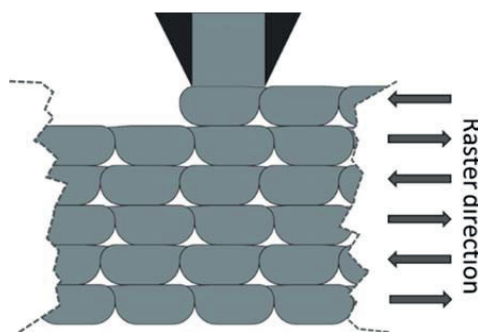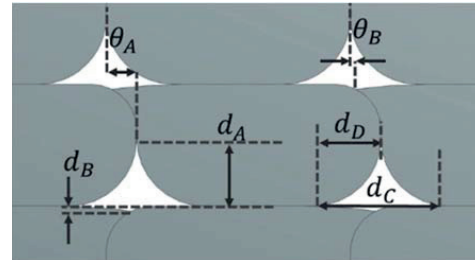

Fig. 10 Geometric measures of voids

lowest performance, with a reported degradation of tensile strength from 22 to 90% [4, 6] compared to the bulk material. Some work using PLA reports an 8–16% reduction of strength of transversal specimens compared with longitudinal ones [18, 19]. However, this work seems to suffer from print quality issues and specimen printing orientations requiring support structures, which might have influenced the results. Specimens that are printed out of x-y plane are often omitted, possibly due to the non-symmetric manufacturing conditions. When creating on-bed standing tensile specimens, the temperature history, the vibrations and thereby the specimen characteristics would vary along its length. Especially voids tend to be smaller close to the heat bed than further away [20].

Many different materials are available on the market; a selection of them, alongside some of their mechanical properties, can be seen in Fig. 6 and Fig. 7. These could be provided as pure, copolymer or filled (carbon/glass/wood/silica), where the most used materials are unfilled PLA and unfilled ABS. Here, the dominant one is PLA due to its relatively low melting point and low shrinkage from solidification to room temperature, which make it easy to use for FDM. Compared with ABS, PLA has very good strength, stiffness and fracture toughness, but low elongation properties make it less suited
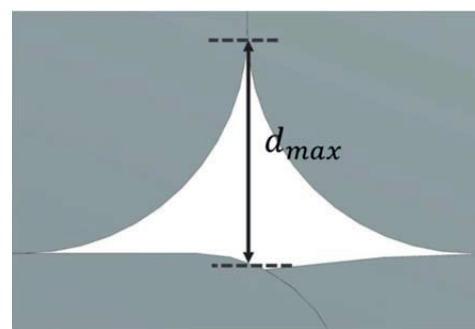

Fig. 9 Near triangular voids in zigzag pattern

Fig. 11 Size and position of the maximum vertical measure of a void, which will be used later in the paper

Table 1 Process characteristics for production of specimens	Layer height	0.3 mm
	Extrusion multiplier	1.0
	Nozzle temperature	210 °C
	Heat bed temperature	55 °C
	Print speed	60 mm/s
	Nozzle size	0.4 mm

for components that utilise the material for springs and spring-like components (e.g., snap fits).

3 Anisotropy and voids

Extruded filament lines have a cross section spanning from oval to a near flattened appearance, where the main drivers for the geometry are:

- Flow rate
- Path placement
- Fluid/solid mechanics of the material
- Layer height

The origin of the shape can partly be explained from fluid mechanics, and the circular shape of the nozzle as Hagen–Poiseuille flow through the nozzle should be expected, using viscous materials such as molten plastics. This implies that the velocity of the material through the nozzle is highest at the centre and declining toward the nozzle wall. This, along with the circular shape of the nozzle, results in less extruded material away from the centreline of the extrusion path (or said otherwise, it would be difficult to extrude a perfectly rectangular line of molten material using a circular nozzle). In addition, the filament is commonly extruded into a corner made up by the previous layer and the previous line of filament, constraining the flow of material and hence flattening its boundaries. As these cross sections do not form sharp corners, placing many filaments alongside each other creates an almost uniform pattern of voids, as illustrated in Fig. 8.

How these voids form, depending on process characteristics, and their effect on mechanical behaviour has been investigated by Rodriguez et al. [6, 7]. Their findings show that the
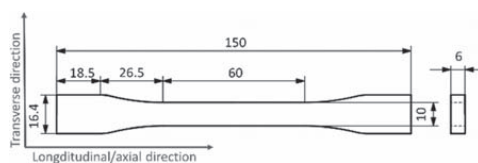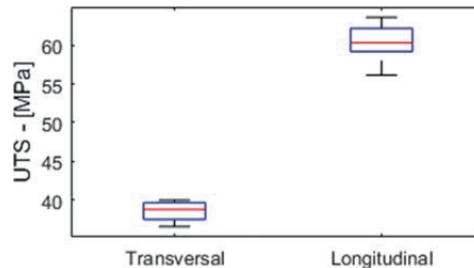

Fig. 13 Ultimate tensile engineering stress for the samples using cross section area based on its exterior dimensions

strength increases with decreased void sizes. Moreover, these voids are not rhombic but tend to extend more upwards than downwards, forming a kite/diamond shape. Some researchers report contradicting findings to this, however, suggesting that the voids extend less upward than downward [21, 22], attributed to, e.g., gravitational forces. However, our experience is in accordance with Rodriguez et al. [7], i.e., the observed asymmetry increases with increased flow rate or overlap of paths. High flow rate or overlap results in near triangular voids, alternating raster directions spread into a zigzag pattern as illustrated in Fig. 9.

We have defined the following geometric values, as measured from the layer boundary or filament boundaries, also shown in Fig. 10 and Fig. 11:

d_A maximum upwards extension of void
d_B maximum downwards extension of void
d_C maximum horizontal measure of void
d_D distance from left contact point to position of d_A
d_{max} maximum vertical measure of void
θ_A misalignment of filament intersections
θ_B misalignment of maximum upwards and downwards measure

Other geometric measures that have a significant effect on fracture behaviour would be the corner radii.
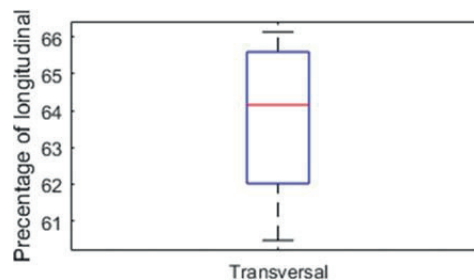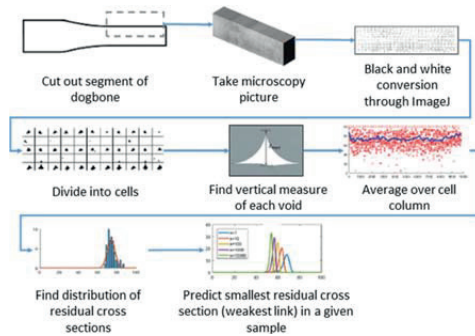

Fig. 12 Tensile specimen geometry

Fig. 14 Results from the transversal specimens compared with the mean of the longitudinal ones

Fig. 15 Approach for analysis of residual cross section

How these voids form, or more correctly, how the bonds between filaments form, have been investigated by many researchers as this is a major factor to the strength of FDM parts. Li et al. [21] used geometric considerations to calculate the void density and bond geometry. Bellehumeur et al. [20] modelled the bond formation between two filaments, depending on temperature, while Sun et al. [13] investigated the temperature profile for some printing processes and its effect on void formation. Coogan and Kazmer [23, 24] modelled the strength of single filament-to-filament bonds, including the contribution of the reduced cross section, and effects of diffusion of polymer chains.

These efforts mainly sought to increase the understanding of the phenomenon of void/bond formation. When expanded to handle more complicated parts than single filament-to-filament bond, they could be of high value for predicting part strength. However, the approaches lack the stochastic perspective that would need to be incorporated for investigating real-world applications and performances. As noted by Gurralla and Regalla, the void sizes are not consistent [25], and a deterministic approach would therefore be insufficient.

To fill this gap, we would explore the statistical effect of void size distribution on ultimate tensile strength of transversely printed FDM parts. Our hypothesis is that it is possible to predict with reasonable accuracy the performance of a transversely printed specimen, compared to a longitudinally printed one, from the distribution of the maximum vertical measure of voids, and hence the distribution of residual cross

sections along the specimen. We further assume that the residual strength of the specimens compared with the ultimate tensile strength of the material is proportional to the estimated residual cross section compared with the net cross section. It is worth noting that the researchers mentioned above have mainly used ABS for their investigations, whereas we will use PLA in this study.

There are other theoretical models for describing fracture due to inherent voids, where the most widespread one is probably the Gurson model [26]. The essence of this model is that it describes the role of hydrostatic pressure in nucleation and growth of voids, hence explaining the pressure dependency of some materials. However, this model is mainly applicable for materials with ductile behaviour. This could exclude PLA, which is reported as brittle [27–29], typically worsened by ageing and exposure to moisture [30]. Also, because the voids are not randomly distributed, but regularly structured holes running across the whole cross section, the Gurson model would need extensive modification to work for FDM specimens.

Another approach for predicting the strength of FDM-printed specimens could be through linear elastic fracture mechanics (LEFM), as the voids mentioned could be seen as subcases of periodic notches/holes [31]. Notably, methods for estimating the stress intensity factors for closely placed rhombic holes with sharp edges, based on numerical calculations, are developed, e.g., the work of Savruk and Kazberuk [32]. Research has also been done on fracture toughness of FDM parts [8, 19]. However, using this as a predictive approach—i.e., investigating the development of cracks between each single void—LEFM would need sufficient control over the critical stress intensity factors in each domain of the tensile specimen. This would be difficult due to highly non-consistent thermal history and hence crystallinity and other material parameters [33].

It is worth noting that our method is not intended to describe the fundamental material mechanics around the voids, but rather to work as an engineering assessment of what to expect from FDM-printed parts due to reduction in residual cross section. Understanding the impact of this factor would be crucial for further investigating the influence of other phenomena such as diffusion of polymer chains, fracture mechanics and residual strain.

Fig. 16 Microscopy picture of dimensions 2570 × 724 compiled of three individual pictures
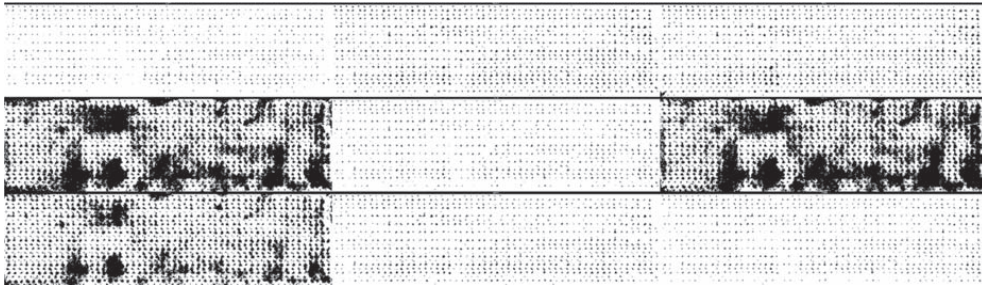
Fig. 17 Different threshold methods tried out, from upper left corner—Sauvola, Phansalkar, Otsu, Niblack, Midgrey, Median, Mean, Contrast and Bernsen. Auto local threshold method, with local radius of 200 pixels

4 Printing, tensile testing and microscopy preparation of samples

First, a total of eight transversely printed and eight longitudinally printed samples were made simultaneously in an unmodified Prusa i3 MK2 printer, with the process specifications given in Table 1.

To keep the research as scientifically controlled as possible (introducing few polymer additives), while maintaining it relevant for most practitioners, uncoloured PLA filament with a 1.75-mm diameter was chosen for the experiment. The PLA was stored in vacuum until printing and tested 2 days after printing, where stored in an air tight container.

A dog bone geometry based on *ISO 527-2-1B* was employed (as seen in Fig. 12), but its clamp section was made 16.4 mm wide (compared with the standard 20 mm clamp section) to make it fit into the clamps of the tensile test bench. The lay-up was equal to the 0° and 90° specimens in Fig. 5.

All samples were tested under quasi-static conditions with a displacement rate of 0.2 mm/min. An assortment of the results is seen in Fig. 13 and Fig. 14. The average ultimate tensile stresses (UTS) were 38.5 and 60.4 MPa for the transversal and longitudinal specimens, respectively, with standard deviations of 1.2 and 2.4 MPa.

The failure load of the transversal specimens falls in between 61 and 66% compared with the mean UTS of the longitudinal printed specimens. As the latter failed in the rounded fillet, possibly affected by stress concentrations inherent to the production method (from the discrete stepping seen in

Fig. 5, also noted by Ahn et al. [4]), these could have failed prematurely.

5 Method and analysis

The proposed method will aim to find the residual cross section through microscopy images of a segment of the tensile specimens. The strategy employed is summarised in Fig. 15.

One segment of a single, transversely printed specimen was cut along its centre axis, sanded and polished for inspection. Before inspection, the specimen was treated with dye penetrant for contrast enhancing, however avoiding dye penetrant extractor (white fluid used for extracting dye penetrant, and hence improve the visibility of cracks and defects) as this tends to give a misleading geometry/size of voids.

Three individual microscopy images of the sample were taken and combined, giving a total sample length of 29 mm and a resolution of 2570 × 724 pixels. Due to global colour gradients (colour differences not due to voids but miscolouring), a simple global greyscale threshold for identifying the voids would lead to misinterpreting the sizes of voids. Therefore, the image was processed through *ImageJ* using the *Auto Local Threshold* algorithm, which estimates the suitable threshold of each pixel based on the colour of the pixels within a radius of 100 pixels. There are different methods for deciding the threshold level, where the *Contrast* method captured the voids more accurately, i.e., giving the largest voids without
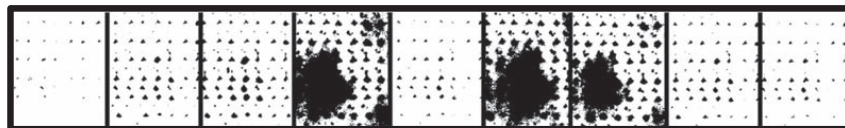
Fig. 18 Detail of same area with, from left to right—Sauvola, Phansalkar, Otsu, Niblack, Midgrey, Median, Mean, Contrast and Bernsen

exhibiting unnatural artefacts, and was therefore used in the rest of the study (see Figs. 16, 17, and 18).

The image was then divided into cells, containing one "filament intersection" each, as shown in Fig. 19. Each cell was scanned to identify the vertical pixel column in the cell with the highest number of black dots (finding d_{max}^{ij}, where ij denotes the row/column index of the cell), assuming this value to be constant throughout the cross section. The residual cross section factor (r^{ij}) of each cell was then taken as:

$$r^{ij} = 1 - \frac{d_{\max}^{ij}}{d_{\text{cell}}} \tag{1}$$

where d_{cell} is the height of the cell. These values were then averaged over the column of cells, creating an average residual cross section factor for each column (R^j), as shown in Fig. 20. Using equal cell heights, R_j is calculated as:

$$R^j = \sum_{i=1}^{n} \frac{r^{ij}}{n} \tag{2}$$

where n is equal to the number of rows in the specimen. This is the factor assumed to be proportional to the ultimate strength of a single cross section, based on the gross cross section of the specimen divided by the strength of the bulk material.

Referring to the measures from Fig. 19, the gross cross section of the specimen (A_{gross}) and the residual cross section (A_{res}) for each column j read:

$$A_{\text{gross}} = W \cdot H \tag{3}$$

$$A_{\text{res}} = A_{\text{gross}} \cdot R^j \tag{4}$$

The approach allowed for the maxima of voids in each cell column to be horizontally misaligned to some extent without affecting the results. This implies that triaxiality was neglected since this is difficult to incorporate without considering more complex analysis, such as finite element analysis (FEA).
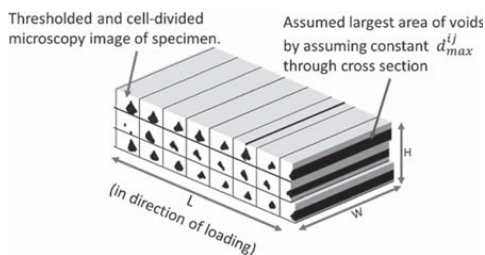

Fig. 20 The magnitude and position of each cell residual cross section fraction (r^{ij}) shown as red crosses, and average over whole column of cells (R^j) shown as blue line

The next step was then to estimate the weakest link W, representing the minimum residual cross section from a given sample size:

$$W = \min_{j=1 \to m} R^j \tag{5}$$

where m is the total number of columns in a given sample. When estimating the weakest link in a sample size, and not the specimen, it is necessary to incorporate a statistical perspective. The general procedure is assuming a Gaussian distribution of the residual cross-sectional factors and finding the distribution of the expected weakest link within a sample. An approximative Gaussian distribution, using mean and standard deviation from the distribution of the residual cross sections, from a microscopy picture, is shown in Fig. 21.

Denoting the probability density function (PDF) for the residual cross section factors and the cumulative distribution function f_R and F_R, respectively, these provide the following relationship:

$$F_R = \int_0^x f_R \, dx \tag{6}$$

The cumulative distribution function (CDF) for the probability of the weakest link in a sample of size m would then be the following:

$$F_W^m = 1 - (1 - F_R)^m \tag{7}$$

Fig. 19 Detail of the cell division of the black and white picture, together with the assumed geometry of the voids through the cross section. Cells are shown sliced at $d_{\max}$
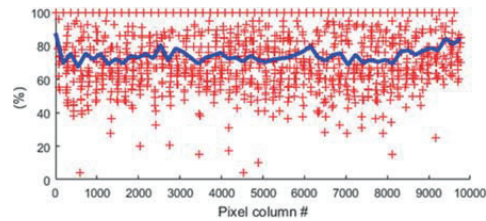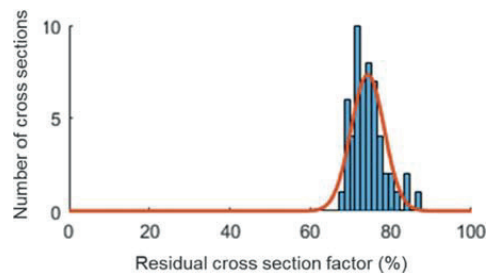

Fig. 21 Real distribution of residual cross section minimums, alongside the probability density function of standard Gaussian distribution scaled to the same numbers of samples

⌕ Springer

which is a Weibull distribution, often seen in weakest link problems. Moreover, its associated probability density function is:

$$f_W^m = \frac{d}{dx} F_W^m \tag{8}$$

This gives the probabilities for a sample of arbitrary size m and print quality equal to the printed specimens, shown in Fig. 22.

It is observed that as the sample size grows large, alongside its decreasing value of the weakest link, the variance decreases, as shown in Fig. 23. This should make the failure load estimations more correct for larger samples. Due to the weakest link effect, the distribution shows a steeper decline than incline, indicating very low probability of a high strength outcome. As a "rule of thumb", for this print quality and size in the range of 100 lines of filament, it would be unlikely for a specimen to achieve a strength of more than 70% of the strength of a void free sample.

6 Comparison with experimental tensile test data

The above probability values are all compared to a solid cross section. Hence, to compare it to longitudinally printed ones, this must be scaled accordingly as these also exhibit cross-sectional reduction. As voids for longitudinally printed
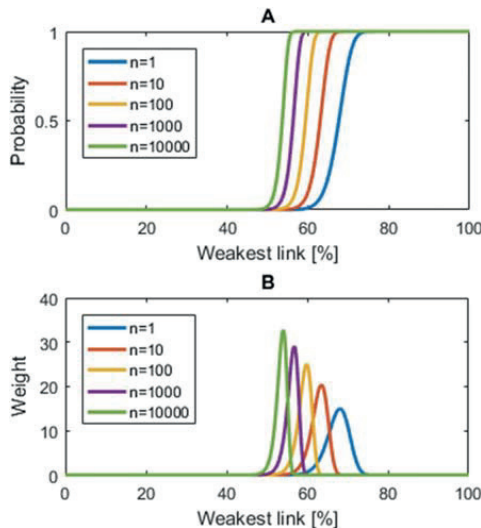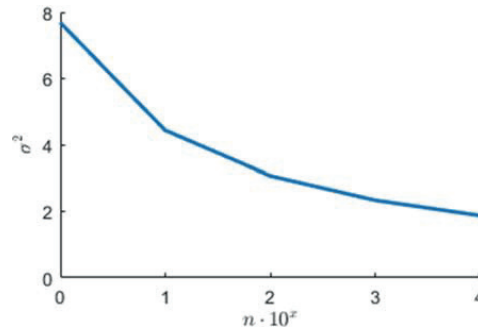
Fig. 23 Variance as function of sample size

specimens run along the axis of loading, the volume fraction would be a sufficient scaling factor. Estimating the volume fraction from the microscopy picture, yields $v_f = 0.9525$. Also, the print strategy used on the transverse specimens results in a wavy surface on its edges as shown in Fig. 24 (where the nozzle changes direction), which collocates with the cross-section minimums. An average over 15 "valleys" result in a reduction in cross-sectional area of 5.8% (denoted $\varepsilon_{\text{edges}}$), and variation in this measure is neglected.

The test samples had a straight section of 60 mm, which results in $m = 150$ filament lines, when using a line width of 0.4 mm. Moreover, it is assumed that tensile failure would arise when the axial stress in the weakest link reaches a critical level and that this level is the same as for the longitudinal printed specimens. Formally, this can be stated as:

$$\frac{F_{\text{transverse}}}{A_{\text{gross}} \cdot W \cdot (1 - \varepsilon_{\text{edges}})} = \frac{F_{\text{longitudinal}}}{A_{\text{gross}} \cdot v_f} \tag{9}$$

Under the above assumptions, this yields the probability density function and cumulative distribution function for the ultimate tensile strength shown in Fig. 25 and Fig. 26.

Fig. 22 **a** Cumulative distribution function. **b** Probability density function for the weakest link in a sample of size n, in percentage of a solid cross section
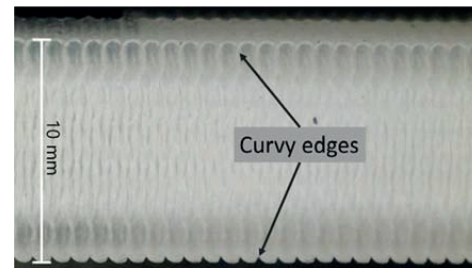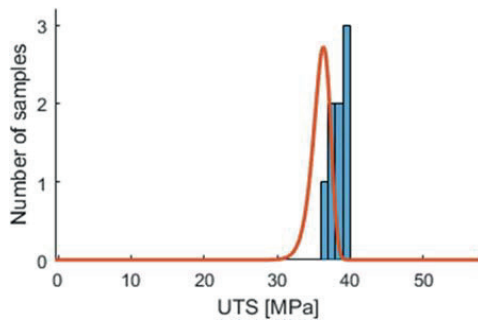
Fig. 24 Curvy edges on the sides of the transversely printed specimens, narrowing the specimen at the locations of maximum void concentrations
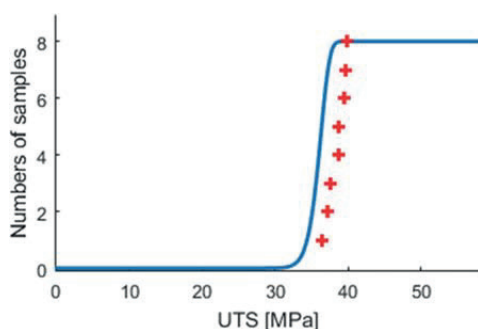
Fig. 25 Scaled probability density function (continuous line) for model alongside experimental data (bars) for ultimate tensile stress using gross cross section (calculated from exterior dimensions of the specimen) of the transversely printed specimens

For our data, the model gives a close yet slightly conservative estimate (about 5 MPa discrepancy) and a matching shape of the continuous distribution.

7 Discussion, limitations and further work

The method proposed herein gives a close estimate on the expected distribution of failure loads of transversely printed specimens based on the failure load of longitudinally printed specimens. However, in this case, the method predicts a lower outcome than the physical experiments. As the approach neglects incomplete atomic diffusion and fracture mechanics, it would lead one to assume that the estimate would predict a higher strength than the physical experiments. The discrepancy could be explained by possible premature failure of the longitudinally printed specimens due to stress concentrations in the fillets of the tensile samples. The residual cross section

Fig. 26 Scaled cumulative distribution function (continuous line) for model alongside experimental data (markers) for ultimate tensile stress using gross cross section for the transversely printed specimens

estimation method using a series of microscopy pictures could also be the origin of this under-prediction of strength.

However, according to our proposed model, there is reason to believe that for specimens of PLA, much of the anisotropic behaviour could be explained directly by the reduction in residual cross section. Due to this effect, the probability of achieving a relatively high strength sample diminishes fast with increased specimen length.

The proposed method is only suitable for the prediction of failure loads for transversely printed specimens. Also, our method is only assessed for PLA, which is the dominant material in practitioner's usage, although less used in previous research.

The method should be further verified by design of experiment techniques, such as Taguchi methods or factorial design, to investigate the influence of different printing conditions on the void sizes and position, and whether the resulting voids can explain the changes in tensile capacity. This approach could also be validated for different printing orientations, or for finding the influence of void sizes on other capacity measures such as ultimate compressive strength and ultimate shear strength.

Another important aspect that should be investigated is the through-thickness properties of the voids. The element of stress triaxiality and fracture could also be investigated, using, e.g., FEA and experimental fracture toughness tests. The mentioned aspects would all be important for future application of this model, whose ultimate aim is to link the bulk material properties and the structural properties of a printed part.

Publisher's Note Springer Nature remains neutral with regard to jurisdictional claims in published maps and institutional affiliations.

References

1. Tronvoll SA, Elverum CW, Welo T (2017) Prototype experiments: strategies and trade-offs. Procedia CIRP 60:554–559
2. Wohlers T. (2016) Wohlers report 2016. Wohlers Associates, Inc.
3. Chen L, He Y, Yang Y, Niu S, Ren H (2017) The research status and development trend of additive manufacturing technology. Int J Adv Manuf Technol 89:3651–3660
4. Ahn S, Montero M, Odell D, Roundy S, Wright PK (2002) Anisotropic material properties of fused deposition modeling ABS. Rapid Prototyp J 8:248–257

5. Ahn SH, Baek C, Lee S, Ahn IS (2003) Anisotropic tensile failure model of rapid prototyping parts—fused deposition modeling (FDM). Int J Mod Phys B 17:1510–1516

6. Rodríguez JF, Thomas JP, Renaud JE (2001) Mechanical behavior of acrylonitrile butadiene styrene (ABS) fused deposition materials. Experimental investigation. Rapid Prototyp J 7: 148–158

7. Rodriguez JF, Thomas JP, Renaud JE (2000) Characterization of the mesostructure of fused-deposition acrylonitrile-butadiene-styrene materials. Rapid Prototyp J 6:175–186

8. Torres J, Cotelo J, Karl J, Gordon AP (2015) Mechanical property optimization of FDM PLA in shear with multiple objectives. JOM 67:1183–1193

9. Torres J, Cole M, Owji A, DeMastry Z, Gordon AP (2016) An approach for mechanical property optimization of fused deposition modeling with polylactic acid via design of experiments. Rapid Prototyp J 22:387–404

10. Sood AK, Chaturvedi V, Datta S, Mahapatra SS (2011) Optimization of process parameters in fused deposition modeling using weighted principal component analysis. J Adv Manuf Syst 10:241–259

11. Casavola C, Cazzato A, Moramarco V, Pappalettere C. Materials & design 2016;90:453–458

12. Mahmood S, Qureshi AJ, Goh KL, Talamona D (2017) Tensile strength of partially filled FFF printed parts: experimental results. Rapid Prototyp J 23:122–128

13. Sun Q, Rizvi GM, Bellehumeur CT, Gu P (2008) Effect of processing conditions on the bonding quality of FDM polymer filaments. Rapid Prototyp J 14:72–80

14. Chacón JM, Caminero MA, García-Plaza E, Núñez PJ (2017) Additive manufacturing of PLA structures using fused deposition modelling: effect of process parameters on mechanical properties and their optimal selection. Mater Des 124:143–157

15. Liu X, Zhang M, Li S, Si L, Peng J, Hu Y (2017) Mechanical property parametric appraisal of fused deposition modeling parts based on the gray Taguchi method. Int J Adv Manuf Technol 89: 2387–2397

16. Thrimurthulu K, Pandey PM, Venkata Reddy N (2004) Optimum part deposition orientation in fused deposition modeling. Int J Mach Tools Manuf 44:585–594

17. Panda SK, Padhee S, Sood AK, Mahapatra SS (2009) Optimization of fused deposition modelling (FDM) process parameters using bacterial foraging technique. Intell Inf Manag 01:89–97

18. Letcher T, Waytashek M (2014) Material property testing of 3D-printed specimen in PLA on an entry-level 3D printer, ASME 2014; IMECE2014–39379

19. Song Y, Li Y, Song W, Yee K, Lee K-Y, Tagarielli VL (2017) Measurements of the mechanical response of unidirectional 3D-printed PLA. Mater Des 123:154–164

20. Bellehumeur C, Li L, Sun Q, Gu P (2004) Modeling of bond formation between polymer filaments in the fused deposition modeling process. J Manuf Process 6:170–178

21. Li L, Sun Q, Bellehumeur C, Gu P (2002) Composite modeling and analysis for fabrication of FDM prototypes with locally controlled properties. J Manuf Process 4:129–141

22. Wang J, Xie H, Weng Z, Senthil T, Wu L (2016) A novel approach to improve mechanical properties of parts fabricated by fused deposition modeling. Mater Des 105:152–159

23. Coogan TJ, Kazmer DO (2017) Healing simulation for bond strength prediction of FDM. Rapid Prototyp J 23:551–561

24. Coogan TJ, Kazmer DO (2017) Bond and part strength in fused deposition modeling. Rapid Prototyp J 23:414–422

25. Gurrala PK, Regalla SP (2014) Part strength evolution with bonding between filaments in fused deposition modelling. Virtual Phys Prototyping 9:141–149

26. Gurson AL et al (1977) Continuum theory of ductile rupture by void nucleation and growth: Part I—Yield criteria and flow rules for porous ductile media. J Eng Mater Technol 99:2–15

27. Todo M, Park S-D, Takayama T, Arakawa K (2007) Fracture micromechanisms of bioabsorbable PLLA/PCL polymer blends. Eng Fract Mech 74:1872–1883

28. Todo M, Shinohara N, Arakawa K (2002) Effects of crystallization and loading-rate on the mode I fracture toughness of biodegradable poly(lactic acid). J Mater Sci Lett 21:1203–1206

29. Arakawa K, Mada T, Park S-D, Todo M (2006) Tensile fracture behavior of a biodegradable polymer, poly(lactic acid). Polym Test 25:628–634

30. Kim E, Shin Y-J, Ahn S-H (2016) The effects of moisture and temperature on the mechanical properties of additive manufacturing components: fused deposition modeling. Rapid Prototyp J 22:887–894

31. Pilkey WD (1997) Holes. In: Peterson's stress concentration factors. John Wiley & Sons, Inc., Hoboken, pp 175–376

32. Savruk MP, Kazberuk A (2009) Stresses in an elastic plane with periodic system of closely located holes. Mater Sci 45:831–844

33. Park S-D, Todo M, Arakawa K (2005) Effects of isothermal crystallization on fracture toughness and crack growth behavior of poly (lactic acid). J Mater Sci 40:1055–1058

A new method for assessing anisotropy in fused deposition modelled parts using computed tomography data

Sigmund A. Tronvoll, Nils Petter Vedvik, Christer W. Elverum & Torgeir Welo
Department of Mechanical and Industrial Engineering
NTNU - Norwegian University of Technology and Science

Abstract

Voids in *fused deposition modeled* (FDM) parts are assumed to be a key driver for the anisotropic behavior of components in polylactic acid, with high relative density. However, these assumptions are based on investigations providing only 2D data (microscopy images). This paper presents a new method to measure such voids by analyzing 3D-data of computed tomography (CT) results, using the OpenCV software library for image processing. The first part of this article elaborates on a proposed method to estimate the reduction in cross sections due to voids in dense cubes of PLA. The second part presents an investigation of the void configurations in different samples, aiming to understand how variation in extrusion rate and compensation for non-linear dynamic extrusion behavior affects the void sizes. The third part displays how this information could be further related to global mechanical properties, using a multiscale finite element approach.

The present method of CT-data analysis gives a clear graphical view of the spatial variation of the void geometry, and the findings suggest that the size of voids have a large non-random spatial variation, decreasing in size towards the turn points of the toolpaths. The void sizes also decline towards the end of each layer due to accumulation of excess material. Printing at a low extrusion rate increases the void sizes considerably, while implementation of an extrusion dynamics compensation algorithm was found to only insignificantly influence the void sizes.

The multiscale finite element approach predicts anisotropic elastic behavior with significant softening in the vertical and transversal direction, relative to the printing direction of the infill. It also displays a non-isotropic energy density throughout the specimen, where the location and magnitude of the most energy dense locations vary significantly for different directions of loading, which implicates an anisotropic behavior in terms of failure in accordance with literature.

1. Introduction

Components manufactured by FDM is found to result in an anisotropic cellular material behavior [1-3]. For low relative density components, the internal structure, also called *infill*, typically consists of either rectilinear webs, as variations of a [0°,90°] or [0°,60°,120°] alternating raster structures, or honeycombs. For structures with high relative density, the most common methods are rectilinear or concentric infills, and as the relative density approaches unity, the voids left in the structure appear mainly in terms of small channels made by aligning four filaments alongside each other as seen in Figure 1.
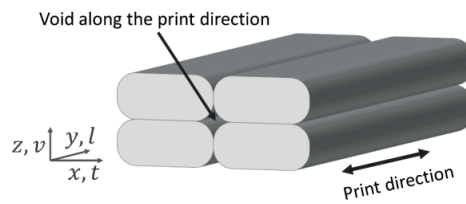
Figure 1 - Drawing of simplified cellular material structure of 4 filament lines placed alongside another, creating a void in the enclosed center region. Longitudinal and transverse direction, l and t, is defined relative to the axis of printing.

The parameters governing the geometry of these voids are numerous, including anything from machine resolution and machine dynamics, to temperature-dependent transient material flow and toolpath placement. Attempts have been made in modelling some of the processes involved in fusing filament segments [4–7], but there is still a long way to go to model the whole system. However, it is possible to investigate the end result of the printed component. This has previously been done by both scanning electron microscope (SEM) and microscopy [1,8]. Unfortunately, these methods do only capture the void sizes along a single surface, and through thickness variations are therefore usually neglected in further analysis. In a previous study the statistical distribution of void sizes combined with a *weakest link* approach was found to be the main driver for anisotropic strength characteristics of tensile specimens in PLA [3]. The method used a microscopy picture of a center slice of a specimen to estimate the void sizes, and the distribution was then analyzed and the expected weakest link of a given sample length was predicted. The theoretical results corresponded well with experimental ones, yet the estimated failure load distribution was lower than that found in experimental results. One of the possible explanations for this under-prediction was that the voids in the center slice are not representative for the full spatial distribution of voids, hence leading to a non-accurate prediction of strength. Investigating this hypothesis is thus one of the main motives for conducting this research. The contributions of this paper can be stated as follows:

- A method to assess void geometries throughout the specimen;
- A demonstration of how this method can be used to assess influence of process parameters on the voids, and investigate the effect of altering *flow rate* and *pressure advance* parameters;
- A demonstration of how this method can be used to assess the voids influence on mechanical parameters as stiffness and failure parameters.

The method presented analyzes volumetric data from x-ray computed tomography (CT-scan), and measures the void sizes throughout a small cubic volume of near-dense FDM parts. The data is analyzed using the *OpenCV* image processing library through *Python* programming. Volumetric data from parts made by FDM has been researched earlier with a focus on dimensional accuracy and porosity [9,10]. However, to our knowledge, this has not been done with the focus on voids as a driver for anisotropy. In response to this gap in prior research, this article reports on the first attempt in relating 3D void geometries based on experimental volumetric information, to anisotropy properties.

To demonstrate how this analysis can be used for obtaining mechanical parameters of the resulting cellular material, a multiscale simulation method is developed. This method is capable of capturing the global elastic behavior and local strain energy density distribution, which can further be used to explore mechanical aspects of failure in FDM manufactured specimens. This is achieved through a 1st order homogenization method using finite element analysis, using the geometrical configuration of the voids found through the CT-data analysis.

The reminder of the article is structured as follows: Section 2 presents previous literature on void formation in FDM. Section 3 describes the invented method used for analysis. Section 4 gives a brief overview of the process parameters investigated. The multiscale modeling approach is presented in section 5. Section 6 display the attributes and procedure for manufacturing of the samples.

Experimental results and discussion from void analysis are given in Section 7, while experimental results and discussion from multiscale analysis are presented in Section 8. Finally, summary and key takeaways are found in Section 9.

It is important to note that there is a large variation in the design and performance of FDM-systems, so that numerical results would most possibly be different from machine to machines. But we expect the trends to be similar, especially for the most popular *Open Source* systems, building on the *Marlin Firmware*, and even more so if also using a *direct extruder design* with both hot-end and extruder co-located on the print head (as opposed to a *Bowden design*).

2. Voids in fused deposition modeling

The most conventional method of manufacturing internal structures by FDM, stacking small strings of filament, creates a cellular material with unit cells in the meso-scale. The resulting cellular material properties are usually anisotropic [1,11]. There are three important strength reduction mechanisms for parts produced by FDM, illustrated in Figure 2, including:

- Reduction of cross section due to voids;
- Void-induced stress concentrations;
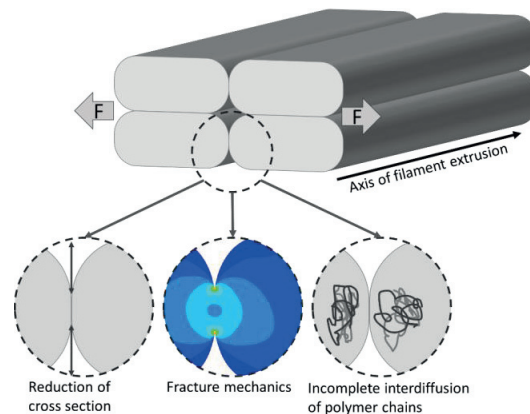- Incomplete interdiffusion of polymer chains.

Figure 2: Strength reduction mechanisms for transverse loading in FDM manufactured specimens.

The reduction in solid cross section explain most of the discrepancy between *transverse* (extrusion paths are transverse to the loading direction) and *longitudinal* (extrusion paths along the loading direction) tensile capacity [3,12]. General findings show that transverse loading results in a plane inter-filament fracture, longitudinal loading creates a fracture surface transverse to the printing direction, while vertical loading separates the layers, as illustrated in Figure 3 [1,8]. The bonding between layers is therefore the key governing mechanism determining tensile capacity.
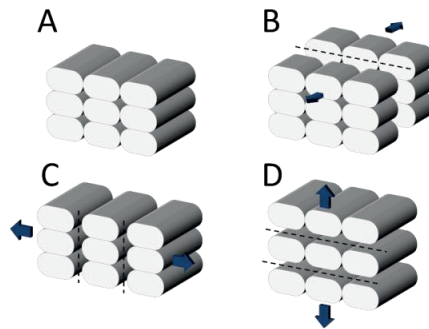
Figure 3: A) virgin sample, B) failure due to longitudinal loading (filament fracture), C) failure due to transverse loading (inter-filament fracture), D) failure due to vertical loading (inter-layer fracture).

In contrast to voids in cast/molded components, the occurrence of voids in parts made by FDM is of a highly repetitive and structured nature, as they are dictated by the toolpaths of the printer. However, the size and shape of these voids are influenced by several process parameters, as well as inaccuracies and variations inherited by the FDM process. Moreover, machine dynamics, resolution and accuracy of the setup, and complex material flow involving molten plastics in a near-solid-phase, would all affect the size and shape of the voids. Furthermore, when the filaments are placed side-to-side, small fluctuations in material flow or unevenness of the print surface will propagate from one filament line to the next, generating a wash-boarding effect. This is especially evident for first-layer printing, where the print quality is very dependent on the evenness of the print surface. In this connection, an uneven surface would often lead to excessive deposition of material in some regions, while leaving other regions insufficiently infilled, as seen in Figure 4.

Figure 4 - First-layer-defects due to A) excessive accumulation of material where the nozzle is too close to the print bed, generating a wash-boarding effect, and B) insufficient infill due to too large distance between nozzle and bed.

For layers located further away from the print bed, the filament shape is more consistent as the deposition surface (the previously printed layers) has been levelled out. The top of each layer is smoother than the bottom, resulting in voids that resemble up-side-down kites or triangles as reported in [3].
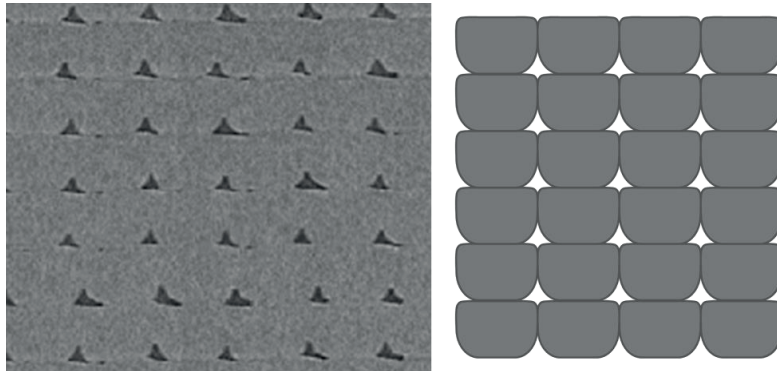
Figure 5: Shape of voids from CT-scan data, with an assumed model of the filament boundaries.

3. Method of CT-Data analysis

The following procedure extracts information about the sizes of voids in a sample of cellular material where the voids are:

1. Known in number.
2. Periodically distributed (as opposed to randomly distributed).
3. Possible to isolate (each void is contained by four adjacent lines of material).

The method is based on analyzing computed tomography (CT) data, but would work for any dataset representing a voxel-based 3D structure with material data that could be used to separate voids from solid material. The proposed method applies the following procedure:

1. Obtain volumetric data from specimen.
2. Threshold the data/images, separating air and solid material.
3. Set up a cell-grid, where each cell covers an area where one would expect one void.
4. Characterize the height and width of each void.
5. Identify the largest void in each cell.
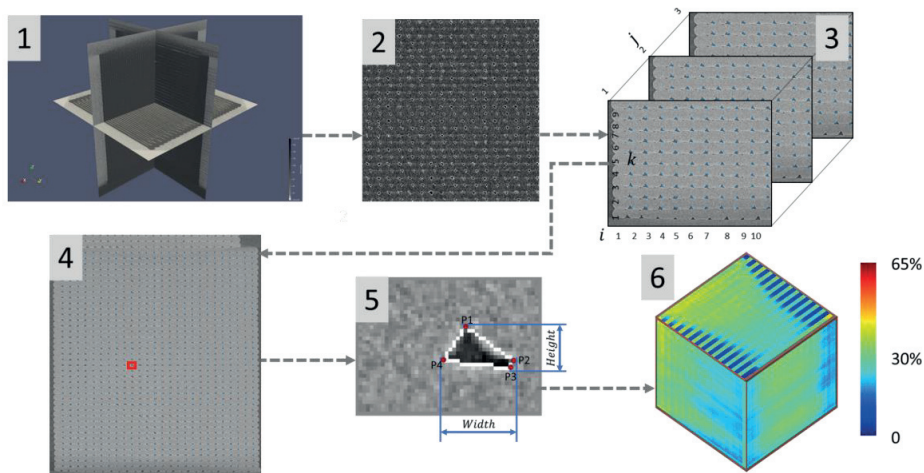6. Analyze the through-thickness properties.

Figure 6: Procedure for measuring voids: 1)Obtain volumetric data from specimen. 2)Threshold the data/images, separating air and solid material. 3) Set up a cell-grid, where each cell covers an area where

one would expect one void. 4) Characterize the height and width of each void. 5) Identify the largest void in each cell. 6) Analyze the through-thickness properties.

This approach, finding the void geometries rather than the conventional method of analyzing the neck geometry [6,12,13] (distance between the voids) allows for more computationally efficient analysis, as one do not need to find the nearest neighboring voids.

To be able to extract continuous data about every single void, a coordinate mapping system is used to estimate the position of the voids. This is done to compensate for specimen misalignment during the CT-scan. Two CT-scan slices at 1/3 and 2/3 width positions of the cubes, taken normal to the longitudinal direction of voids/filament lines, is used to set up this coordinate system. The coordinates of the corner voids of the two slices are named N1 to N4, and N5 to N8, respectively, as displayed in Figure 7. The coordinates of each void are then found through linear interpolation, as follows:

$$
\begin{aligned}
[x,z] = \quad & N_1(\eta - 1)(\xi - 1)(\psi - 1) \\
& + N_2(\eta)(\xi - 1)(\psi - 1) \\
& + N_3(\eta)(\xi)(\psi - 1) \\
& + N_4(\eta - 1)(\xi)(\psi - 1) \\
& + N_5(\eta - 1)(\xi - 1)(\psi) \\
& + N_6(\eta)(\xi - 1)(\psi) \\
& + N_7(\eta)(\xi)(\psi) \\
& + N_8(\eta - 1)(\xi)(\psi)
\end{aligned}
\tag{1}
$$

where the void row, columns and image number relate to these values in the following way:

$$
\eta = \frac{i - 1}{l - 1}
\tag{2}
$$

$$
\xi = \frac{k - 1}{m - 1}
\tag{3}
$$

$$
\psi = \frac{j - n}{p - n}
\tag{4}
$$

Here i, j and k are the void's column, slice, and row number, respectively, as seen in Figure 8, l and m are the total column and row numbers, respectively, while n and p are the numbers of the first and second frame used for setting up the coordinate system. The reason for not using the first and last frames for setting up the coordinate system is due to geometry inconsistencies in those areas, experienced through trial and error.
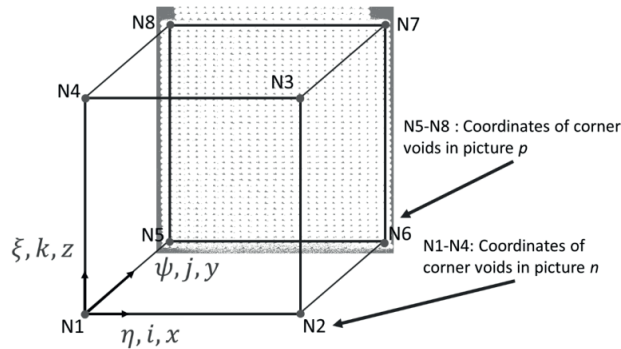

Figure 7: Linear interpolation of coordinates for setting up a grid for finding voids. The nodes N are the [x,z] coordinates of the outermost voids in the two slices used for interpolation.
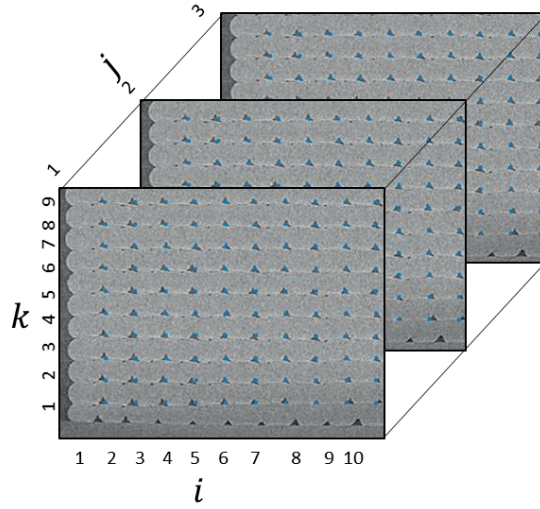
Figure 8: The column, slice and row index of the voids.

As seen in Figure 9, for all calculated void positions a slice of the dataset with height and width, corresponding to the layer height and filament width, was scanned for voids. This was achieved by using *Python* and the *OpenCV* library functions *mean threshold* and *find contour*. If more than one contour was found in one cell, only the largest one was stored. Noise was filtered out by using a minimum required contour length of seven pixels.
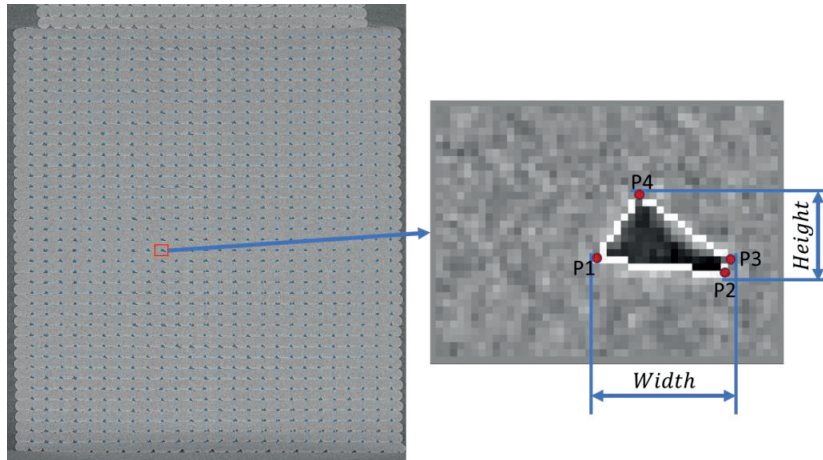
Figure 9: CT-slice with indications for each interpolated void position, and a rectangular box indicating the current cell, together with detail of a cell and its void maxima.

The maximum extension in *x* and *y* direction was found as seen in Figure 9, and displayed as fractions of layer height *H* and filament width *W* of the void:

$$C_h^{ijk} = \frac{h}{H} = \frac{z_4 - z_2}{H} \tag{5}$$

$$C_w^{ijk} = \frac{w}{W} = \frac{x_3 - x_1}{W} \tag{6}$$

where $[x_n, z_n]$ are the coordinates from points P_n for the voids in cell ijk. The area was simplified, using the outer points:

$$a^{ijk} = \frac{x_1 z_1 - x_2 z_1 + x_2 z_3 - x_3 z_2 + x_3 z_4 - x_4 z + x_4 z_1 - x_1 z}{2} \tag{7}$$

$$C_a^{ijk} = \frac{a^{ijk}}{HW} \tag{8}$$

When written as a one or two index average value; e.g. $\bar{C}^{ij}$ denotes the average over the missing indexes, in this case the row index k. As some cells have more than one void (in the case of much noise or irregular void shapes), all voids in each cell are analyzed, and only the maximum values for these coefficients are used.

The geometrical discontinuities at the edges were neglected by defining the boundaries 1 mm from the edges, as illustrated in Figure 10.
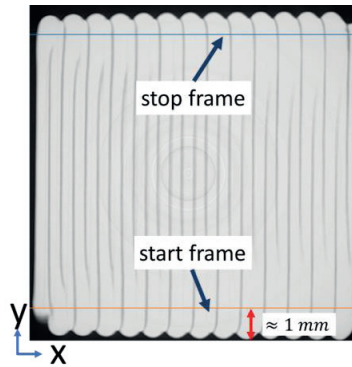

Figure 10: Position of start and stop frame/slice for analysis, as seen from a horizontal slice of the specimen.

4. Parameter selected for investigation

Two parameters are selected for a brief investigation of their influence on the void size and spatial distribution, namely flow rate and pressure advance.

Flow rate, also called extrusion multiplier, refers to relative increased or decreased feeding velocity of raw material/filament. Although the rotational velocity of the filament feeder, and its radius will give an approximate relationship between the rotational velocity of the feeder and volumetric extrusion rate of material, experimental results from Bellini et al. [14] show that this deviation could be large. Tuning of this parameter is therefore crucial to achieve the correct amount of the extruded material [15]. This parameter is highly connected with tensile capacity [1,11], and is therefore assumed to have a significant influence on the void sizes.

Pressure advance is a compensation algorithm for reducing unwanted extrusion defects found in areas of high acceleration or deacceleration and is therefore assumed to decrease eventual variation in void size. The specific algorithm used in this research was *linear advance v1.0* as implemented in the *Marlin v1.1.8* firmware. The algorithms' influence on the mesostructure or mechanical performance of FDM parts has not been investigated earlier *(Reference to Paper 2 in this thesis)*

5. Multiscale simulation approach

As the material is clearly non-uniform, the part's response to uniform (axial) loading is also expected be non-uniform. As a proposal of a multi-level approach for finding the global behavior, and generating local responses of strain energy density, we have adopted a multiscale finite element-based simulation strategy, as illustrated in Figure 11. The approach includes the following steps:

1. Use the previously described method to obtain the shape and area of the inherent voids.
2. Find the distribution of void sizes and average void shape.
3. Create unit cell simulation models for cells with a range of void sizes, but same shape as found in step 2, and obtain effective homogenized material constants.
4. Map these onto a finite element model using the distribution data from step 1.
5. Simulate the uniaxial loading response of the model.
6. Find the global stress/strain response and energy storage in each element.
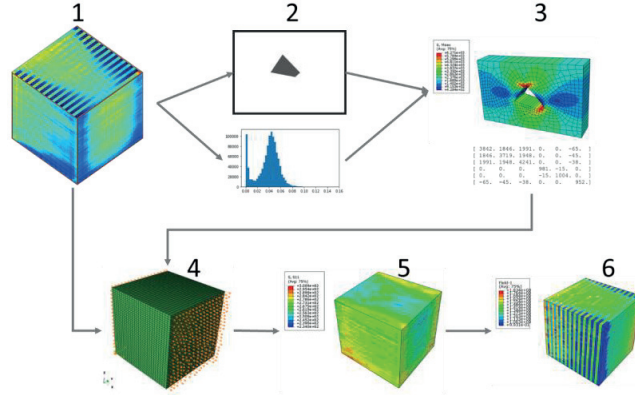

Figure 11: Proposed method for finding stiffness of a uniaxially printed FDM part, and its internal stresses.

In theory, one could have made a simulation model for each void shape and size, but this would be computationally expensive. To increase efficiency, therefore, a characteristic shape was used to represent the void geometry found through averaging the relative positions of the corners for all voids. Naming the x and y position of the q-th corner of the void with index ijk, $[x_q^{ijk}, z_q^{ijk}]$, the average relative position $[\overline{\Delta x_q}, \overline{\Delta z_q}]$ using $[x_1^{ijk}, z_1^{ijk}]$ as reference point in each void (excluding cells without voids) is calculated as:

$$[\overline{\Delta x_q}, \overline{\Delta z}] = \sum_{i,j,k=1,1,1}^{l,m,n} \frac{[x_q^{ijk}, z_q^{ijk}] - [x_1^{ijk}, z_1^{ijk}]}{ijk - N_{zero}} \tag{9}$$

where N_{zero} is the number of cells where the processing method did not identify any voids. It was assumed that the location of the voids inside each unit cell could be approximated by positioning the average of the x and y maximums in the center of the cell; hence,

$$\frac{\overline{\Delta x_1} + \overline{\Delta x_3}}{2} = \frac{W}{2} \tag{10}$$

$$\frac{\overline{\Delta z_2} + \overline{\Delta z_4}}{2} = \frac{H}{2} \tag{11}$$

The finite element analysis was performed using the commercial finite element code *ABAQUS, release 6.14*. Models were created using the Python scripting interface supported in ABAQUS/CAE meshed with 8-node elements of type C3D8R.

The unit cell response was found through a 1st order homogenization approach, as described by Geers et al. [16] using periodic boundary conditions and linear stress responses. The method assumes an insignificant strain gradient across the homogenized structure. Periodic boundary conditions for the unit cell response were implemented by identifying pairs of parallel surfaces $\{A, B\}$ on the unit cell, and applying the following constraint equations:

$$u_i^A - u_i^B = \varepsilon_{ji}\left(x_j^A - x_j^B\right) \qquad (12)$$

where x_i is the i-coordinate of the surface, u_i is the displacement of the surface in the i-direction and ε_{ji} are the imposed macro-strains applied as six different deformation modes.

$$\varepsilon_{1\ldots6} = \{[1\ 0\ 0\ 0\ 0\ 0], \ldots, [0\ 0\ 0\ 0\ 0\ 1]\} \qquad (13)$$

i and j should in this context not be confused with the column and image index previously described. The resulting average stresses from solutions of the individual load cases applied on the unit cell were calculated by multiplying the stresses at the centroid of each element by its volume fraction relative to the unit cell volume, and summing all elements in the model as shown:

$$\bar{\sigma}_{ij} = \frac{1}{V}\int \sigma_{ij}\,dV = \frac{1}{V}\sum_{n=1}^{N}\sigma_{ij,n}V_n \qquad (14)$$

The resulting stress vectors represent the rows of the stiffness matrix, and the resulting effective elastic properties were extracted from the compliance matrix by inverting the stiffness matrix. The Poisson's ratio in the simulation was set to 0.35 [17]. While irrelevant due to normalization of results, the Youngs modulus was set to 3000 MPa. The effect of element size was investigated in a few convergence studies for selected void sizes, and was found to have insignificant effect on the displacement results on the boundaries. Mapping of the cellular material properties from the cell-level simulations onto the global finite element model was done with reduced resolution in y-direction, so that the model could be simulated with 26×100×39 elements rather than 26×1100×39, which was the resolution from the CT-scan data analysis. The C_a used for each element was therefore the average over neighboring ± 5 data points taken in the y-direction.

The loading of the global simulation model was applied as unit displacement between the faces normal to the direction of loading, and these faces were also constrained from out-of-plane displacements. An illustration of the constraints for x-directional loading is shown in Figure 12. The results were then used for obtaining the global stiffness by obtaining the resultant forces.
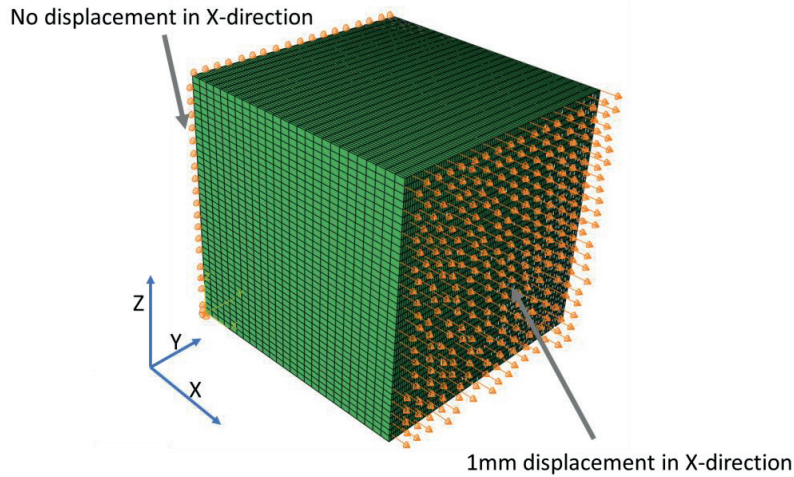

No displacement in X-direction

1mm displacement in X-direction

Figure 12: Loads/boundary conditions for loading in x-direction.

For relating the result to strength parameters through fracture mechanics, strain energy density is found to be a key factor. Griffith and Irwin [18,19] proposed approaches using strain energy release rates as basis for fracture in linear elastic materials, while Rice [20] developed approaches for non-linear elastic and elastic-plastic behavior. Although this article will not go the full length and provide predictive approaches for failure in FDM parts, we will provide the strain energy distribution of the loaded structures. The strain energy density results are normalized, so that the energy density in each element is divided by the average energy density for an isotropic homogenous cube of with bulk material properties, loaded with the same resultant force. For loading in the *n*-direction, this normalized strain energy density, u_{norm} for each cell i, j, k, could be found through:

$$u_{norm}^{ijk} = \frac{u^{ijk}}{\frac{1}{2} F \delta_{bulk}} \tag{15}$$

where u^{ijk} is the energy density for each element, while F is the forces acting on the boundaries of the system and δ_{bulk} is the boundary displacement for a dense cube of the same bulk material, loaded with same resultant force. This can be found through:

$$\delta_{bulk} = F \frac{l_n}{E A_n} \tag{16}$$

with Young's modulus E, length and cross section of cube in loading direction (n), l_n and A_n, respectively. Stiffness reductions factors R are calculated by:

$$R = 1 - \frac{F \, l_n}{E A_n \delta_u} \tag{17}$$

where δ_u is the unit displacement applied in the simulation.

6. Manufacturing and CT-scanning of samples

The cubes used in this analysis were produced with dimensions as seen in Figure 13, which is a trade-off between capturing a great number of voids and achieving a decent spatial resolution from the CT-reconstruction. The cubes are printed with the same uniaxial toolpaths for each layer, as shown in Figure 14. Three samples were printed in transparent polylactic acid filament provided by *Flashforge*, with variation in flow rate *F*, and pressure advance parameter *K* as seen in Table 1. Printing temperature was set to 210°Celsius. All samples were printed on a Prusa i3 MK2S, and due to firmware conventions, the *pressure advance parameter* is applied with a scaling factor of 512. All samples were scanned using a NIKON XT H 225 ST X-ray CT scanner with 1571 projections.
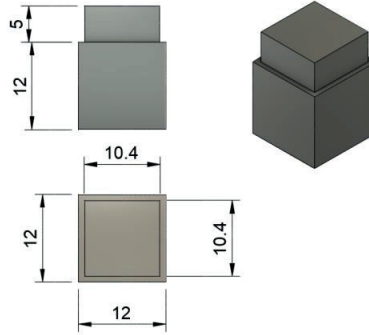
Figure 13: Drawing of the printed cubes used in this study. A small pedestal is added to give some spacing between the specimens and the rotating base while CT-scanning. Specimens are scanned up-side down rotating around the vertical axis.
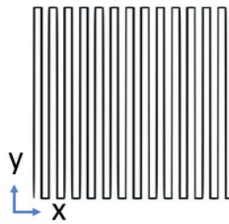
Figure 14: Toolpaths for printing a single layer of the cubes. All layers start in the lower left corner. All specimens were placed at the center of the print bed.

Table 1: Print variations for the three samples.

Sample no.	F	K [s]
1	1	0
2	0.9	0
3	1	0.06

7. Void analysis results and discussion

By visual reference only, there is clearly a large difference on the void sizes between samples with flow rate 1 and 0.9, as seen in Figure 15, while there is little difference when including pressure advance.

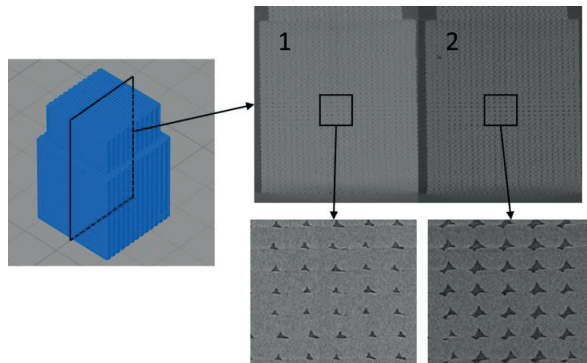*Figure 15: Detail from sample 1 and 2 showing large difference in void size.*

The analysis results comparing the different specimens are seen in Figure 16 to Figure 24. For the three-dimensional illustrations in Figure 16 to Figure 23, the faces of the cubes are showing the through-thickness average values in this direction.
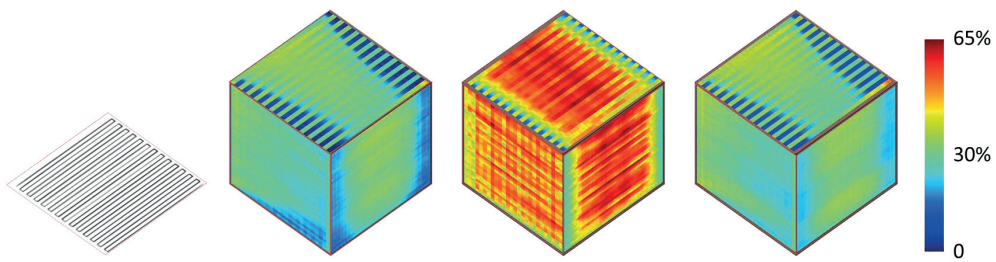
Figure 16: Through-specimen average void heights ($\bar{C}_h^{ik}$, $\bar{C}_h^{jk}$ and $\bar{C}_h^{ij}$ for left, right and upper faces respectively) in percentage of layer heights. Specimen 1 to 3, from left to right. Raster pattern shown to the left.

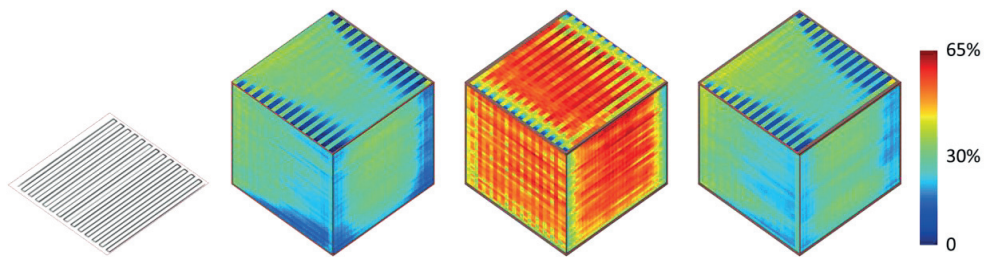*Figure 17: Through-specimen average of void width as percentage of filament widths ($\bar{C}_w^{ik}$, $\bar{C}_w^{jk}$ and $\bar{C}_w^{ij}$ for left, right and upper plane respectively).*
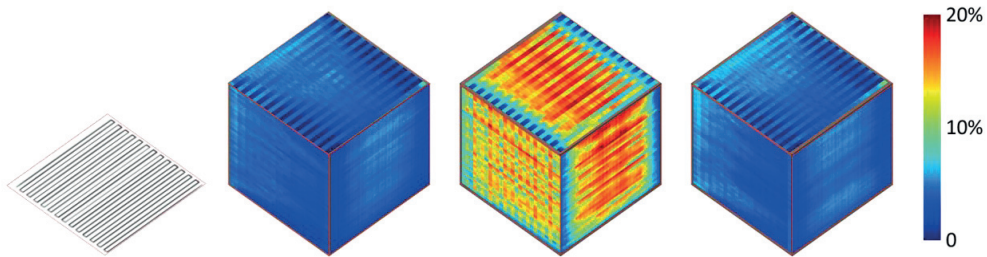
Figure 18: Through-specimen average of void area divided by unit cell area ($\bar{C}_a^{\,ik}$, $\bar{C}_a^{\,jk}$ and $\bar{C}_a^{\,ij}$ for left, right and upper plane respectively).

The first observation is that the void sizes are not randomly distributed, as they show clear signs of spatial dependency through non-random patterns both in transverse, longitudinal and vertical directions. The non-random size distribution also implies non-uniform stress distribution during uniaxial loading—especially for the force flow for transverse loading. The results also show that the voids are smaller close to the print bed than further up, especially for the 3-5 first layers, which is in accordance with literature [6] (also illustrated in Figure 24 as $\bar{C}_w^{\,k}$). As seen from Figure 19, the void size at the sides where the toolpath changes direction is significantly higher than for the rest of the structure, and creates a relatively stiffer bond on those sides. As the boundary of the analysis is 1mm from the edge of the specimen, the actual solid turning point is not a part of the analysis. It is therefore believed that the temperature of the end of the previous line is sufficiently high, so that it sinters together with the new line to a higher degree than the more distant areas. Figure 19, the void size at the sides where the toolpath changes direction is significantly higher than for the rest of the structure, creating a relatively stiffer bond on those sides. As the boundary of the analysis is 1mm from the edge of the specimen, the actual solid turning point is not a part of the analysis. It is therefore assumed that the temperature of the end of the previous line is sufficiently high, so that it sinters together with the new line to a higher degree than in the more distant areas.
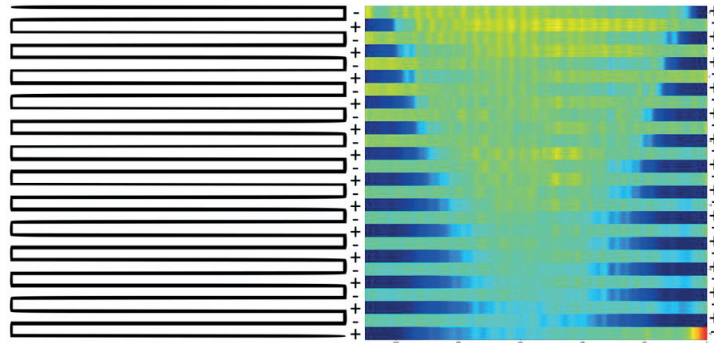

Figure 19: x-y plane with $\bar{C}_a^{\,ij}$ of specimen no. 1, start in upper left corner, and color scale as in Figure 20 Results show alternating side of toolpath direction-change affecting void sizes, which creates an alternating strong bond (+) and weak bond (-) on opposite sides of the specimen.
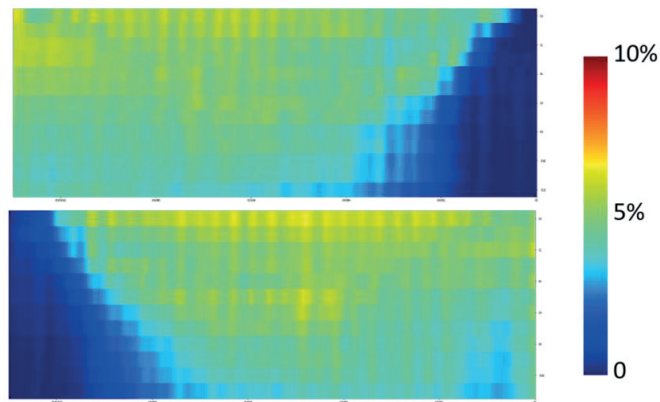
Figure 20: $\bar{C}_a^{ij}$ for voids with left and right turning point, displaying largest void sizes mid to end of void, opposite to turning point (Previous figure split into odd and even column numbers).
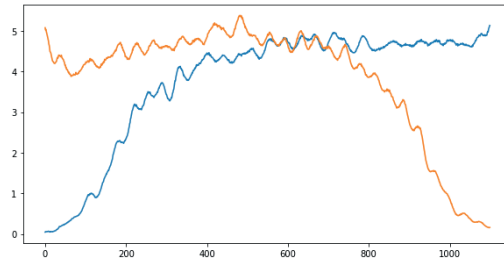
Figure 21: $\bar{C}_a^j$ for voids with left (blue) and right (green) turning point (averaged values from previous illustration).

As seen from Figure 19 to Figure 21, the voids are increasing in size from the turning point until approximately the mid plane of the specimen where it reaches a plateau. The oscillation in void size is also significantly higher near the middle of the sample. It is suspected that this is due to the fact that the velocity of the printer is higher in these areas. There is also a high void size at the end-of-print for all specimens, which is assumed to be a print defect due to effects while stopping the material extrusion and removing the nozzle

High void size in end-of-print

Figure 22: Defects in end-of-print location for each layer.

For the two specimens with default extruder multiplier, results from the x-z plane show that the void sizes decrease considerably throughout each layer. The most plausible explanation for this effect is accumulation of excess material due to inaccuracies. There are indications of machine or extrusion dynamics playing a role, as there is some oscillating variation along each void, where $\bar{C}_a^{ij}$ for the two densest samples show oscillating values of 2−3%, as seen in Figure 23.

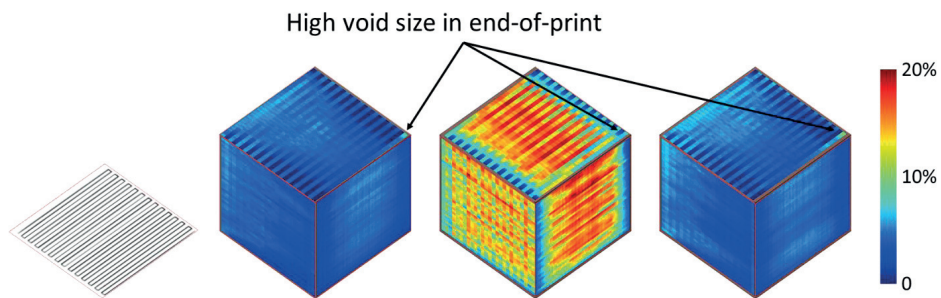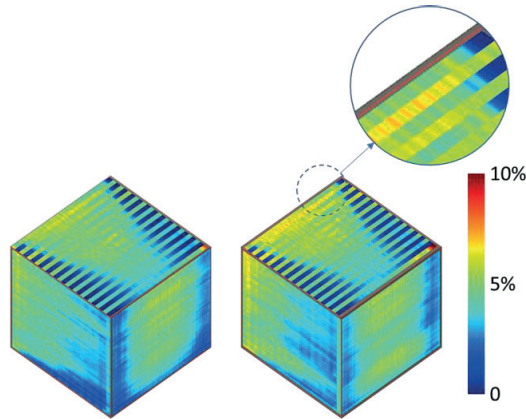Figure 23: $\bar{C}_a$ illustrated using different color scale for sample 1 and 3 for higher resolution. Detail of fluctuating void sizes, possibly due to machine dynamics.

Average values for void height, area and width for each cross section normal to longitudinal, transverse and vertical direction respectively is shown in Figure 24, and total maximum and average values are shown in Table 2 and Table 3.
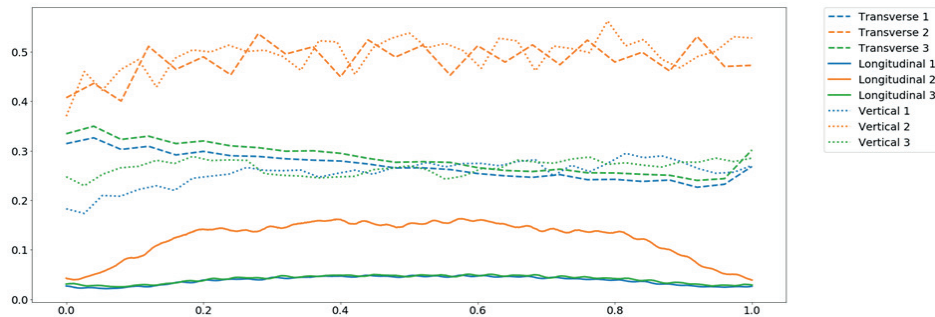
Figure 24: Average cross section reduction in the transverse ($\bar{C}_h^{\ i}$), longitudinal ($\bar{C}_a^{\ j}$) and vertical ($\bar{C}_w^{\ k}$) direction for the three specimens (1 to 3). All positional values taken starts at origin in the coordinate system in Figure 7, and are relative to specimen size.

Comparing Samples 1 and 3 reveals that incorporating a linear pressure advance of 0.2 s does not impact the void sizes to a large extent. Comparing Samples 1 and 2, however, reveals that under-extrusion of 10% impacts the void sizes considerably. It triples the void's cross section, while increasing the height and width approximately 70%, compared with Sample 1. Tuning the flow rate correctly is therefore a crucial task for achieving the smallest voids possible, which has been emphasized in literature [11,21,22].Total averages are seen in Table 3, where C_a would be equal to the porosity.

Table 2: Maximum reduction in cross section along each axis. Maximum values for transverse ($\bar{C}_h{}^i$), longitudinal ($\bar{C}_a{}^k$) and vertical ($\bar{C}_w{}^j$) void measures.

Sample	Max $\bar{C}_h{}^i$	Max $\bar{C}_a{}^k$	Max $\bar{C}_w{}^j$
1	33%	4.9%	29%
2	54%	16%	55%
3	35%	5.1%	29%

Table 3: Total average coefficients.

Sample	$\bar{C}_h$	$\bar{C}_a$	$\bar{C}_w$
1	27%	3.8%	25%
2	48%	12%	49%
3	28%	4.1%	26%

8. Results and discussion of multiscale approach

The average void shape is shown in Figure 25. A histogram of the void size values is shown in Figure 26.
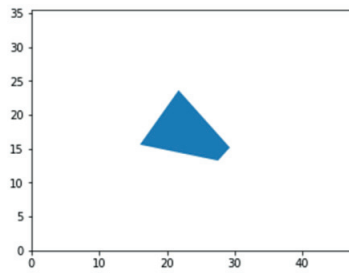
Figure 25: Average void shape, based on relative distances between the corner voids, excluding cells without voids. Dimensions are in pixels, at approximately 119 pixels per mm.
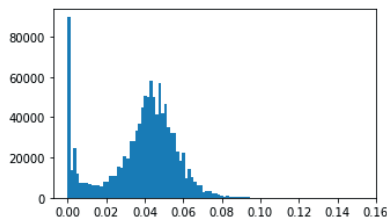
Figure 26: Histogram of the C_a values for sample 1.

Unit cell simulation models were made for 100 different void sizes, with C_a ranging from 0 to 0.16 (equivalent to void cross section areas from 0 to 0.0192 mm^2) where the void shape was a scaled version of the geometry seen in Figure 25, uniformly scaled in x and z-direction. These were then mapped onto the global structure.

The results from the simulations show a reduction in stiffness in all directions, with the largest reduction in z and x-direction, as these are dependent on the void height and width. The reduction in stiffness in z-direction, 3.8%, is the same as the value for $\bar{C}_a$ for this specimen. For a geometry with uniform voids this should be expected as C_a would be equal to the reduction in cross section for that

direction, and hence the reduction in stiffness should be equal [19]. The non-uniform void size that these parts exhibit does, however, seem to not affect this value.

Table 4: Stiffness reduction in each direction compared with bulk material.

Direction	Stiffness reduction
X	10.7 %
Y	3.8 %
Z	13.5%

Normalized strain energy densities for transverse (x), longitudinal (y) and vertical (z) loading are shown in Figure 27 to Figure 32, displaying a considerable spatial dependency. Note that there are different legend scales for the three load cases. Based on the assumptions of planar fracture surfaces as shown in Figure 3, Figure 28, Figure 30 and Figure 32 display the strain energy densities for each cross section perpendicular to the direction of loading.

Figure 27: Normalized strain energy density for loading in transverse direction (exterior only).
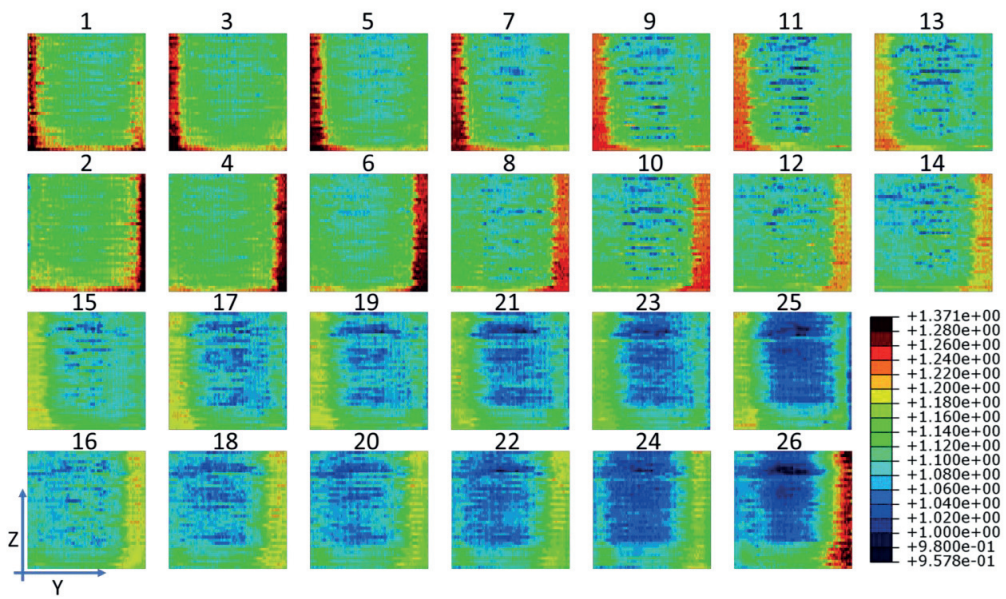
Figure 28: Normalized strain energy density for loading in transverse direction. Each cross section (column index i) shown. Images are divided into odd and even numbers for illustrative purposes due to alternating compliant and stiff side.

Figure 29: Normalized strain energy density for loading in longitudinal direction (exterior only).
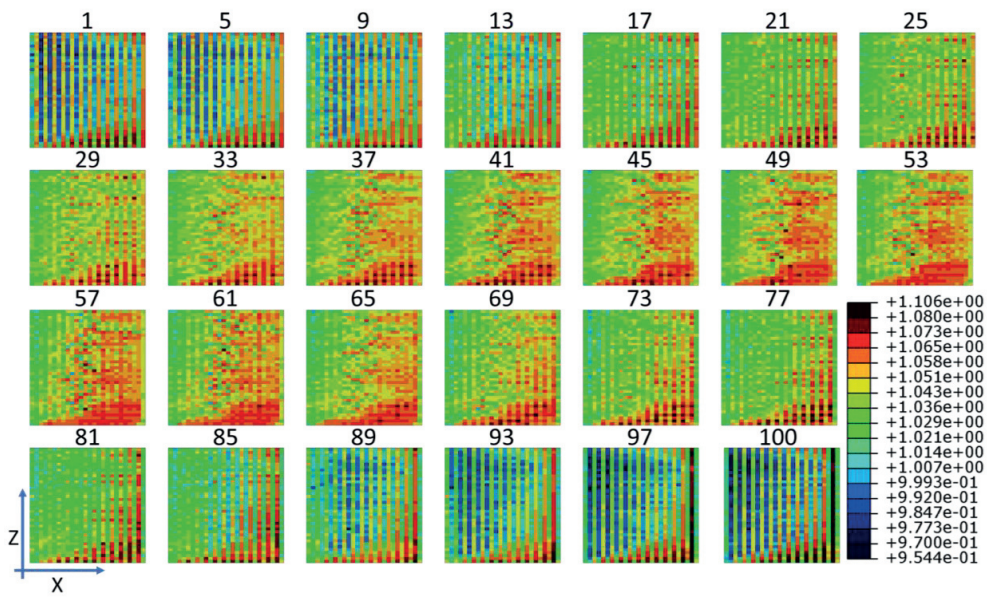
Figure 30: Normalized strain energy density for loading in longitudinal direction. Cross section (slice index j) shown.
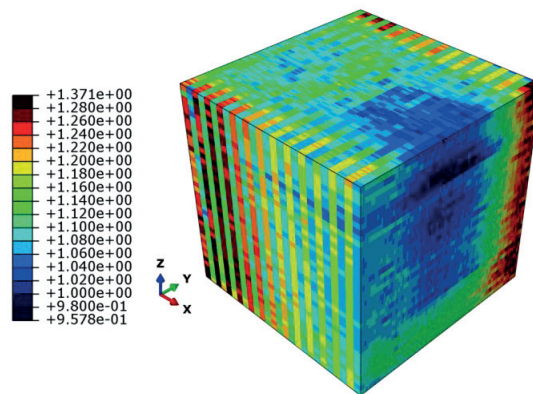

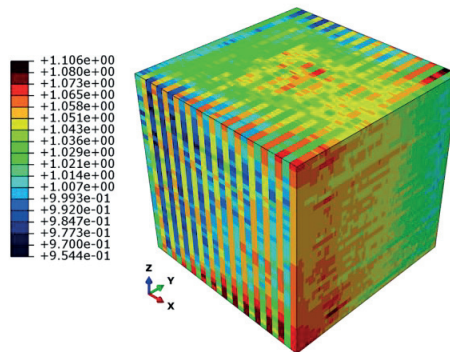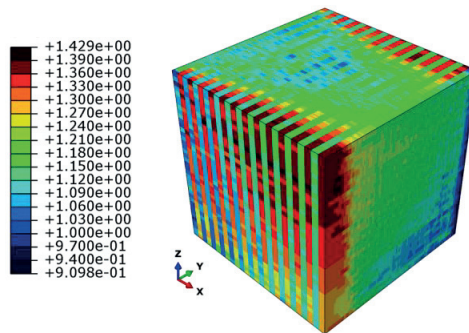*Figure 31: Normalized strain energy density for loading in vertical direction (exterior only).*
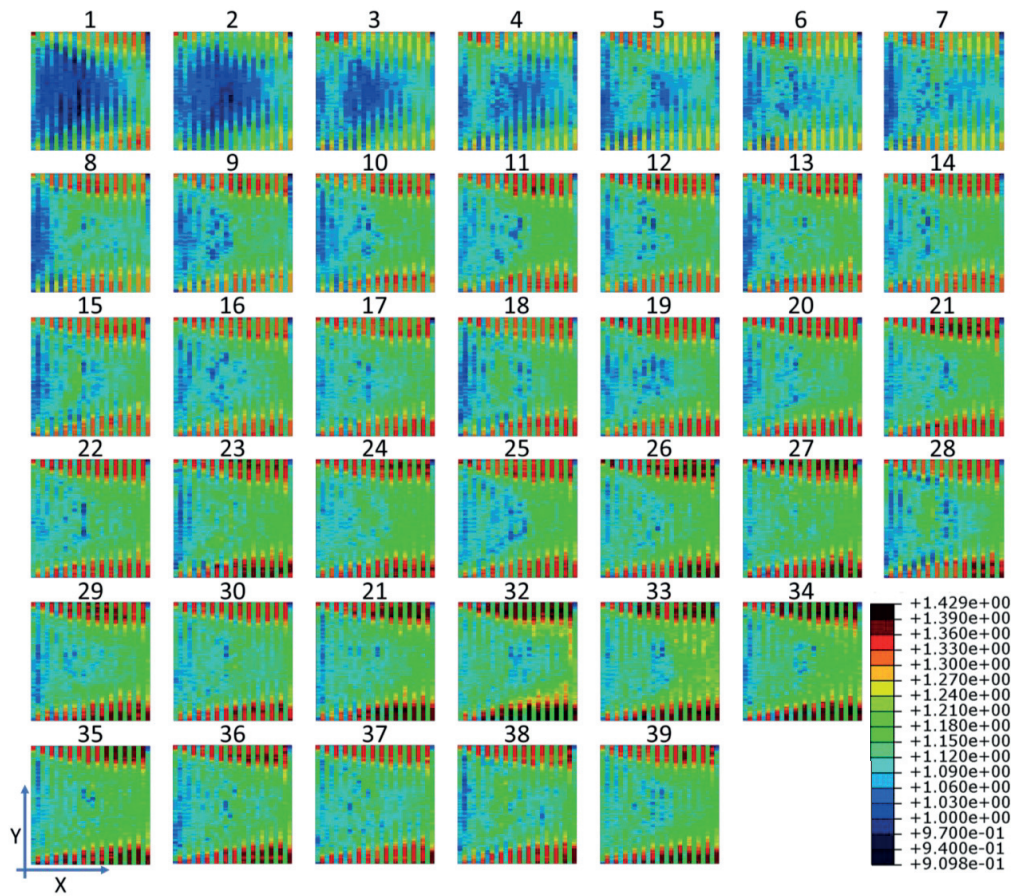
Figure 32: Normalized strain energy density for loading in vertical direction. Each cross section (row index k) shown.

From the results, it is very clear that one introduces more energy into the system for loading in transverse or vertical direction compared with loading in longitudinal, using the same force. While the most energy dense elements for y-directional loading has approximately 10% more energy than for loading an isotropic cube of bulk material, x and z-directional loading have 37% and 43%, respectively. This could explain much of the cellular material anisotropy reported from FDM specimens.

The regions of high energy density also differ from load case to load case. For transverse direction loading, the highest energy levels are found on the compliant sides as discussed in Figure 19. The energy density is also highest for the first columns due to the large void sizes, and on the very last, because of the large defects during print. Conversely, for loading in vertical direction, the high energy density levels are found on the stiff sides. For loading in longitudinal direction, the high-energy density elements are somewhat more randomly distributed, but tends to be higher in the stiff region in the end of each layer (right hand side for each image in Figure 30).

An important aspect is that many of the high-energy density areas are located at or near the boundaries of the geometry, especially for loading in the transverse and vertical directions. This observation may be due to edge effects playing a considerable role for eventual crack initiation and growth.

9. Conclusions and further work

This article has presented a novel method for automatically capturing void sizes from CT-scan data. In accordance with literature, the method is capable of identifying effects of decreasing flow rate on the void sizes, which increases the void sizes significantly, from approximately 27 and 28% of the cell height and width, to 47% and 49% from sample 1 to 2 (10% decrease in flow rate). Incorporating pressure control using an *advance algorithm* increases the void sizes marginally, but not enough to conclude o any relationship. The results also show a clear spatial dependency of void sizes; hence, prior research must be approached with care as most often single microscopy images are used for geometry assessments, and through- thickness variations are thereby omitted.

Further, the research has shown how geometry data of the voids can be used in investigating cellular material properties, linear elastic properties and energy density distribution through a novel multiscale approach based on a 1st order homogenization. This approach is applied on the default material sample under no *pressure advance* or altering of *flow rate*. The results show that the introduction of voids soften the structure significantly for loading in the vertical and transverse direction, providing respectively 13.5% and 10.7% lower stiffness than for a cube with no porosity. For the longitudinal direction loading, the structure is softened with 3.8%, which is the same magnitude as the porosity for the sample. It is also shown that the energy densities are much higher for loading in the vertical and transverse directions compared with loading in the longitudinal direction. The highest cell-average strain energy densities for the sample investigated is 37% (transverse loading), 11% (longitudinal loading) and 41% (vertical loading) higher than it would have been for a non-porous sample with the same loading. This suggests anisotropic cellular material performance in terms of failure, but as there is a large spatial variation in strain energy densities, no conclusion on failure loads are made.

Further work on the method of capturing the geometry of voids should try to optimize process parameters for minimizing void sizes. Here it is of interest to investigate whether this has any influence on the strength of FDM specimens by making comparison with experimental data. Another important extension of this work on void analysis would be to further develop the method to be able to analyze CT-data from geometries with an alternating layup (e.g. [0°,90°]) or more complex non-cubic geometries.

As failure in unidirectionally printed FDM specimens would propagate in the interface between layers or columns of filament lines for transverse or vertical loading, further work on the multiscale simulation method should try to establish methods for identifying the weakest layer or column intersection. However, as most of the high-strain energy density areas are on the geometry boundaries, such an assessment should aim to include edge effects. When such a method is in place, each cross section can be analyzed individually, and be used to map the strain field from the global simulation onto the identified weakest cross section, before further investigating the link between FDM mesostructure and failure.

Acknowledgements

References

[1] Ahn S, Montero M, Odell D, Roundy S, Wright PK. Anisotropic material properties of fused deposition modeling ABS. Rapid Prototyping Journal 2002;8:248–57.
[2] Sung Hoon Ahn, Changil Baek, Sunyoung Lee, In Shup Ahn. Anisotropic Tensile Failure Model of Rapid Prototyping Parts - Fused Deposition Modeling (FDM). International Journal of Modern Physics B: Condensed Matter Physics; Statistical Physics; Applied Physics 2003;17:1510.
[3] Tronvoll SA, Welo T, Elverum CW. The effects of voids on structural properties of fused deposition modelled parts: a probabilistic approach. Int J Adv Manuf Technol 2018:1–12.

[4] Coogan TJ, Kazmer DO. Healing simulation for bond strength prediction of FDM. Rapid Prototyping Journal 2017;23.

[5] Bellehumeur C, Li L, Sun Q, Gu P. Modeling of Bond Formation Between Polymer Filaments in the Fused Deposition Modeling Process. Journal of Manufacturing Processes 2004;6:170−8.

[6] Q. Sun, G.M. Rizvi, C.T. Bellehumeur, P. Gu. Effect of processing conditions on the bonding quality of FDM polymer filaments. Rapid Prototyping Journal 2008;14:72−80.

[7] Crockett RS, Calvert PD. The Liquid-To-Solid Transition in Stereodeposition Techniques n.d.:8.

[8] Gurrala PK, Regalla SP. Part strength evolution with bonding between filaments in fused deposition modelling. Virtual and Physical Prototyping 2014;9:141−9.

[9] Ihab El-Katatny, S.H. Masood, Y.S. Morsi. Error analysis of FDM fabricated medical replicas. Rapid Prototyping Journal 2010;16:36−43.

[10] Ho ST, Hutmacher DW. A comparison of micro CT with other techniques used in the characterization of scaffolds. Biomaterials 2006;27:1362−76.

[11] Montero M, Roundy S, Odell D, Ahn S-H, Wright PK. Material characterization of fused deposition modeling (FDM) ABS by designed experiments. Proceedings of rapid prototyping and manufacturing conference, SME, 2001, p. 1−21.

[12] Coogan TJ, Kazmer DO. Bond and part strength in fused deposition modeling. Rapid Prototyping Journal 2017;23:414−22.

[13] Jose F. Rodriguez, James P. Thomas, John E. Renaud. Characterization of the mesostructure of fused-deposition acrylonitrile-butadiene-styrene materials. Rapid Prototyping Journal 2000;6:175−86.

[14] Bellini A, Güçeri S, Bertoldi M. Liquefier Dynamics in Fused Deposition. Journal of Manufacturing Science and Engineering 2004;126:237.

[15] Gary H, Ranellucci A, Moe J. Slic3r Manual - Flow Math n.d. http://manual.slic3r.org/advanced/flow-math (accessed April 10, 2018).

[16] Geers MGD, Kouznetsova VG, Brekelmans WAM. Multi-scale computational homogenization: Trends and challenges. Journal of Computational and Applied Mathematics 2010;234:2175−82.

[17] Imre B, Keledi G, Renner K, Móczó J, Murariu M, Dubois P, et al. Adhesion and micromechanical deformation processes in PLA/CaSO4 composites. Carbohydrate Polymers 2012;89:759−67.

[18] Griffith Alan Arnold, Taylor Geoffrey Ingram. VI. The phenomena of rupture and flow in solids. Philosophical Transactions of the Royal Society of London Series A, Containing Papers of a Mathematical or Physical Character 1921;221:163−98.

[19] Irwin GR. Onset of fast crack propagation in high strength steel and aluminum alloys. NAVAL RESEARCH LAB WASHINGTON DC; 1956.

[20] Rice JR. A path independent integral and the approximate analysis of strain concentration by notches and cracks. Journal of Applied Mechanics 1968;35:379−386.

[21] Rodríguez JF, Thomas JP, Renaud JE. Mechanical behavior of acrylonitrile butadiene styrene (ABS) fused deposition materials. Experimental investigation. Rapid Prototyping Journal 2001;7:148−58.

[22] Chin Ang K, Fai Leong K, Kai Chua C, Chandrasekaran M. Investigation of the mechanical properties and porosity relationships in fused deposition modelling-fabricated porous structures. Rapid Prototyping Journal 2006;12:100−5.

Errata to article *Prototype experiments: strategies and trade-offs*

Reference list entries [11]-[24] corrected due to numbering errors.

27th CIRP Design 2017

Prototype experiments: strategies and trade-offs

Sigmund A. Tronvoll*, Christer W. Elverum, Torgeir Welo

NTNU - Norwegian University of Science and Technology - Department of Mechanical and Industrial Engineering,
Richard Birkelands vei 2B, 7491 Trondheim, Norway.

* Corresponding author. Tel.: +47-905-20-107. *E-mail address:* sigmund.tronvoll@ntnu.no

Abstract

Throughout the whole product development process, there is always a question on whether the proposed product is "up to its task", and often it is up to the engineer or designer to answer these questions. In many cases, this calls for experiments in form of prototype testing, to explore, verify, and validate the product performance. This paper connects the overall approach of the development process, in form of point-based, set-based, and agile strategies, and connects them to what seems to be the fundamental tradeoff in prototype experiments, exemplified by real cases from an industrial-academic development project.

Keywords: agile development; set-based engineering; point-based engineering; prototyping; experimentation

1. Background and introduction

As product development methodologies come and go, some aspects of product development remain invariant. Redesign, rework or iterative work cycles in its simplest form exists in all engineering activities [1], as changing measures of a machine drawing due to interference of parts, choosing different color of a part after seeing a rendered CAD model, or larger failures as rebuilding a late-stage prototype due to a weak design.

Going back to the basics, engineering design is about fulfilling a need. Some of these can be parametrized into equations, and mathematically solved, resulting in a solution that will work. An example could be deciding the needed cross section for a cantilever beam to hold a certain load without overshooting its yield strength. However, the transition from needs to design for something as simple as a bar stool proves difficult when considering all possible inflicting parameters as fatigue life, material defects and user preferences and behavior.

When digging into the problem, designers and engineers therefore introduce simplifications and assumptions to confine the problem into a neater package of solvable bits and pieces of problems and sub-problems. Based on these models, a qualified (or unqualified) guess for a suitable solution is composed and evaluated against its requirements through some form of experiment. As these are in fact guesses, the resulting design will sometimes fail, either due to lack of understanding of what the product should do or withstand, or due to overly crude simplifications and assumptions. The solution must therefore subsequently be redesigned and tested again. The cost of such rework often depends on the level of commitment introduced after the initial work is done, and tend to be more expensive the further you get into the process [2]. Or more accurately; the sunk cost of the initial faulty work that must be discarded could have been substantial, while rework is the means of correcting those faults.

These, almost unavoidable, cycles are the background for the term iterative design cycles, which are celebrated and formalized in some cultures (as *design thinking* [3] and *agile development* [4]) and doomed in others (as *quality function deployment* [5] and *total quality management* [6]). The difference is not whether they exist in different cultures, but how they are perceived. Does the culture emphasize tuning each design decision to perfection before committing to it, or do they acknowledge that early design decisions will be flawed, and therefore iterates with larger changes between each cycle? Do the culture lean towards "do it right the first time" or "just do it"?

To increase confidence in solutions, engineers often utilize different dimensioning tools as *allowable stress design* and *limit state design*. In addition to this, engineers and designers try to reduce the cost of rework through design strategy and improved analysis/tests of design proposals. Elverum, Welo and Tronvoll [7] have earlier proposed guidelines for choosing prototyping methods for design and evaluation, based on contextual factors. To be able to expand on these contextual guidelines, this paper investigates and clarifies the trade-offs associated with choosing approach for experimenting with prototypes. Two examples from an academic/industrial collaborative project are displayed, to show how the iterative nature of product development, together with the strategy of the product development task, affects the experiment trade-off.

2. The four strategies

Before going into how prototype experiments are conducted, it is important to set their purpose in a strategic context. In what overall development strategy are the experiments utilized? There are in principle four different approaches to progress a design task. The choice depends on the extent to which a proposed solution is refined/fixated, and what backup plans are built into the product or the process:

1. **Point-based design** - Make sure that the chosen solution would be suitable/work, and stick with it. Use as much resources as needed to be able to proceed with a design, only when you have achieved a very high confidence in its performance. If the design appears to be missing its target, redo the process (no backup plan), similar to trying to implement the stage/phase-gate approach as a development process rather than a management tool [8].
2. **Set-based solution array -** Create an array (set) of solutions/designs that potentially could perform at certain level and hope that at least one would be suitable. Screening/convergence is based on continuous or stage-wise estimation of performance and gradual elimination of weak alternatives (as opposed to searching for the best alternatives) [9].
3. **Performance set investigation -** Instead of choosing multiple solutions, choose the most promising one, and investigate its performance thoroughly so that it's capability could be represented as a range of performance rather than the traditional compliance with requirements. Postpone committing to design decisions, which will constrain the design, until they can be validated. This will eventually lead to a gradual convergence of the design [9,10]. The capabilities and performance ranges are also named sets in some literature.
4. **Flexible design** - Design a best-guess solution so that eventual necessary design changes are easily implementable. Fixate, but allow for change (for example through extensive use of modularization). Validate when possible and change direction if needed [4]. This is the only strategy actually designed for

iterating, while the others try to mitigate uncertainty in other ways.

The twofold use of 'set' is only to point out that they are essential to set-based concurrent engineering, in which they are combined [11]. As strategy 2 and 3 stems from studies of Toyota, they are naturally described as components of Lean Product Development [9,12]. There is currently a lack of naming convention on the two aspects of set-based strategies, so their naming in this paper does only reflect their function.

The term flexible could as well be replaced by agile, as used in the software industry. However, the second and third principle are also useful tools to achieve an agile development process [13] for physical goods.

Although the strategies have been graphically presented in various ways in earlier work (as set-based in Smith [13] and agile-like in Steinert and Leifer [14]), the essential difference between the strategies boils down to how the concepts evolve in a design space/time diagram, as seen in figure 1.
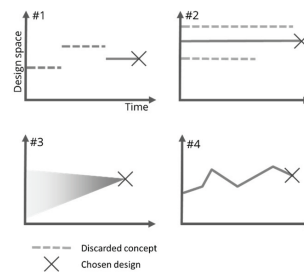

Figure 1: Design progress of the four different strategies. 1) Point based design, 2) Set based solution array, 3) Performance set investigation, 4) Flexible design.

Design teams rarely stick with one of the strategies exclusively, as this would be mentally difficult and impractical. Furthermore, the differences between the strategies are fuzzy when it comes to real-world application as they are mostly combined. What is certain is that designers and engineers tend to intentionally or unintentionally change between the different strategies. It would be rational to differentiate between systems design and component design, where systems are often designed and evaluated using strategy 3 and 4, while the components are designed using strategies 1-3. This is due to the number of variables/components in larger systems, which introduces a lot of uncertainty in the start and would need the flexibility of performance set investigation and flexible design to handle this uncertainty. On the other hand, keeping a sufficient set-based solution array for large systems is cumbersome, and point based design would likely fail due to the uncertainty. Contrary, functions of sub-components are easier to identify, easier to create solution sets of, cheaper to replace, and less cumbersome to fully redesign if they fail. Other researchers have also identified that as the development process is getting closer to finish, the process often tends to approach point-based [13].

3. Iteration through prototype experiments

Iterative development cycles have been a widespread concept for a long time (see Figure 2), probably first formally introduced by Simon [15] as the *generate-test cycle* for explaining how artificial intelligence might contribute to engineering and design. This has later been expanded to the *design-build-test cycle* from [16] to fit for the problem solving cycles in the Japanese automotive industry, or the *design-build-run-analyze cycle* from Thomke [17] stressing the analyze part as an essential activity to learn from the cycle.

The basic of iterative development is however the fact that design tasks consist of cycles with divergent and convergent activities, where one propose, create and test solutions, and subsequently re-create, re-design and re-test if the initial results are not satisfying.

Experimentation, borrowing Smith's description [13] can be described as "you provoke a situation and see how it responds". The reason for explicitly using the term *prototype experiments* rather than prototypes as an isolated artefact, is that a prototype is made for evaluation through some form of experiment. A prototype experiment often targets generating knowledge about different attributes of a proposed design which is not identified by simple reflection. This could be screening of solutions, milestone tests, fulfilment of requirements, proof of concept/manufacturing, integration etc.

In contrast to many researchers which are using the term prototype as a tangible artefact, as opposed to virtual prototypes, we choose in this paper to keep the term as open as possible. Ulrich and Eppinger's definition of prototypes as "… an approximation of the product along one or more dimensions." [18] would to a large extent cover most product development experiments.

Clark et al. [16] identified that different prototype experiments were used in the Japanese automotive industry, during so called "problem solving cycles", in classical set-based engineering; "Inside the problem solving cycles, alternative solutions are created or retrieved, and their consequences are simulated through physical, mental, or computer experiments". It must be noted that the term *computer experiment* should be rephrased to *analytic calculations,* as this is what they are, only as a system of many calculations done at the same time. In this paper we disregard investigating mental experiments, although probably the least cost intensive, as this is a matter of brain power and not strategic experimentation.

The choice of arms would depend on the problem, the wanted form of the output and the capability of the development team, but the main goal must be finding the consequence of a solution through the most favorable type of experiment.

An important fact about prototype experiments is that in addition to including an incomplete model of the product (the prototype), the test also most often includes an incomplete model of its environment [19], and unanticipated behavior often tend to happen when either of the models are replaced by a more comprehensive one [17,18]. The test environment, in contrast to the prototype, can in theory span over an infinite range of scenarios, as it is difficult for a product developer to

know in advance how the product will be used. In addition to the variety of the scenarios and load cases, the uncertainty of their duration and occurrence throughout their life span makes all prototype testing incomplete. This is especially significant for consumer durables, as they in contrast to capital goods, are rarely designed for each individual buyer/user and also suffer from less contact with producer/designer, both before, under and after purchase.

Generalized, the test environment attributes are possible to fit within one or more of the categories of human interaction, physical environment, and product structure. Often, many experiments must be performed to target the span of anticipated scenarios and types of environment the product is supposed to be subjected to. Drawing the analogy to the iterative design-build-test cycle, this would be extended with a parallel loop with iterations around the test environment [20] (see figure 2), to illustrate how the environment is iteratively changed to test a prototype for different cases.
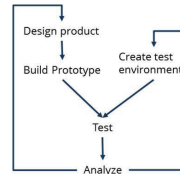

Figure 2: The iterative prototype experiment cycle

Some test setups are created for being able to test multiple prototypes, which allows for experimenting with different solutions which has been shown to be useful for set-based techniques [10].

4. Dimensions of experimental tests in product development

Assessing the important attributes of an experimental test, we could say that the most important result is the increase in the industrial performance parameters, or the general (not project specific) usefulness of the experiment. An experiment should therefore aim for either of these improvements:

- Reduce development cost
- Shorten development time
- Increase total product quality
- Create reusable physical assets
- Create reusable knowledge

Point 1-3 are the general product development performance parameters introduced by Clark and Fujimoto [21], which target the single project performance, while parameter 4 and 5 target the project-to-project asset transfer emphasized in *knowledge based engineering* [22], and *front loading* tactics [23]. All these factors are also emphasized in Lean Product Development [12], focusing on project performance, knowledge, and asset generation, especially for the use in continuous improvement (Kaizen).

However, these are the measures of an outcome, and not the dimensions of the experiment itself, and are difficult to assess on forehand. The dimensions of an experiment should capture how the experiment recreates its real physical counterpart. To what cost, in what way and to what extent does an experiment, present the behavior and performance of the real product in a real environment. The factors of influencing this are:

1. Iteration cost (What is the cost of the experiment)
2. Iteration time (What is the time used on an experiment)
3. Approximation level (How correct is the result)
4. User level (How easy is it to use)
5. Result presentation implicit/explicit (How easy it is to draw conclusions from the data)
6. Experiment flexibility (How easy it is to change conditions)

Dimension 1-3 are quite directly linked to general process performance, while 4-5 are parameters less focused on through research. However, dimension 4-6 might hold the key to why designers, engineers, and managers choose the approach they do.

4.1. Iteration cost

As one of the attributes directly linked to general product development performance, this is a natural component of the experimentation trade-off. However, it must be noted that the overall process performance and the experiment iteration cost is not necessarily directly correlating. If taking into account that approximately 80% of the life cycle costs of a product are committed to after spending 20% of the product development cost [2], there are reasons to believe that somewhat costly experiments in the early phase, that could be giving high learning value could often be beneficial.

Some forms of experimentation, as simulations, can often be iterated again and again, with negligible marginal cost, while destructive testing of physical prototypes often have the same marginal as initial cost.

4.2. Iteration time

As with iteration cost, this is a quite obvious part of any performance measure. And as identified by Thomke et. al.[23], using time and resources on extensive testing and knowledge creating in the start of a project (termed *front-loading*), could result in time savings for the overall project performance.

Reproducing all loads and durations acting on a consumer durable throughout it's safe-life is rarely done in product development, as their safe--life do often extend the product development phase by orders of magnitude. One does therefore often create a more compact load scheme (or scenario), or test multiple similar prototypes on different cases in parallel. Especially in software industry, where users are often granted permission to use not-yet-launched products (as a part of the later stages of the development; *beta testing),* and in return get user statistics, error messages, and bugs which the software exhibits. As an example, Windows 7 had 8 million individual, non-paid, testers [24]. That did not only free up time for the

development team, but made a much more extensive test than any in-house testing facilities could have done.

4.3. Level of approximation

This is one the main counterarguments against computer simulations. Engineers, and maybe especially managers will often prefer tangible experiments for tangible artefacts as exemplified by Iansiti and MacCormack [25]. The world is transient, non-linear, non-conservative, multi-physical, stochastic, and continuous in extent. Reducing this to a, very often, single physics, steady state simulation, is an extreme simplification, and often requires very high knowledge about the situation and limitations of the simulation procedure. If these qualifications are not present, this would often lead to crude results (crap-in, crap out).

Lean management relies heavily on observing the real problems in order to understand and solve them. This has been named *San-Gen Shugi* (*the three reals*): *Gemba*, *Gembutsu* and *Genjitsu*, which translates to *the real place*, *real item* and real *situation/data* [26]. In case of production, this is possible, as these are physical entities, while for product development it can be a bit more difficult due to the fact that all the "real physicals" only exist in the future, after product deployment.

Some have given "dimensions" to the approximation on whether the prototype is either rich/low on functions/attributes and how accurate the representation of these functions are. This has been named by some as fidelity vs. resolution [27] or horizontal vs. vertical prototyping [28,29]. Ulrich and Eppinger [18] has a different way of describing prototypes, as whether they are focused/comprehensive (the amount of functions implemented), and analytical/physical, giving a dimension on whether they are to be tested in the real world, or by analytic calculations/estimations.

4.4. User level

What knowledge and capabilities is needed to conduct the experiment is important when choosing mode of experimentation. This would often be one of the main indicators for whether the experiment can be conducted in-house or must be outsourced to other companies. This is where physical experiments have one of its great advantages. As physical prototyping methods and physical testing most often consists of familiar and tangible processes, it will be a higher possibility that the whole product development team understands the construction of the prototype, the design of the experiment and the implications of the results.

Choosing a toolset common for the whole design team (or the team is able to learn within reasonable time) for experimentation, could be beneficial as it not only allows the team to ask questions about the product performance, but also enables them to answer them.

4.5. Results presentation

Although performance measures, qualitative analysis and visual appearance can be described in words and numbers, a thorough analysis and understanding of the results often require

a more graphical appearance, in form of graphs, plots, videos and statements. Often, to get a feel for how the prototype performs, the result is then frequently showcased against some baseline performance (market leaders, nominal values, legislative values etc.), which often calls for experimenting with in market products also.

4.6. Experiment flexibility

This parameter targets the possibility of changing the experiment, either in terms of the product or the test environment. Fully functional prototypes facilitate testing a large part of their life-cycle scenarios, while a focused prototype might only fit for a very specific case.

5. Examples from an academic-industrial collaborative project

As a part of improving and developing products for property level flood protection, two parallel development tasks were performed, where one was mainly targeting improving water tightness of temporary flood barriers which could be implemented into the already existing product and new products, and the other case targeted developing all-new type of flood protection barriers.

6. Improving water tightness

This was a project initiated to improve the water tightness of self-stabilizing bookstand flood barriers, as shown in Bjerkholt and Lindholm [30]. The first round of experiments was done as a screening of sealing solutions against each other, in a set-based solution array driven development phase.

Figure 3 - First experiment setup of investigating sealing performance

The first experimental setup was designed to be able to replicate a general flood barrier, and the team used a plywood tank and half scale flood barrier. The ground was replicated using pebbles glued on with bed-liner, and the replica of the modules was constructed to accommodate a wide range of sealing solutions. There was no measuring of the leakage, but rather a visual estimation of much/less/no leakage, which was found to be sufficient for the experiment.

The team found two distinct sealing solutions which they favored, but in addition, gained a lot of knowledge about the coupling between leakage and structural stability.

The second experiment was based on the results from the first one, using one of the sealing solutions (a foam gasket), and explored the influence of water pressure vs. gasket pressure, in addition to being able to test different widths of the gasket. The new setup isolated the key sealing mechanism, to be able to draw quantifiable data, and neglected the overall failure effects

observed when testing with a more realistic setup. The setup consisted of a bucket with a texture plate encircling a draining hole in the bottom, and on top of this a plate with a glued on circular gasket as seen in figure 8. The setup also incorporated automatic water leveling and input water measuring to be able to log performance data.
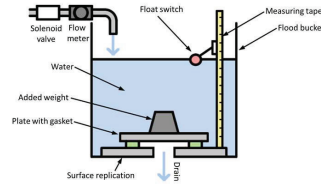

Figure 4: Second experiment setup [31], giving a more rigorous testing of performance parameters of a more constrained type of sealing solution.

The latter experiment reduced the flexibility of the setup, and would only accommodate seals of "gasket like" functionality. But in return allowed for exploring the effect of gasket pressure and water pressure on the leakage rate, [31]. This makes the latter experiment more of an investigation of the performance set of the chosen solution, rather than the set-based solution array nature of the first experiment.

So in terms of tradeoffs committed, somewhat higher iteration time and iteration cost of the setup (due to the data logging system), heightened user level, reduced flexibility, in trade of more explicit data. The approximation in the setup is decreased in terms of data extraction, but it neglects the potential instability issues found using the first setup, making it less accurate in terms of overall accuracy.

6.1. All new concept

This was a project initialized to develop a flood barrier for the consumer market (rather than business to business which is the company's main market segment). The proposed product consisted of tripods holding a canvas (as seen in figure 5).

Figure 5: First prototypes, and tests, of canvas-tripod solution.

The first round of experiments was a *classical proof-of-concept prototype*. As there were uncertainties about the structural integrity of the concept, the overall purpose was to investigate whether it would work or not. The product was built in half scale, and tested in a steel tank. Due to the number of uncertainties, as a potential need of a rod for holding the canvas between the modules, length of canvas, tripod feet spread, flexibility of tripod, flexibility in all these factors were designed into the product. This was achieved using a high degree of modularity, allowed for features to be altered,

removed and introduced in multiple iterations (although keeping most of the concept fixed) throughout the experiment.
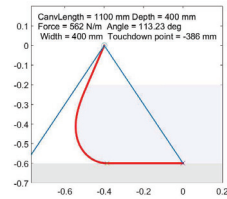

Figure 6: Second round of experimentation – Computer simulation of geometry and loading of canvas.

After getting some peculiar failure modes in the physical testing, the team wanted to know more about the loads and geometry of canvas subjected to a hydraulic pressure. Especially what canvas lengths would be safe, or alternatively introduce unstable behavior.

Although a simplified 2D form of the problem is governed by a very simple equation (cylindrical hoop stress equation) it results in a non-linear partial differential equation. Due to the apparent complexity in the problem, this could not be solved easily in normal structural simulation software, and was therefore hard coded in MATLAB. The results gave a clear overview of the limit between unstable and safe behavior of the barrier. As this experiment was limited to a single solution, for exploring its capabilities thoroughly, this leans toward a *performance-set investigation* type of experiment.

The tradeoff committed was increased user level, decreased flexibility, increased approximation, in trade of a more extensive results presentation, including canvas tension in addition to instability, less iteration cost and time.

7. Concluding remarks

Throughout a development project, designers and engineers shift their strategy to be able to answer the questions at hand. A lot of potential might lie in choosing the most appropriate method of experimentation within that strategy, which in turn calls for investigating its advantages, pitfalls, limitations and implications. The trade-off given when confining a real world problem into a prototype experiment, is characterized by six attributes; iteration time, iteration cost, approximation level user level, result presentation and experiment flexibility. These factors do not say much about the success of the overall product development, but they do give some key points for how the experiment can transform design parameters into valid data to support decision-making.

8. Aknowledgements

9. References

[1] Smith RP, Tjandra P. Experimental observation of iteration in engineering design. Research in Engineering Design 1998;10:107–17.
[2] Haskins C, Forsberg K, Krueger M, Walden D, Hamelin D. Systems engineering handbook. INCOSE, 2006.
[3] Dow SP, Klemmer SR. The Efficacy of Prototyping Under Time Constraints. In: Meinel C, Leifer L, Plattner H, editors. Design Thinking, Springer Berlin Heidelberg; 2011, p. 111–28.
[4] Beck K, Beedle M, Van Bennekum A, Cockburn A, Cunningham W, Fowler M, et al. Manifesto for agile software development 2001.
[5] Mohamed Zairi, Mohamed A. Youssef. Quality function deployment: a main pillar for successful total quality management and product development. International Journal of Quality & Reliability Management 1995;12:9–23.
[6] Harari O. Ten reasons why TQM doesn't work. Management Review 1993;82:33.
[7] Elverum CW, Welo T, Tronvoll S. Prototyping in New Product Development: Strategy Considerations. Procedia CIRP 2016;50:117–22.
[8] Cooper RG, Kleinschmidt EJ. New product processes at leading industrial firms. Industrial Marketing Management 1991;20:137–47.
[9] Ward A, Liker JK, Cristiano JJ, Sobek DK. The second Toyota paradox: How delaying decisions can make better cars faster. Sloan Management Review 1995;36:43.
[10] Kennedy BM, Sobek DK, Kennedy MN. Reducing Rework by Applying Set-Based Practices Early in the Systems Engineering Process. Systems Engineering 2014;17:278–96.
[11] Sobek DK, Ward AC, Liker JK. Toyota's Principles of Set-Based Concurrent Engineering. Sloan Management Review 1999;40:67–83.
[12] Welo T. On the application of lean principles in Product Development: a commentary on models and practices. International Journal of Product Development 2011;13:316–43.
[13] Smith PG. Flexible product development: building agility for changing markets. John Wiley & Sons; 2007.
[14] Steinert M, Leifer LJ. "Finding One"s Way': Re-Discovering a Hunter-Gatherer Model based on Wayfaring. International Journal of Engineering Education 2012;28:251.
[15] Simon HA. The sciences of the artificial. Cambridge, Mass.: MIT Press; 1969.
[16] Clark KB, Fujimoto T. Lead time in automobile product development explaining the Japanese advantage. Journal of Engineering and Technology Management 1989;6:25–58.
[17] Thomke SH. Managing experimentation in the design of new products. Management Science 1998;44:743–762.
[18] Ulrich KT, Eppinger SD. Product design and development. 5th ed. McGraw-Hill; 2012.
[19] Thomke SH. Simulation, learning and R&D performance: Evidence from automotive development. Research Policy 1998;27:55–74.
[20] Tronvoll SA, Elverum CW, Welo T. Test Environments in Engineering Design: A conceptual study. DS 85-1: Proceedings of NordDesign 2016, Volume 1, 2016.
[21] Clark KB, Fujimoto T. Product Development Performance: Strategy, Organization, and Management in the World Auto Industry. Harvard Business Press; 1991.
[22] Studer R, Benjamins VR, Fensel D. Knowledge engineering: Principles and methods. Data & Knowledge Engineering 1998;25:161–97.
[23] Thomke S, Fujimoto T. The Effect of "Front-Loading" Problem-Solving on Product Development Performance. Journal of Product Innovation Management 2000;17:128–42.
[24] Protalinski E. Windows 7 had 8 million testers, biggest beta ever. Ars Technica 2009. www.arstechnica.com (accessed November 8, 2016).
[25] Iansiti M, MacCormack AD. Team New Zealand (A). Harvard Business Publising, 1996.
[26] Hill AV. The Encyclopedia of Operations Management: A Field Manual and Glossary of Operations Management Terms and Concepts. FT Press; 2012.
[27] McCurdy M, Connors C, Pyrzak G, Kanefsky B, Vera A. Breaking the fidelity barrier: an examination of our current characterization of prototypes and an example of a mixed-fidelity success. Proceedings of the SIGCHI Conference, ACM; 2006, p. 1233–1242.
[28] Beaudouin-Lafon M, Mackay W. Prototyping tools and techniques. Human Computer Interaction-Development Process 2003;122–142.
[29] Floyd C. A Systematic Look at Prototyping. In: Budde R, Kuhlenkamp K, Mathiassen L, Züllighoven H, editors. Approaches to Prototyping, Springer Berlin Heidelberg; 1984, p. 1–18.
[30] Bjerkholt JT, Lindholm OG. An Innovative Semi-permanent Flood Protection Structure-Alternative to Sandbags and Supplements to Conventional Earth Embankments. Advances in Urban Flood Management 2007:461.
[31] Haaland KV, Walderhaug ØB. Master Thesis. Prototyping and testing of novel flood protection systems. 2016.